SIGNATURES OF NEW PARTICLES AT HIGH ENERGY COLLIDERS

Anthony Robert Allan B.Sc. Dunelm

Abstract

We discuss the experimental signatures of new particles, predicted by the Standard Model and by Supersymmetry, in high energy proton-antiproton and, or, electron-positron colliders. A review of the theory of the Standard Model and of Supersymmetry, and a general discussion of collider physics is included.

We review various Higgs boson production mechanisms, and consider one, Higgs boson production via Bremsstrahlung from electroweak gauge bosons, in detail. We find that the clearest signature is seen in the invariant mass distribution of the electron pair in the process $\bar{p}p \longrightarrow X$ ($Z \longrightarrow He^{+}e^{-}$). However, the event rate is small, and, unless the Higgs boson can be identified from its decay products, such events may be misidentified as ordinary $Z \longrightarrow e^{+}e^{-}$ events.

We analyse UA1 jet-plus-large-missing-p_T events in terms of a supersymmetric model with a light photino and with $m_{\tilde{g}} < m_{\tilde{g}}$. If these events are due solely to scalar quark production, we find that, in our scenario, the scalar quarks must have a mass in the range 20 - 35 GeV, and the gluino mass must be greater than O(60) GeV.

We study the production of scalar electrons in $e^{+}e^{-}$ collisions on and above the Z resonance. By calculating the cross-sections for $e^{+}e^{-} \longrightarrow e^{+}e^{-}\tilde{\gamma}\tilde{\gamma}$ we show that scalar electrons with mass above the beam energies ($\sqrt{s}/2$) can be identified. In particular, if a zino exists with mass $m_{\tilde{Z}} < \sqrt{s}-m_{\tilde{e}}$, then zino production and decay can give a contribution which dominates the γ-exchange contributions. In this case the presence of both the $\tilde{e}$ and $\tilde{Z}$ may be revealed by a distinctive signature in the electron momentum distribution.

SIGNATURES OF NEW PARTICLES AT HIGH ENERGY COLLIDERS

Thesis

for the degree of

DOCTOR OF PHILOSOPHY

Department of Physics
University of Durham

Anthony Robert Allan B.Sc. Dunelm
— Collingwood College —

1. April 1986

Acknowledgements

I would like to thank Fred Gault, for his infectious enthusiasm and encouragement in the early days, and Alan Martin, for taking me on for the last two years or so. I would also like to thank all the other members in the Theory Group who contributed to the stimulating and convivial atmosphere in which what follows was cobbled together: Peter Collins, Mike Pennington, Chris Maxwell, Stuart Grayson, Tim Spiller, James Webb, Anthony Worrall, Neil Speirs, King-Lun Au, Martin Carter, Tony Peacock, Yanos Michopoulos, Simon Webb, Nick Brown and, in particular, Nigel Glover, for his continued criticism and encouragement. Further thanks are due to Stuart and Nigel, for their collaboration on work incorporated in Chapter 4 of this thesis, and to Nick, for his help in unravelling some knots in Chapter 5.

Thanks are also due to my friends in Collingwood and Trevelyan Colleges, for providing pleasant diversions from this work throughout the past three years or so.

I thank the Standing Committee for the award of a University of Durham Reseach Studentship.

To all those without whom ...

Errata

page i	*line 18*	*for* Reseach *read* Research
page 3	*line 20*	*for* quark spectroscopy *read* hadron spectroscopy
page 6	*line 6*	*for* concerved *read* conserved
page 47	*line 5*	*for* unkown *read* unknown
	line 26	*for* HIggs *read* Higgs
page 113	*ref. 11*	*for* T. Wada *read* W.W. Wada

Contents

Chapter 1

The Standard Model of strong and electroweak interactions and Supersymmetry

Chapter 2

Collider physics

Chapter 3

Higgs boson production via Bremmsstrahlung from electroweak gauge bosons

Chapter 4

Signatures for scalar quark production at the $\bar{p}p$ Collider

Chapter 5

Scalar electron and zino production

on and beyond the Z resonance in $e^+ e^-$ annihilation

Chapter 6

Conclusions

Appendix

Monte Carlo integration and event simulation

References

Signatures of New Particles at High Energy Colliders

"Is it within the power of one man to divine the secret nature of the world, or is even the whisper of that wish a supreme egotism, punishable by a visitation from the White Knight?"

- from *The Small Stones of Tu Fu* by Brian Aldiss

Chapter 1

THE STANDARD MODEL OF STRONG AND ELECTROWEAK INTERACTIONS AND SUPERSYMMETRY

The world embarasses me, and I cannot dream
That this watch exists and has no watchmaker
- Voltaire

1.1 Introduction

1.1.1 *The Classical World*

Many Ancient Greek philosophers considered the question, *Of what is the World made?* Naturally, different philosophers at different times gave different answers. Thales (?624-?546 B.C.) proposed that the primary substance, or element, of the Universe was water, Anaximenes (C6th B.C.) air, and Heraclitus (?535-?475 B.C.) fire. Empedocles (?490-430 B.C.) suggested that there could be more than one element, and to the list of water, air, and fire added a fourth, earth. A different concept was the atomist theory of Leucippus (C5th B.C.) and Democritus (?460-?370 B.C.), in which all matter is composed of indivisible particles, or atoms, of the same stuff but with differing shapes. Aristotle (384-322 BC) accepted the doctrine of four elements, combining in different proportions to form divers Earthly matter, and thus made it the canonical theory for over two thousand years.

Both Democritus's atomism and the Aristotelian world-view are elegant and compelling in their conceptual simplicty; however, each has one fundamental flaw - it is wrong!

Nevertheless, Greek philosophy paved the way for the scientific investigation of the same question in recent centuries. Boyle was the first to propose the existence ofchemical elements in the 17th century; Dalton provided a physical justification for Boyle's ideas with his atomic theory in the 19th. Mendeleev's periodic table of chemical elements (1871) showed a pattern which suggested that there was some ordered substructure to Dalton's atoms as, indeed, has been subsequently evinced by the work of Rutherford and others.

In this century, the nucleons, mesons, and other sub-atomic particles were discovered. The patterns in the properties of these hadrons (the Eightfold Way of Gell-Mann and Ne'eman (1964)) suggested that these "elementary" particles, too, had a substructure, and that the fundamental constituents of matter were still to be discovered ...

1.1.2 *The Modern World*

In recent years there has been significant progress towards an understanding of the fundamental structure of Nature. In particular, it appears that, at the current limit of resolution, all matter is composed of point-like spin-$^1/_2$ fermionic particles, the leptons and quarks (see Table 1.1). These particles undergo three types of interaction -- the electromagnetic, weak, and strong interactions -- which can be successfully described by gauge theories and are mediated by vector guage bosons (see Table 1.1). (The gravitational interaction is not included in the Standard Model since i) its effect is negligible at current

Table 1.1

The SM Particle Spectrum

The particles of the Standard Model with recent values of their masses, and some of their quantum numbers. Spin (j) is given in units of $\hbar$, and electromagnetic charge (Q) is defined such that the electron charge is -1.

The fermions are all spin-$^1/_2$ objects. S, C, B, T are strangeness, charm, beauty and truth quantum numbers. Free quarks are not seen and the mass represents the current quark mass felt via electroweak interactions. All quarks and leptons have antiparticles (with opposite Q,S,...). Each quark flavour comes in three colours (r, g, b). Three generations are known; the existence of any further generation(s) is very speculative.

All the bosons have zero baryon and lepton numbers (B, L). The vector bosons mediate the electroweak and strong interactions; the scalar Higgs boson arises as a consequence of the electroweak symmetry breaking.

(a) Fermions

Quarks ($B=+^1/_3$)								Leptons ($L=+1$)		
Flavour		Mass (GeV)	Q	S	C	B	T		Mass (GeV)	Q
down	d	0.008	$-^1/_3$	0	0	0	0	e^-	0.0005	-1
up	u	0.004	$^2/_3$	0	0	0	0	ν_e	0	0
strange	s	0.15	$-^1/_3$	-1	0	0	0	μ^-	0.105	-1
charm	c	1.2	$^2/_3$	0	1	0	0	ν_μ	0	0
bottom	b	4.7	$-^1/_3$	0	0	-1	0	τ^-	1.8	-1
top	t	35 (?)	$^2/_3$	0	0	0	1	ν_τ	0	0

(b) Bosons

		Mass (GeV)	j	Q
photon	γ	0	1	0
weak bosons	W	82.2	1	±1
	Z^0	93.2	1	0
gluons	g_i	0	1	0
Higgs boson	H^0	?	0	0

energies, and ii) there is no successful description of gravity as a gauge theory.)[1,2]

The first group of fermions is the leptons, particles which do not experience the strong force of hadronic interactions. There are three known charged leptons (e^-, μ^-, and τ^-), which undergo electromagnetic and weak interactions; each of these has an associated neutrino (ν_e, ν_μ, and ν_τ), which interacts only weakly. All the leptons seem to be point-like; no structure down to about 10^{-2} fm has been seen in $e^+ e^- \longrightarrow e^+ e^-$ and $e^+ e^- \longrightarrow \mu^+ \mu^-$ scattering experiments.[3] A lower limit on the size of the charged leptons ($< 10^{-6}$ fm) can be deduced from the fact that their anomalous magnetic moments -- g-2 -- agree with the predictions of QED (see §1.2.1), to a few parts in 10^{10} for the electron.[4]

Quarks also react electromagnetically (they have fractional electric charges) and weakly; however, unlike leptons, they undergo strong interactions. This force is so strong as to confine the quarks within hadrons (p, ...; π, ...) such that no quark has been seen in isolation. Despite this, the physical presence of quarks within hadrons has been clearly indicated bye the results of deep inelastic e, μ, and ν scattering experiments on protons.[5,6] Baryons are composed of three (valence) quarks, e.g. $|p\rangle = |uud\rangle$, and mesons of a quark and anti-quark, e.g. $|\pi^+\rangle = |u\bar{d}\rangle$.[1] The quark model of quark spectroscopy has been remarkably successful.

Five flavours of quarks (d[own], u[p]; s[trange], c[harm];

b[ottom]) have been established experimentally. There is also evidence for the existence of a sixth, the t[op] quark, with a mass 30 GeV < m_t < 50 GeV.[7]

It will be noted that Table 1.1 groups quarks and leptons together in different generations. Apart from the obvious similarity of quarks and leptons as point-like fermions having electromagnetic and weak interactions (though only the former undergo strong interactions; i.e. leptons have a neutral strong "charge," just as neutrinos are electrically neutral), there are also theoretical reasons[8] (the Adler-Bell-Jackiw anomally) for believing that the sum of the charges of the fundamental fermions must vanish. From Table 1.1, we see that

$$Q_e + Q_\nu + 3(Q_u + Q_d) = 0 \qquad (1.1)$$

(where the factor of 3 stems from the three colours of quarks; see §1.2.2), so the relation is satisfied by each generation of fermions separately.

Some authors have proposed the existence of a fourth generation of fermions composed of a heavy charged lepton (λ^-) and its associated neutrino (ν_λ), and two heavy quarks (a[mity], v[itality]).[9] Though there is no experimental or (within the Standard Model) theoretical reason why this cannot be so, neither is there any strong justification for this extension of the established pattern.

The gauge boson of electromagnetism, the photon (γ), has been experimentally well established for many decades. The presence of the gluons, which mediate the strong interaction,

within hadrons has been revealed by deep inelastic scattering experiments.[10] Finally, the gauge bosons of the weak interaction (or, more accurately, the massive gauge bosons of the electroweak interaction; see §1.2.3) have recently been observed by the UA1 and UA2 Collaborations at CERN.[11,12]

The discovery of the gauge bosons has lent support to the description of particle interactions in terms of the $SU(3)_C * SU(2)_L * U(1)_Y$ gauge theory of the Standard Model. This model is discussed in some detail in the next section. Though the Standard Model has had some notable successes, there are also serious shortcomings; these are discused in §1.2.4, together with an outline of some of the "cures."

One of the most attractive theories to go beyond the scope of the Standard Model is Supersymmetry. This retains the description of particle interactions in terms of gauge theories, but also includes a symmetry between fermions and bosons. A consequence of this is that all the known particles have superpartners differing by half a unit of spin. If this Fermi-Bose symmetry is unbroken, the particles and their superpartners should be degenerate in mass; since this is manifestly not the case, supersymmetry must be broken at some high energy. The Standard Model remains as a low-energy effective theory within Supersymmetry. A brief theoretical description of Supersymmetry is given in Section 1.3, together with a description of the likely particle spectrum and a general discussion of the likely phenomenology.

1.2 The Standard Model of Strong and Electroweak Interactions

1.2.1 *Quantum Electrodynamics*

The underlying principle of gauge theories is the invariance of the fundamental Lagrangian under various phase transformations. This phase invariance, or gauge symmetry, leads to a conserved current and, hence, to a concerved charge (Nother's theorem).

Consider the Lagrangian (strictly, the Lagrangian density) for a non-interacting spin-$^1/_2$ fermion, ψ, with mass m:

$$\mathcal{L} = i\bar{\psi}\gamma_\mu\partial^\mu\psi - m\bar{\psi}\psi \,, \tag{1.2}$$

where $\bar{\psi} \equiv \psi^\dagger\gamma^0$, and γ_μ are the usual Dirac matrices. The Euler-Lagrange equations for this Lagrangian lead to the familiar Dirac equation,[2]

$$i\gamma_\mu\partial^\mu\psi - m\psi = 0 \,. \tag{1.3}$$

The Lagrangian is invariant under the global phase transformation,

$$\psi \dashrightarrow \exp(i\alpha)\,\psi \,, \tag{1.4}$$

giving rise to a conserved current,

$$j_\mu = \bar{\psi}\gamma_\mu\psi \,. \tag{1.5}$$

As only one parameter, α, is involved, this is said to be a U(1) symmetry. In pratice, the invariance under such a global phase transformation (global gauge invariance) means that the phase is immeasurable and, hence, can be chosen arbitrarily. A more general invariance (local gauge invariance) arises if the phase is space-time dependant: $\alpha = \alpha(x)$.

The Lagrangian for quantum electrodynamics (QED) is given

by[13]

$$\mathcal{L}_{QED} = \bar{\psi}(i\gamma_\mu\partial^\mu - m)\psi + e\bar{\psi}\gamma_\mu A^\mu\psi - {}^1/_4 F_{\mu\nu}F^{\mu\nu} \qquad (1.6)$$

where ψ is the fermion field and e its electric charge (a coupling constant) , A_μ is the photon field, and $F_{\mu\nu}$ is the electromagnetic field strength tensor

$$F_{\mu\nu} = \partial_\nu A_\mu - \partial_\mu A_\nu \ . \qquad (1.7)$$

This Lagrangian is invariant under the local gauge transformation

$$\psi \dashrightarrow \exp(i\alpha(x))\psi \qquad (1.8)$$

if A transforms as

$$A_\mu \dashrightarrow A_\mu + {}^1/_e\partial_\mu\alpha(x) \ , \qquad (1.9)$$

the usual gauge transformation for the electromagnetic potential. The field strength tensor is invariant under the transformation, of course. The fermion-photon coupling term is required to cancel unwanted terms generated by the local gauge transformation, and must be of this form. The $F_{\mu\nu}F^{\mu\nu}$ term represents the kinetic energy of the photon.

One consequence of requiring local gauge invariance is that a mass term like $m^2A_\mu A^\mu$ is not allowed; i.e. the photon must be massless. The success of QED and the 'natural' way in which both the fermion-photon coupling and the masslessness of the photon arise suggest that local gauge invariance is a good thing; thus, attempts have been made to describe the strong and weak forces in the same way.

1.2.2 Quantum Chromodynamics: The Theory of the Strong Interaction

Would they ever change their hue
As the light chameleons do,
Suiting it to every ray
Twenty times a day?
- P.B. Shelley

The gauge transformations $\exp(i\alpha(x))$ of QED form an Abelian unitary gauge group, $U(1)_Q$. Quantum chromodynamics (QCD)[10,14] is based on a non-Abelian special unitary group, SU(3) of colour. In contrast to the single generator of $U(1)_Q$, $SU(3)_C$ has eight (32-1) generators, T^a, and, consequently, there exist eight vector fields (gluons) which mediate the interaction. Each quark lies in the fundamental triplet represention of the group; the gluons lie in the adjoint octet representation. The eight generators T^a (a=1,8) form the Lie algebra

$$[T^a, T^b]_- = if^{abc}T^c \qquad (1.10)$$

where f^{abc} are the structure constants of the group, and are antisymmetric in all indices. In the adjoint representation, the T^a are traceless 3x3 matrices.

In analogy with QED, we can construct the Lagrangian of QCD:

$$\mathcal{L}_{QCD} = \bar{\psi}_q(i\gamma_\mu\partial^\mu - m)\psi_q - g(\bar{\psi}_q\gamma_\mu T^a\psi_q)G^{\mu a} - {}^1/_4 G_{\mu\nu}{}^a G^{\mu\nu a} \ , \qquad (1.11)$$

where ψ_q is a quark field of mass m, $G_\mu{}^a$ (with colour label a=1,8) the octet of gauge fields, $G_{\mu\nu}{}^a$ the gluon field strength tensor, and g the strong coupling constant. Each term in the Lagrangian is a colour singlet.

This Lagrangian must be invariant under the local gauge transformation

$$\psi_q \dashrightarrow \exp(i\alpha^a(x)T^a)\psi_q \qquad (1.12)$$

which, for infineitessimal $\alpha^a(x)$, leads to the requirement that

$$G_\mu{}^a \dashrightarrow G_\mu{}^a - {}^1/_g\partial_\mu\alpha^a(x) - f^{abc}\alpha^b(x)G_\mu{}^c \qquad (1.13a)$$

if

$$G_{\mu\nu}{}^a = \partial_\nu G_\mu{}^a - \partial_\mu G_\nu{}^a - gf^{abc}G_\mu{}^b G_\nu{}^c \ . \qquad (1.13b)$$

As with QED, there exist no quadratic terms in $\mathcal{L}_{QCD}$ corresponding to a mass term, so gluons, like photons, are massless. The non-Abelian nature of the group (i.e. $f^{abc} \neq 0$) leads to triple and quartic gluon interactions in the kinetic energy term, $G_{\mu\nu}{}^a G^{\mu\nu a}$. That is, in QCD the gluons themselves carry the colour charge to which they couple, whereas in QED (an Abelian theory) the photon is electromagnetically neutral.

A consequence of the gluon self-interactions is that the one-loop β-function (that is, the coefficient of the terms in the effective quark-gluon coupling generated by one-loop graphs), $\beta = 11 - {}^2/_3N_f$, is positive (if the number of active quark flavours, N_f, is less than 17), unlike the β-function of QED ($\beta_0 = -{}^4/_3$).[10] This implies that the running coupling constant of QCD,

$$\alpha_0(Q^2) = g^2/4\pi = 4\pi/\beta_0 \ln(Q^2/\Lambda^2) \qquad (1.14)$$

(where g is the effective coupling and Λ is an arbitrary mass scale of the theory), decreases as Q^2 increases; i.e. $\alpha_0(Q_1{}^2) < \alpha_0(Q_2{}^2)$ if $Q_1{}^2 > Q_2{}^2$.

Furthermore, $\alpha_0(Q^2) \dashrightarrow 0$ as $Q^2 \dashrightarrow \infty$, and asymptotic freedom is achieved;[13] that is, at small distances, corresponding to high momentum, coloured objects appear to be free. Moreover, as $\alpha_0(Q^2)$ is small at large Q^2, sensible perturbation theory

expansions are permitted, and testable predictions can be made.[16] However, at large distances (and low momentum), $\alpha_s(Q^2)$ is not small and the non-perturbative region of hadronic, rather than parton (quark & gluon), physics is entered. It is currently believed that this increase with decreasing energy of the strong coupling constant leads to confinement of coloured objects within hadrons. Precise tests of this non-perturbative region are necessarily difficult, but many of its predictions (e.g. the occurance of hadronic jets) have been successfully tested.[10]

1.2.3 *The Weinberg-Salam Model of Electroweak Interactions*

(a) Spontaneous Symmetry Breaking and Electroweak Unification

The impressive success of QED and QCD suggests that the weak interaction, too, may be described by a locally gauge invariant theory. However, the short range nature of the interaction indicates that the mediating particles have large masses (O(100) GeV), whereas gauge invariance forbids mass terms like $m^2A_\mu A^\mu$ for the gauge fields. Nevertheless, weak interactions have been described described successfully in terms of a gauge theory which also achieves unification of weak and electromagnetic interactions.

Since the weak vector bosons are massive, the gauge symmetry must be broken. In giving mass terms to the vector fields, care has to be taken to preserve renormalisability and not to break unitarity requirements. This is achieved via spontaneous symmetry breaking, where we construct a locally gauge invariant theory with

a non-invariant ground state. The particular structure of the ground state leads to well defined symetry breaking effects that preserve the important features of the theory.

The Weinberg-Salam (WS) model of electroweak unification[17] uses the Higgs mechanism,[18] and has been shown to be renormalisable.[19] It is based on an SU(2) * U(1) gauge theory with four gauge bosons (3 of SU(2) & 1 of SU(1)) coupled to an SU(2) doublet of complex scalar Higgs fields, viz:

$$\phi = \begin{pmatrix} \phi^+ \\ \phi^0 \end{pmatrix} = \begin{pmatrix} \phi_1 + i\phi_2 \\ \phi_3 + i\phi_4 \end{pmatrix} \tag{1.15}$$

The Lagrangian is

$$\begin{aligned} \mathcal{L}_{EW} &= |(\partial_\mu - igT^a W_\mu{}^a - ig'YB_\mu)\phi|^2 + V(\phi^\dagger\phi) \\ &\quad - {}^1/_4 W_{\mu\nu}{}^a W^{\mu\nu a} - {}^1/_4 B_{\mu\nu} B^{\mu\nu} \end{aligned} \tag{1.16}$$

where $W_\mu{}^a$ (a=1,3) and B_μ are the gauge fields of the SU(2) and U(1) symmetry groups and $W_{\mu\nu}{}^a$ and $B_{\mu\nu}$ their field strength tensors. The couplings of the SU(2) and U(1) groups are g and g', and their generators are T^a (weak isospin, a=1,3) and Y (weak hypercharge).

The scalar potential V is

$$V(\phi^\dagger\phi) = \mu^2\phi^\dagger\phi + \lambda(\phi^\dagger\phi)^2 \tag{1.17}$$

where $\lambda > 0$ so V is bounded below. If $\mu^2 > 0$ then V has a minimum at $\phi^\dagger\phi = 0$ and the ground state is gauge invariant. However, if we take $\mu^2 < 0$, V has a minimum at $\phi^\dagger\phi = v^2/2$ where $v^2 = \mu^2/\lambda$. When the fields are expressed as perturbations from this ground state the theory is no longer gauge invariant. Expanding about one of the minima,

$$\phi(x) = {}^{1}/_{\sqrt{2}}\begin{pmatrix} 0 \\ v + H(x) \end{pmatrix} \tag{1.18}$$

where $\phi_{vacuum} = v/\sqrt{2}$, the first term in the Lagrangian becomes

$$\mathcal{L}_{EW}^{(1)} = {}^{1}/_{2}\partial_\mu H \partial^\mu H + {}^{1}/_{2}\left(\frac{g\,v}{2}\right)^2 (W_\mu{}^1 W^{\mu 1} + W_\mu{}^2 W^{\mu 2})$$

$$+ {}^{1}/_{2}\left(\frac{v}{2}\right)^2 ((gW_\mu{}^3 - g'B_\mu)(gW^{\mu 3} - g'B^\mu)) \tag{1.19}$$

$$+ \text{cubic and quartic interaction terms}$$

Making the substitutions

$$W_\mu^{\pm} = (W_\mu{}^1 \mp iW_\mu{}^2)/\sqrt{2} \tag{1.20a}$$

$$Z_\mu = \cos\theta_W W_\mu{}^3 - \sin\theta_W B_\mu \tag{1.20b}$$

$$A_\mu = \sin\theta_W W_\mu{}^3 + \cos\theta_W B_\mu \ , \tag{1.20c}$$

where $\tan\theta_W = g'/g$, we can rewrite (1.19) in the suggestive form

$$\mathcal{L}_{EW}^{(1)} = {}^{1}/_{2}\partial_\mu H \partial^\mu H + M_W{}^2 (W_\mu{}^+ W^{\mu +} + W_\mu{}^- W^{\mu -}) + M_Z{}^2 (Z_\mu Z^\mu) \tag{1.21}$$

with

$$M_W = gv/2 \ ; \quad M_Z = gv/2\cos\theta_W \ . \tag{1.22}$$

In general, the spontaneous breaking of the symmetry results in the occurence of three massless scalars, as a consequence of the Goldstone theorem.[20] In fact, we can make a gauge transformation which will eliminate these Goldstone bosons from the Lagrangian; this corrsponds to our definition of ϕ (Eq. (1.18); such that H is real) and the gauge fields. That is, the gauge fields have "eaten" the Goldstone bosons and become massive; the scalar degrees of freedom have become the necessary longitudinal polarisations of the massive vector bosons.

Since one combination of gauge fields, A_μ, has no mass term,

there remains an unbroken U(1) gauge symmetry; if this is identified as $U(1)_Q$ then A_μ is the photon. Given this, we can write the identity

$$e = g\sin\theta_W = g'\cos\theta_W \qquad (1.23)$$

To account for the phenomenological V-A structure of the weak interaction, the fermions are introduced in left-handed doublets and right-handed singlets of SU(2), e.g.

$$\begin{pmatrix} \nu_e \\ e \end{pmatrix}_L , \; e_R \; ; \quad \begin{pmatrix} u \\ d \end{pmatrix}_L , \; u_R , \; d_R , \qquad (1.24)$$

where $f_{R,L} = {}^1/_2(1\pm\gamma_5)f$. As the weak interactions are left-handed, the SU(2) group usually carries an "L" subscript. All the fermions are singlets under the original U(1) group and posses a weak hypercharge, Y. Hypercharge and the 3-component of weak isospin are related to electromagnetic charge, viz:

$$Q = T^3 + Y \qquad (1.25)$$

(c.f. the Gell-Mann - Nishijima relationship for hadrons).

The $SU(2)_L * U(1)_Y$ Lagrangian for fermion-gauge boson interactions is

$$\mathcal{L}_{int} = - \bar{L}\gamma_\mu(gT^aW^{\mu a} + g'YB^\mu)L - \bar{R}\gamma_\mu(g'YB^\mu)R \qquad (1.26)$$

where L (R) denotes a left-(right-)handed fermion doublet (singlet). This may be rewritten to show the $U(1)_Q$ structure explicitly:

$$\mathcal{L}_{int} = - e\bar{L}\gamma_\mu QA^\mu L - e\bar{R}\gamma_\mu QA^\mu R - (g/\sqrt{2})\bar{L}\gamma_\mu T^+W^{\mu+}L$$
$$- (g/\cos\theta_W)\bar{L}\gamma_\mu(T^3-\sin^2\theta_W Q)Z^\mu L - (g/\cos\theta_W)\bar{R}\gamma_\mu(-\sin^2\theta_W)Z^\mu R \; . \qquad (1.27)$$

Note that the γ and Z couple to both left- and right-handed fermions, while $W^\pm$ couple only to left-handed fermions.

(b) KM Mixing and the Generation of the Fermion Masses

The left-handed quark-doublets which undergo weak interactions are not the same as the physical mass eigenstates. For 3 generations we have

$$\begin{pmatrix} u \\ d_w \end{pmatrix}_L , \begin{pmatrix} c \\ s_w \end{pmatrix}_L , \begin{pmatrix} t \\ b_w \end{pmatrix}_L , \tag{1.28}$$

where d_w, s_w, b_w are weak-interaction eigenstates which are mixtures of the mass eigenstates d, s, b described by

$$\begin{pmatrix} d_w \\ s_w \\ b_w \end{pmatrix}_L = U \begin{pmatrix} d \\ s \\ b \end{pmatrix}_L \tag{1.29}$$

where U is a 3x3 unitary matrix. In general, the matrix U is described by 9 independant parameters. However, we can transform each quark field as $q \rightarrow \exp(i\alpha(q))q$, where $\alpha(q)$ is a flavour-dependant phase parameter, such that five of the parameters of U can be eliminated. One choice of the 4-parameter matrix U, due to Kobayashi and Maskawa (KM),[21] is

$$U = \begin{pmatrix} 1 & 0 & 0 \\ 0 & c_2 & s_2 \\ 0 & -s_2 & c_2 \end{pmatrix} \begin{pmatrix} c_1 & s_1 & 0 \\ -s_1 & c_1 & 0 \\ 0 & 0 & 1 \end{pmatrix} \begin{pmatrix} 1 & 0 & 0 \\ 0 & 1 & 0 \\ 0 & 0 & e^{i\delta} \end{pmatrix} \begin{pmatrix} 1 & 0 & 0 \\ 0 & c_3 & s_3 \\ 0 & -s_3 & c_3 \end{pmatrix} \tag{1.30}$$

where $s_i = \sin\theta_i$, $c_i = \cos\theta_i$; $0 < \theta_i < \pi/2$, $-\pi < \delta < \pi$. Showing U as a product of matrices is suggestive; the angles θ_i emerge as Euler angles describing the rotation amongst the 3 flavours d, s, & b. The fourth parameter, the phase δ, is chosen such that the coefficients of d_w are real. This phase can lead to CP violation, e.g. in the neutral kaon system.

The four KM mixing parameters, θ_i and δ, are arbitrary; they are not predicted by the electroweak theory and must be determined from experimental data.

The quark-gauge boson interaction term in the Lagrangian (1.26) can be written in terms of charged weak currents, viz:

$$\mathcal{L}_{int}^{W} = -(g/\sqrt{2})\bar{L}\gamma_\mu T^+ W^{\mu+} L = -(g/\sqrt{2}) j_\mu^+ W^{\mu+} \quad , \tag{1.31}$$

where

$$j_\mu^- = (u\ c\ t)_L \gamma_\mu U \begin{pmatrix} d \\ s \\ b \end{pmatrix}_L \quad ; \quad j_\mu^+ = (j_\mu^-)^\dagger \quad . \tag{1.32}$$

Since the right- and left-handed fermions transform differently under $SU(2)_L$, a fermion mass term of the form m(LR+RL) is forbidden. An attractive feature of the Higgs mechanism is that it alows fermions to acquire masses via a Yukawa coupling to the scalar Higgs field in terms of the form (for the electron multiplets)

$$\mathcal{L}_{m_e} = -G_o(\bar{\nu}_o\ \bar{e})_L\ e_R + h.c. \tag{1.33}$$

which is gauge invariant. After spontaneous symmetry breaking, in terms of the new Higgs fields we get

$$\begin{aligned} \mathcal{L}_{m_e} = &- (G_o v/\sqrt{2}) (\bar{e}_L e_R + \bar{e}_R e_L) \\ &- (G_o/\sqrt{2}) (\bar{e}_L e_R + \bar{e}_R e_L) H(x) \ ; \end{aligned} \tag{1.34a}$$

chosing $G_e = \sqrt{2} m_e/v$ we can write this

$$\mathcal{L}_{m_e} = - m_o \bar{e} e - (m_o/v)\bar{e} e H \quad , \tag{1.34b}$$

which shows the electron mass explicitly. The generalisation to other leptons is trivial.

Quark masses are generated in a similar fashion, but, in order to give masses to the upper member of the quark doublet, we must introduce the conjugate Higgs doublet:

$$\phi_c = -i\tau_2\phi^* = \begin{pmatrix} -\bar{\phi}^0 \\ \phi^- \end{pmatrix} \qquad (1.35)$$

such that

$$\begin{aligned} \mathcal{L}_m &= -G_d^{ij}(\bar{u}_i\ \bar{d}_i)_L\phi d_{jR} \\ &\quad - G_u^{ij}(\bar{u}_i\ \bar{d}_i)_L\phi_c u_{jR} \qquad + \text{ hermitean conjugate} \\ &\text{-SSB->} -m_d\bar{d}d - m_u\bar{u}u - (m_d/v)\bar{d}dH - (m_u/v)\bar{u}uH\ . \end{aligned} \qquad (1.36)$$

Note that we have allowed for KM mixing between the quark families, i. The Yukawa couplings, G_f, are arbitrary; they are not predicted by the theory and must be input from experimental measurement of the fermion mass. Each massive fermion introduces another free parameter into the electroweak model!

We note also that the Higgs-fermion couplings are proportional to the fermion masses; i.e. Higgs bosons couple preferentially to heavier fermions. This has important consequences for Higgs phenomenology (see Chapter 3).

(c) Limits on the Mass of the Higgs Scalar

Writing the terms in the Lagrangian involving the Higgs scalar only:

$$\mathcal{L}_H = {}^1/_2(\partial_\mu\phi)^2 - ({}^1/_2\mu^2\phi^2 + {}^1/_4\lambda\phi^4)$$

$$\text{-SSB->}\ {}^1/_2(\partial_\mu H)^2 - \lambda v^2H^2 - \lambda vH^3 - {}^1/_4\lambda H^4 + \text{const.}\ , \qquad (1.37a)$$

we see that the physical Higgs scalar, H, has a mass term such that

$$m_H = \sqrt{2\lambda v^2} = \sqrt{-2\mu^2}\ . \qquad (1.37b)$$

Though we can determine v from experimental measurement (e.g. of M_W, given $\sin^2\theta_W$), λ (and, hence, μ) is unknown, and, therefore, the mass of the Higgs scalar is not predicted. However,

theoretical lower and upper bounds do exist.[22]

The lower bound comes from a consideration of the radiative corrections to the Higgs potential from scalar and gauge boson loops. If we make the assumption that $\mu^2 = 0$ (which is attractive, as it removes the only dimensionful parameter in the Lagrangian, which is classically scale invariant), then the Higgs mass is calculable. To one-loop[23]

$$m_0^2 = \frac{3\alpha^2 v^2}{4\sin^4\theta_W}(1 + {}^1/_2\sec^4\theta_W) \simeq (10\ \text{GeV})^2 , \qquad (1.38)$$

the exact value depending on the choice of α and $\sin^2\theta_W$. For $\alpha(M_W^2) = {}^1/_{128.5}$ and $\sin^2\theta_W(M_W^2) = 0.215$ we have[24] $m_0 = 10.4$ GeV. Including fermion loops reduces this by $0.006(m_t/(15\ \text{GeV}))^4$ GeV for each flavour; this correction is appreciable only in the case of the top quark: ~ 0.3 GeV for $m_t \sim 40$ GeV. If $\mu^2 < 0$ then $m_H > m_0$. However, if $\mu^2 > 0$, because of the radiative corrections to the potential, it is still possible to realise spontaneous symmetry breaking. In this case m_H could be less than m_0; however, if m_H is much less than this the spontaneously broken vacuum is unstable. Hence, we have a general lower limit of approximately $m_0 \simeq 10$ GeV.

The upper limit is softer and comes from the breakdown of perturbation theory. As m_H increases, the scalar coupling, λ, also increases and, for large enough m_H, becomes significantly greater than one. If the scale at which this happens is smaller than the grand unification scale, then perturbation theory has broken down. The validity of perturbation theory is not sacred, merely desirable; e.g. a breakdown of perturbation theory would

play havoc with the concept of grand unifiaction. Within this argument, an upper limit of[25] m_H = 175 GeV has been found. Note that this is significantly smaller than the earlier upper limit of $m_H = \sqrt{(8\pi\sqrt{2}/3G_F)} \sim 1$ TeV found from the requirement that two-body reactions of gauge bosons should respect partial-wave unitarity.

1.2.4 *Limitations of the Standard Model*

At present the SM has been successful in describing quantitatively or (in the absence of precise calculations) qualitatively nearly all available data pertaining to strong, weak and electromagnetic interaction phenomena. This is an amazing state of affairs when one considers that less than twenty years ago there was no theory of weak or strong interactions; apart from QED, particle physics phenomena were at best described by piecemeal phenomenological models with no fundamental theory in sight.

Today, the WS theory accurately describes electroweak phenomena, including the recent experimental discovery of the weak gauge bosons, and it is widely accepted that QCD is the theory of the strong interaction.[26] However, it is generally felt that the SM has some rather unsatisfactory features and does not give a complete description of particle physics phenomenology.

For instance, it contains many arbitrary assumptions and parameters, viz:

- Why are left-handed fermions in SU(2) doublets and right-handed ones in SU(2) singlets?

- Why are there three colours?
- Why is electric charge quantized ($q_d = q_e/3$) ?
- How many generations are there?
- Why do the KM angles and the fermion masses (i.e. the Yukawa couplings) have the values that they do?
- ...

Also the SM is not asymptotically free, so that at some energy scale its interactions become strong, suggesting that, in principle, the SM is the low energy effective theory of a more fundamental one.

However, the biggest problems lie in the Higgs sector. Not only has the Higgs boson predicted by WS not been observed experimentally, but there are also fundamental theoretical problems, inasmuch as the mass of the Higgs boson is unconstrained and may by unstable against radiative corrections. If the Higgs boson mass is of the order of a few TeV, the Higgs self-coupling gets to strong and we should not see the apparent success of perturbation theory at low energy; the full theory should contain a mechanism to inhibit such behaviour.

So far, three kinds of models which try to deal with this problem have emerged. One approach is to describe quarks, leptons and gauge bosons as composite objects;[27] while this eliminates the problem at today's level, it simply displaces it without improving our understanding. A second approach is to eliminate fundamental scalars from the theory by making them composites of new fermions, the "Technicolor" approach.[28] This is a good idea, but at present it has two major flaws: i) it seems to be technically

difficult to construct a workable model, and ii) nearly all models predict the existence of charged Technipions (which behave like charged Higgs bosons) with mass < 25 GeV, which have not been seen experimentally and would be excluded by the observation of semi-leptonic decays of the top quark.

The third approach is to use a higher symmetry to eliminate the quadratic divergence in the Higgs mass; this can be technically arranged in supersymmetric theories where both light and heavy scalars can exist in a natural way. Such theories are discussed in the next Section.

1.3 Supersymmetry

I can believe anything, provided it is incredible.
- from The Picture of Dorian Grey *by Oscar Wilde*

1.3.1 *Why Supersymmetry?*

In supersymmetry (SS) theories[29] we introduce a new symmetry, between bosons and fermions. This implies that for every known (SM) particle there must also exist a "superparticle" which differs in spin by half a unit. Hence, SS can deal straightforwardly with the problem of the quadratic Higgs mass divergence (§1.2.4). For every particle loop in the radiative correction to the Higgs mass we must also include a loop of superpartners; the extra minus sign associated with fermion loops and the supesymmetric relations between masses and couplings guarantee that the coefficients of the divergence is zero. Thus in unbroken SS it is possible to understand why corrections to

scalar boson masses are not large.

However, SS, if it exists, must be broken, since the superpartners are not observed to be degenerate in mass with the SM particles. If the above argument is still to hold in broken SS, then the masses of the superparticles cannot be too large. Crudely speaking, the superpartners should not differ in mass from the SM particles by more than about 250 GeV, which is the weak interaction (Higgs) scale. This is confirmed in models; while there is no compelling model of SS, all those studied produce some detectable superpartners that are light, often with masses well below M_W. (This, of course, makes SS attractive to phenomenologists, as it implies a new spectrum of particles which may be accessible in experiments; this is discussed further in §1.3.3.)

There are several other reasons why theorists find SS attractive, viz:

- Nature has shown that she likes gauge theories, so SS is a logical progression beyond the SM; furthermore, the spin degree of freedom can then be integrated within gauge theory.[30]
- SS is mathematically well behaved, and may be finite.[31]
- Local SS theories relate the generators of SS transformations to the generators of space-time transformations, hence coupling gravity to SS theory.[32]

1.3.2 *An Outline of Supersymmetry Theory*

(a) Rudiments of SS Algebra and SS Breaking

In order to implement the idea of a symmetry between bosons and fermions we must introduce a generator, S, which achieves the transformation of a boson into a fermion and vice-versa:

$$S_\alpha: \text{boson} \longleftrightarrow \text{fermion} \tag{1.39}$$

Note that S carries a spinor label α, since fermions are described by spinors; bosons are described by scalars or vectors. S_α has the character of a spin-$^1/_2$ field under the Lorentz group, so

$$[J_{\mu\nu}, S_\alpha]_- = {}^1/_2(\sigma_{\mu\nu}S)_\alpha \tag{1.40}$$

where

$$\sigma_{\mu\nu} = -{}^1/_2[\gamma_\mu, \gamma_\nu]_- \ . \tag{1.41}$$

S_α does not cause a translation, so $[P_\mu, S_\alpha]_- = 0$. A fermionic field $\psi_\alpha(x)$ may be transformed into a scalar field A(x) by an infinitessimal spinor parameter ε_α by

$$\delta A(x) = -\bar{\varepsilon}\psi(x) \tag{1.42}$$

(where $\bar{\varepsilon} = \varepsilon^\dagger\gamma^0$). A may be varied into ψ by

$$\delta\psi = i(\partial\!\!\!/\varepsilon)A \ . \tag{1.43}$$

We assume that the ε's anticommute with all other spinors, and we have

$$[S_\alpha, S_\beta]_+ = -2(\not{P}C)_{\alpha\beta} \ , \tag{1.44}$$

where C is the charge-conjugation matrix: $C^{-1}\gamma_\mu C = -\gamma_\mu{}^T$. The generators S_α are the square roots of the Poincaré translation generators P_μ.

It is straightforward to extend this algebra to include an

internal symmetry group, SU(N), by adding an index i (=1,N) onto S . This is most convenient to do in the chiral representation, with chiral projectors $^1/_2(1+\gamma_5)$ such that $\psi_{\alpha+} = [^1/_2(1+\gamma_5)\psi]_\alpha$ are the chiral projections of any spinor. Then (1.44) becomes

$$[S_{\alpha+}{}^i,\ S_{\beta-j}]_+ = -2(\not{P}C)_{\alpha+\beta-}\delta^i{}_j \ . \qquad (1.45)$$

This modified algebra is the N-extended SS algebra, SN.

Simple SS combines particles with spins differing by $^1/_2$ into supermultiplets. The simplest example is the pair (A,ψ) with spin $(0,^1/_2)$; however, any pair $(j,j+^1/_2)$ can be combined by SS. Extended SS has more than one generator and so may combine particles spanning a range of spins.

The simplest model of global SS, due to Wess and Zumino,[33] is that based on the multiplet with spins $(0,^1/_2)$. To realise SS, there must be an equal number of Bose and Fermi degrees of freedom; that is we must have one spinor, ψ_α, and two scalars, A and B (which is, in fact, a pseudoscalar, for reasons of parity). We must also have two auxiliary fields, a scalar, F, and a pseudoscalar, G, which are required to allow for closure of the SS algebra off-shell, but which vanish on-shell. We then have the transformations

$$\begin{aligned} \delta A &= -\bar{\varepsilon}\psi \qquad \delta B = -\bar{\varepsilon}\gamma_5\psi \\ \delta F &= -i\bar{\varepsilon}\not{\partial}\psi \qquad G = -i\bar{\varepsilon}\not{\partial}\gamma_5\psi \\ \delta\psi &= [i\not{\partial}(A+\gamma_5 B) + (F-\gamma_5 G)]\varepsilon \end{aligned} \qquad (1.46)$$

and the full Lagrangian invariant under these transformations is

$$\begin{aligned} \mathcal{L} = {}& ^1/_2[(\partial_\mu A)^2 + (\partial_\mu B)^2 + F^2 + G^2] + {}^1/_2\bar{\psi}\not{\partial}\psi + m(^1/_2\bar{\psi}\psi + AF - BG) \\ & + g(FA^2 - FB^2 - 2GAB + \bar{\psi}\psi A - \bar{\psi}\gamma_5\psi B) \end{aligned} \qquad (1.47)$$

Auxiliary fields are necessary in all extended SSs; however, their

description in these cases has proved extraordinarily difficult.

The Wess-Zumino quantum field theory described by $\mathcal{L}$ can be quantised in a manner which preserves SS. Only a single logarithmic ultra-violet divergence is present, leading to a common wave function renormalization of the fields A, B, and ψ.

In order to relate SS to gauge theories we must also construct analogues of non-Abelian gauge theories. The multiplet used to describe this case has spin $(^1/_2,1)$; we have a spinor, λ, and a gauge field, V , as well as a single auxiliary field, D, required to close the algebra off-shell. Under global SS they transform

$$\begin{aligned} \delta V &= \bar{\varepsilon}\gamma_\mu\lambda \\ \delta\lambda &= i(\partial\!\!\!/ A)\varepsilon + i(\gamma_5\varepsilon)D \\ \delta D &= -\bar{\varepsilon}\gamma_5\partial\!\!\!/\lambda . \end{aligned} \qquad (1.48)$$

We may couple this to charged matter, described by a pair of multiplets, $(A,B,F,G,\psi)_i$, forming complex component fields: $A = (A_1 + iA_2)/\sqrt{2}$, etc. The full Lagrangian, in addition to the terms for the matter field (1.47), involves an invariant action

$$\mathcal{L} = \ldots - {}^1/_2 W_{\mu\nu}W^{\mu\nu} + {}^1/_2\bar{\lambda}\partial\!\!\!/\lambda + {}^1/_2 D^2 , \qquad (1.49)$$

where $W_{\mu\nu} = \partial_\mu V_\nu - \partial_\nu V_\mu$.

Since there are no known superpartners of the observed particles, SS must be broken in some way. This may involve various mechanisms.

The breaking may be explicit, by the addition of terms to the Lagrangian which are not SS invariant. Such an approach[34] is

somewhat unappealing; however, in the case of extended SS it appears to be the only way to proceed.

SS may be broken spontaneously, either in the classical equations of motion (tree-level), or dynamically, by radiative corrections. In fact, a superspace analysis shows that if spontaneous symmetry breaking does not occur at tree-level, it cannot occur dynamically, if SS is valid.

When a global symmetry is broken spontaneously, the Goldstone theorem predicts the occurence of a massless scalar boson. In the case of SS we should expect a similar particle, but of spin-$^1/_2$, to occur; this is generally known as the goldstino. When SS is spontaneously broken there is an associated mass splitting between the scalars and fermions. The size of the mass splitting, $(m_o^2 - m_f^2)$ is related to the coupling strength and decay constant of the goldstino.

(b) Extended Supersymmetric Gauge Theories

For N-SS$^{<35}$ there are 2N operators, $S_{\alpha+}^{\ i}$, belonging to the fundamental representation N of SU(N) and 2N conjugate operators belonging to the conjugate representation N. The creation operators, $S_{\alpha+}^{\ i}$, raise helicity by $^1/_2$; thus, a multiplet of states, with ground state $|-\lambda\rangle$ such that $S_{\alpha-i}|-\lambda\rangle = 0$, would have the helicities

$$(-\lambda, -\lambda+^1/_2, \ldots, -\lambda+^1/_2N) \qquad (1.50)$$

Since the operators $S_{\alpha+}^{\ i}$ are mutually anticommuting the degeneracy of the state $(S_+)^r|\lambda\rangle$ is ${}^NC_r$. Thus the set of states with maximum

helicity 1, for N = 2 and 4, will have helicity degeneracy

$$\begin{aligned} N = 2&: \quad (\underline{0}^2, \underline{1/2}^2, \underline{1}) \\ N = 4&: \quad (\underline{0}^6, \underline{1/2}^4, \underline{1}) \end{aligned} \tag{1.51}$$

on combining the set of helicity states (1.50) and their CPT-conjugates with opposite sign. The on-shell gauge theory for N = 3 is the same as for N = 4.

For N = 2 the set of fields includes a gauge vector A_μ, a Dirac spinor x (or a doublet of Weyl spinors, ψ^i), a scalar S and a pseudoscalar, P, all in the adjoint representation of the internal symmetry group, G, with transformations

$$\begin{aligned} \delta A_\mu &= i(\bar{\varepsilon}\gamma_\mu x - \bar{x}\gamma_\mu\varepsilon) \\ \delta P &= \bar{x}\gamma_5\varepsilon - \bar{\varepsilon}\gamma_5 x \\ \delta S &= i(\bar{x}\varepsilon - \bar{\varepsilon}x) \\ \delta x &= (\sigma_{\mu\nu}F^{\mu\nu} + \gamma_5[P,S]_- + i\not{\partial}P\gamma_5 - \not{\partial}S) \end{aligned} \tag{1.52}$$

where $D_\mu = \partial_\mu + igA_\mu$, and $F^{\mu\nu}$ is the usual covariant field-strength. ε is a singlet under G. The formulation in terms of ψ^i has an SU(2) invariance and an additional U(1) chiral invariance.[36]

The case of N = 4 is similar, but has the scalars S, P replaced by a sexplet, A_{ij}, of SU(4), $A_{ij}{}^* = A^{ij} = \varepsilon^{ijkl}A_{kl}$, and a quartet of Weyl spinors, x^i, transforming in the 4 of SU(4); all the fields are in the adjoint representation of G. The form of the SS transformations (and the invariant Lagrangian) are similar to those for the N = 2 case, given the differing set of fields. The form of the N = 4 Lagrangian prevents the extra U(1) invariance possible in the N = 2 case; hence, N = 4 SS has explicit SU(4) invariance, but not U(4).

The great interest in these cases is that N = 4 SS (super-Yang-Mills) is the first quantum field theory discovered to be completely finite to all orders.[37] Such a remarkable result was one of the grails for which quantum field theorists had been searching since the introduction of quantum field theories and the ensuing mainfestation of the problems of ultra-violet divergences.

Since there exists such a beautiful quantum field theory, it is natural to try to apply it to the real world. Various attempts have been made to apply SS to the SM or to GUTs. The global supersymmetry of the N = 4 Lagrangian may be conjectured to be observed in the generation structure, so leading to the expectation of a fourth generation. In order to relate the theory to the known spectrum of particles there are several difficulties which must be overcome.

A serious problem is that spontaneous symmetry breaking of any gauge theory will produce massless neutral currents in an SU(5) or SO(10) gauge group, a result incompatible with low energy phenomenology.[38] However, given at least one extra, non-electromagnetic, U(1), decent to SU(3) * SU(2) * U(1) may avoid the problem. A further difficulty is the existance of mirror fermions, which come about because the supermultiplets containing fermions also have their opposite chirality particles.[39] The symmetry breaking mechanism itself may also cause problems, since, as the generators anticommute, all SSs must be broken if one is; this difficulty does not occur if the SS is broken explicitly.

(c) Supergravity (Local Supersymmetry)

Following the gauge approach, we can construct a theory of fields which is invariant under local SS transformations; i.e. the transformation parameter, ε, is now space-time dependant. The commutator of any two SS transfromations is now a translation vector, $(\bar{\varepsilon}_2\gamma^\mu\varepsilon_1)$, a non-constant coordinate transformation; the gauge approach then requires the presence of gravity in terms of a curved space-time, thus leading to supergravity (SG).

The gauge field of the local SS transformation, $\varepsilon_\alpha(x)$, will be a massless spin-$^3/_2$ field, $\psi_{\mu\alpha}(x)$, the gravitino. If local SS is spontaneously broken, then the resulting spin-$^1/_2$ goldstino can be absorbed into the gravitino to give it mass (the super-Higgs effect). The gauge fields for coordinate transformations are the vierbein, $e^a{}_\mu$, and the spin-connection, $w^{ab}{}_\mu$ $(a,b=0,3)$, which is the gauge field of local Lorentz transformations. $w^{ab}{}_\mu$, can be expressed in terms of $e^a{}_\mu$ and the spinor $\psi_{\mu\alpha}$, and $(\psi_{\mu\alpha}, e^a{}_\mu)$ transforms as a multiplet of N = 1 SS with spin $(^3/_2, 2)$; thus $e^a{}_\mu$ stands for the graviton. The global transformations for such a multiplet are

$$\delta e^a{}_\mu = i\bar{\varepsilon}\gamma^a\psi_\mu\,, \qquad \delta\psi_\mu = (\gamma^\beta\gamma_a\varepsilon)\partial_\beta e^a{}_\mu\,, \tag{1.53}$$

but for local SS

$$\delta\psi_\mu = D_\mu\varepsilon\,; \quad D_\mu = \partial_\mu + {}^1/_2 w^{ab}{}_\mu\sigma_{ab}\,. \tag{1.54}$$

The simplest extension to this N = 1 SG is by the addition of further fields. In order to obtain N-extended SG, the total multiplet including the graviton must be in multiplets of N-extended SS. Suitable multiplets with maximum helicity 2 are

$$\begin{aligned} N = 2&: \quad (\underline{1},\ \underline{3/2}^{2},\ \underline{2}) \\ N = 4&: \quad (\underline{0}^{2},\ \underline{1/2}^{4},\ \underline{1}^{6},\ \underline{3/2}^{4},\ \underline{2}) \\ N = 8&: \quad (\underline{0}^{70},\ \underline{1/2}^{56},\ \underline{1}^{28},\ \underline{3/2}^{8},\ \underline{2}) \end{aligned} \tag{1.55}$$

where PCT-conjugate states have been included. Thus N = 2 SG[40] will have a gauge field, A_μ, and two gravitinos, $\psi^i{}_\mu$, as well as the graviton.

The most important theory is maximal N = 8 SG, since all the others can be obtained by contraction. The N = 8 theory originally proved impossible to construct directly in four dimensions, and it is, in fact, most natural to develop by dimensional reduction from N = 1 SG in 11 dimensions.[41] The eight 4-dimensional spinors (gravitinos) of N = 8 SG can be accomodated in a single 11-dimensional spinor (the Rarita-Schwinger field) in addition to 56 spin-$^1/_2$ spinors. Similarly the 11-dimensional tensor (graviton) can decompose to give a 4-dimensional graviton, seven vector and 28 scalar fields. Further bosonic fields arise from the decomposition of the anti-symmetric potential of N = 1 SG, to make the complete N = 8 multiplet (Eq. (1.55)).

The remarkable feature of N = 1 SG in 11 dimensions is that all the fields are gauge fields, with no matter fields whose number and internal symmetry properties may be arbitrary. This has led to the suggestion that the "extra" 7 dimensions have been spontaneously compactified to dimensions of the order of the Planck length ($\sim 10^{-35}$ m). Indeed, this is just like the Kaluza-Klein approach[42] to the unification of gravity with the other forces, which were to be considered as curvature in other

dimensions, just as gravity is the curvature of 4-dimensional space-time.

Again, as with N = 4 SS, it is tempting to try to describe the elements of the SM in terms of N = 8 SG. The theory is based on the preonic multiplets ($\underline{0}^{70}$, $\underline{1/2}^{56}$, $\underline{1}^{28}$, $\underline{3/2}^{8}$, $\underline{2}$). One possibility is that the 3 known fermion generations are in the preon multiplet; this is appealing, since, after the removal of eight fermionic states to become the massive modes of the gravitinos, there are 48 fermionic states which can allow 3 generations of 16 fermions each (including L and R) of an SU(5) type of symmetry. However, it is difficult to accomodate the SU(3) * SU(2) * U(1) model within the local symmetry of N = 8 SG, unless spontaneous compactification from 11 dimensions occurs in a non-straightforward manner.[43] A more basic problem is that, after suitable breaking of the internal symmetry, the fermions in the theory will be vector-like, since the internal symmetry is not related to the 4-dimensional space-time manifold in terms of which chirality is defined. Because of this, the preons of N = 8 SG must be considered, not as presently observed particles (except for the graviton), but as the truly elementary particles from which presently observed particles would be constructed as composites.

1.3.3 *The Phenomenology of Supersymmetry*

As mentioned earlier in this Section, SS predicts new particles which are the superpartners of all the known particles and which differ in spin by half a unit. In addition, ther total

number of bosonic and fermionic degrees of freedom must be equal. For example, in any model, there are two scalar quarks corresponding to the two helicity components of each quark species. Similarly, we may enumerate the minimal set of superparticles that are needed; this is shown in Table 1.2.

The superparticles carry with them quantum numbers (with the exception of spin) identical to their SM partners; for example, the gluino, like the gluon, is a colour octet, flavour singlet, $C = -1$ object.

It should also be noted that there are two Higgs doublets; this is a consequence of fermion mass generation. With only one Higgs doublet, some interaction terms present in the WS theory would violate SS and so are forbidden, with the result that only quarks of a given charge can acquire mass; therefore, at least two Higgs doublets are needed to give mass to both up- and down-type quarks.

The SS breaking has two effects on the particle spectrum. Firstly, the mass degeneracy of particle and superpartner is removed, such that the mass of the superparticle is lifted above that of its SM partner (enough to avoid experimental detection to date). Secondly, the mass matrices for the superparticles can mix particles which carry the same values of conserved quantum numbers; the particular combinations of interaction eigenstates which form the mass eigenstates would have to be determined by experiment. For example, in addition to super-KM mixing of scalar quarks (Ref. 44; and see Chapter 4), we can also have $\tilde{q}_L$ and $\tilde{q}_R$

Table 1.2

The SS Particle Spectrum

The mass eigenstates of the scalar quarks and scalar leptons are, in general, mixtures of the weak eigenstates of each kind. In addition, there can be super-Kobayashi-Maskawa mixing between the scalar quark flavours.

Again, for the partners of bosons mixing generally occurs among the weak eigenstates. The couplings of weak eigenstates are determined by theory, but the couplings of the mass eigenstates depend on the amount of mixing. The generic names are given in the table; the specific names may reflect the couplings, e.g. wiggsinos for charginos with couplings intermediate between those of winos and higgsinos.

If supersymmetry is a spontaneously broken global symmetry there is also a Goldstone fermion, the goldstino, $\tilde{G}$. In supergravity theories, the goldstino is absorbed into a massive gravitino, the spin-$^3/_2$ superpartner of the graviton.

SM Particles	Weak Interaction Eigenstates		Mass Eigenstates	
	Symbol	Name	Symbol	Name
q (d,u,s,c,b,t)	$\tilde{q}_L$, $\tilde{q}_R$	scalar quark	$\tilde{q}_1$, $\tilde{q}_2$	scalar quark
l (e, μ, τ)	$\tilde{l}_L$, $\tilde{l}_R$	scalar lepton	$\tilde{l}_1$, $\tilde{l}_2$	scalar lepton
(ν_e, ν_μ, ν_τ)	$\tilde{\nu}$	scalar neutrino	$\tilde{\nu}$	scalar neutrino
g	$\tilde{g}$	gluino	$\tilde{g}$	gluino
$W^\pm$	$\tilde{W}^\pm$	wino	$\tilde{\chi}_{1,2}^\pm$	charginos
H_1^+	$\tilde{H}_1^+$	higgsino		
H_2^-	$\tilde{H}_2^-$	higgsino		
γ	$\tilde{\gamma}$	photino	$\tilde{\chi}_1^0$	neutralinos
Z^0	$\tilde{Z}^0$	zino		
H_1^0	$\tilde{H}_1^0$	higgsino		
H_2^0	$\tilde{H}_2^0$	higgsino		

mixing.

If the photino and gluino are massless then there can exist a continuous global symmetry, called R-symmetry. However, there are theoretical reasons why the gluino cannot be masless, in which case this continuous symmetry must be broken, but a discrete R-symmetry[45] (almost) always remains, leading to a multiplicatively conserved quantum number called R-parity.[46] All SM particles are assigned an R-parity of +1 and the superparticles an R-parity of -1. (Formally, the R-parity of any particle of spin j, baryon number B and lepton number L can be defined to be $R = (-1)^{2j+3B+L}$.) This has a number of important consequences.

Firstly, since in experiments the initial state will contain no superparticles, the final state can only contain even numbers of such particles. Secondly, the lightest superparticle must be stable since, due to conservation of R-parity, it cannot decay into only SM particles. In spontaneously broken global SS the massless goldstino is necessarily the lightest superparticle;[47] in currently-favoured supergravity models the goldstino is absorbed into a gravitino[48] (which is seldom the lightest superparticle), and the photino is then the most likely candidate, though the situation can be complicated by mixing with other neutralinos. The third consequence is that the production and interaction cross-sections of any light superparticles are likely to be of weak-interaction size, since the processes will generally involve a massive superparticle propagator. Consequently, the photino will behave in experiments very much like a neutrino.

Thus, we may make the following observation about experimental signatures of SS. Any process involving the production (and subsequent decay, where appropriate) of superparticles will yield final states including two (or 2n) photinos which will elude experimental detection and so appear as missing energy or missing transverse momentum. The photino signature may be distinguished from that of a neutrino as no charged lepton accompanies the photino. We discuss two particular cases, scalar quark and scalar electron production, in Chapters 4 and 5.

Chapter 2

COLLIDER PHYSICS

"And he that breaks a thing to find out what it is has left the path of wisdom."
- from The Lord of the Rings *by J.R.R. Tolkien*

2.0 Preamble

In this work we consider the phenomenology of new particles produced in high-energy colliders. Two kinds of machines are of interest: $\bar{p}p$ colliders (in particular, that at CERN), and the forthcoming e^+e^- colliders (SLC at Stanford and LEP at CERN).

In Section 2.1 we briefly describe the CERN $\bar{p}p$ Collider; we also discuss in some detail aspects of the parton model which are relevant to the calculations of production cross-sections at such a machine. In Section 2.2 we describe the essential features of e^+e^- colliders. The former discussion is pertinent to Chapters 3 and 4, the latter to Chapter 5.

2.1 $\bar{p}p$ colliders and the parton model

2.1.1 *The CERN $\bar{p}p$ Collider*

The recent history of experimental high-energy particle physics has been dominated by the success of one machine, the 540 GeV $\bar{p}p$ Collider at CERN (Conseil Européen pour la Recherche Nucléaire), near Geneva. This was designed and constructed with the principal goal of directly observing the gauge bosons of the

WS model, which it achieved in 1982.[1] The 1984 Nobel Prize for Physics was awarded to Carlo Rubbia and Simon van der Meer for their leading roles in planning and executing the experiments.

The discovery of neutral currents in the mid-seventies[2] strongly supported the gauge theories of (electro)weak interactions,[3] and it became clear that the experimental observation of the gauge bosons, as a direct test of the theory, was essential. However, the experimentally determined value of $\sin^2\theta_W$[4] had led to the expectation that the bosons are very massive ($M > 70$ GeV) and so could not be produced in machines available at that time.

The existing large proton accelerators at CERN and FNAL worked as fixed target machines, such that only a small fraction of the beam energy is available for the creation of new particles; the equivalent total centre-of-mass (c.m.) energy available is given by $s \approx 2ME$, where M is the mass of the target particle ($M \sim 1$ GeV for nucleons) and E is the beam energy. A better way to reach a high $\sqrt{s}$ is by the use of colliding beam machines, where the accelerated particles meet head-on, giving $\sqrt{s} = 2E$, where E is the energy of each beam of equally massive particles. It was quite clear that only colliders would provide the opportunity of producing particles with masses above 50 GeV.

In 1976 Rubbia et al.[5] proposed an alternative to building an entirely new high-energy colliding beam machine (such as ISABELLE or LEP, which were then in the very early planning stage). They proposed to convert an existing fixed-target proton

accelerator (the Super Proton Synchrotron at CERN) into a collider; since the SPS has only one annular beam tube, the counter-rotating beam must be of antiprotons. However, colliders have the disadvantage that the luminosity (and, hence, the reaction rate) is small compared to that obtained in fixed-target machines; in particular, large numbers of antiptrotons are required, and random motion of the antiprotons in the beam must be reduced (one speaks of "beam cooling"). The technical challenge of producing a high-density beam of antiprotons of uniform momentum was met by van der Meer using the technique of "stochastic cooling"[6] (the details of which are beyond the scope of this discussion), which was successfully demonstrated at CERN in 1978.[7]

Construction of an intermediate antiproton accumulator using stocastic cooling and the change in operation of the SPS into a $\bar{p}p$ collider with $\sqrt{s}$ = 540 GeV was started. (Since protons and antiprotons are composed of many partons which share the energy and momentum of the hadrons (see §2.1.2), the subprocess energy, i.e. the c.m. energy, $\sqrt{\hat{s}}$, of two colliding partons, will be substantially less than the $\bar{p}p$ c.m. energy; thus to achieve $\sqrt{\hat{s}} = O(M_{W,Z})$ such a high value of $\sqrt{s}$ is necessary.) Details of the layout and operation of the Collider are given in Fig. 2.1. Six experiments (UA1 to 6),[8] in two underground areas, were accepted to take data at the Collider; of these, only UA1 and UA2 are capable of detecting the electroweak gauge bosons.

The parton nature of the proton and antiproton dictates what kinematic variables can be usefully measured. In particular,

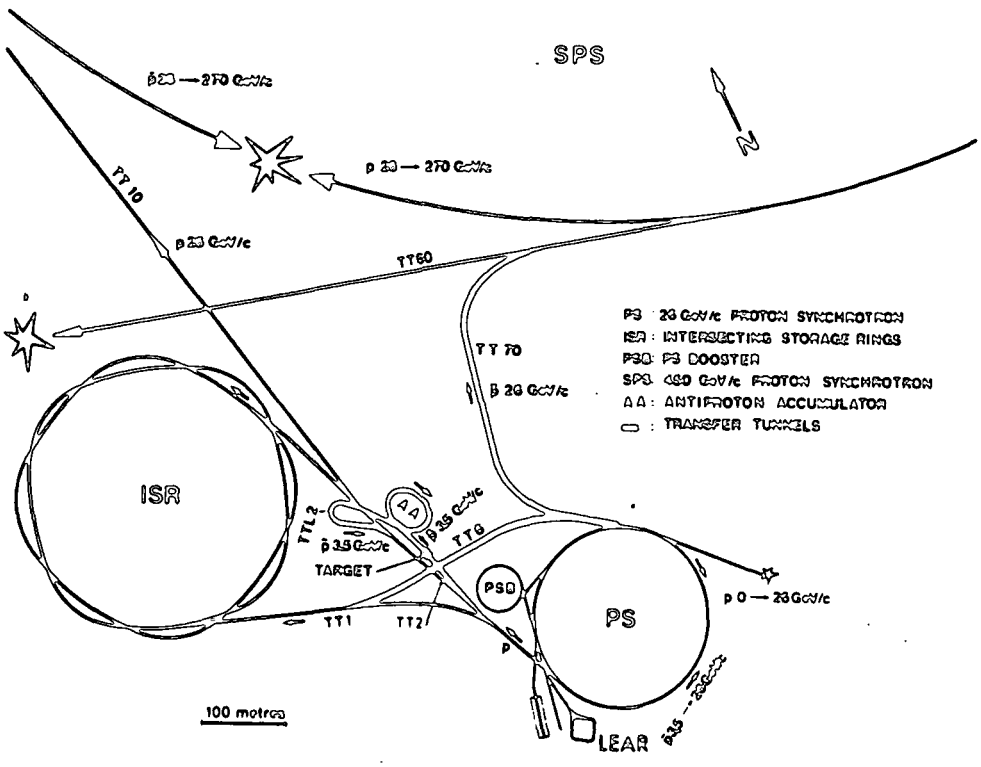

Figure 2.1
A schematic layout of the CERN $\bar{p}p$ Collider.
A beam of protons is accelerated every 2.6 s to an energy of 26 GeV in the PS. This beam is focused on a tungsten target yielding antiprotons which a magnetic horn funnels into the AA. The $\bar{p}$ have a momentum of ~ 3.5 GeV. 60 000 pulses are cooled and stacked in the AA. Once the stack is sufficiently dense, three proton bunches are injected at 26 GeV into the SPS and left there as a coasting beam; three bunches of antiprotons are then injected in the counter-rotating sense. Both beams are then accelerated to 270 GeV, giving a total c.m. energy of $\sqrt{s}$ = 540 GeV.

since the partons have an undefined longitudinal momentum (p_L) in the laboratory frame and negligible transverse momentum (see §2.1.2), only the transverse components of the final-state momenta in the c.m. frame can be determined directly. Because energetic particles can escape down the beam pipe, the event longitudinal momentum cannot be measured, and so the longitudinal components of c.m. momenta cannot be reconstructed. However, if two (or more) particles are detected, their total invariant mass can, of course, be constructed; a sharply peaked invariant mass distribution may indicate the presence of a heavy propagator in the c.m. system.

When a particle, such as a neutrino, with a negligible interaction cross-section is produced, it will not be detected directly. However, its presence may be inferred from an imbalance of momentum in the transverse plane, which should sum to zero; one speaks of events with missing transverse momentum (p_T). In the UA1 experiment (Fig. 2.2(a)) the array of calorimeters and other detectors covers a solid angle of very nearly 4π around the $\bar{p}p$ interaction point, and the transverse momentum sum can be done with precision; this is not so in UA2 (Fig. 2.2(b)) which has a significant opening (~ 20%) about the beam pipe at either end. For example, events in which an energetic electron is accompanied by large missing p_T have been identified[c1] as the decay $W \rightarrow e \bar{\nu}_e$; M_W can be determined from the electron p_T distribution.

2.1.2 *The Parton Model and Structure Functions*

Deep inelastic scattering experiments, in which the

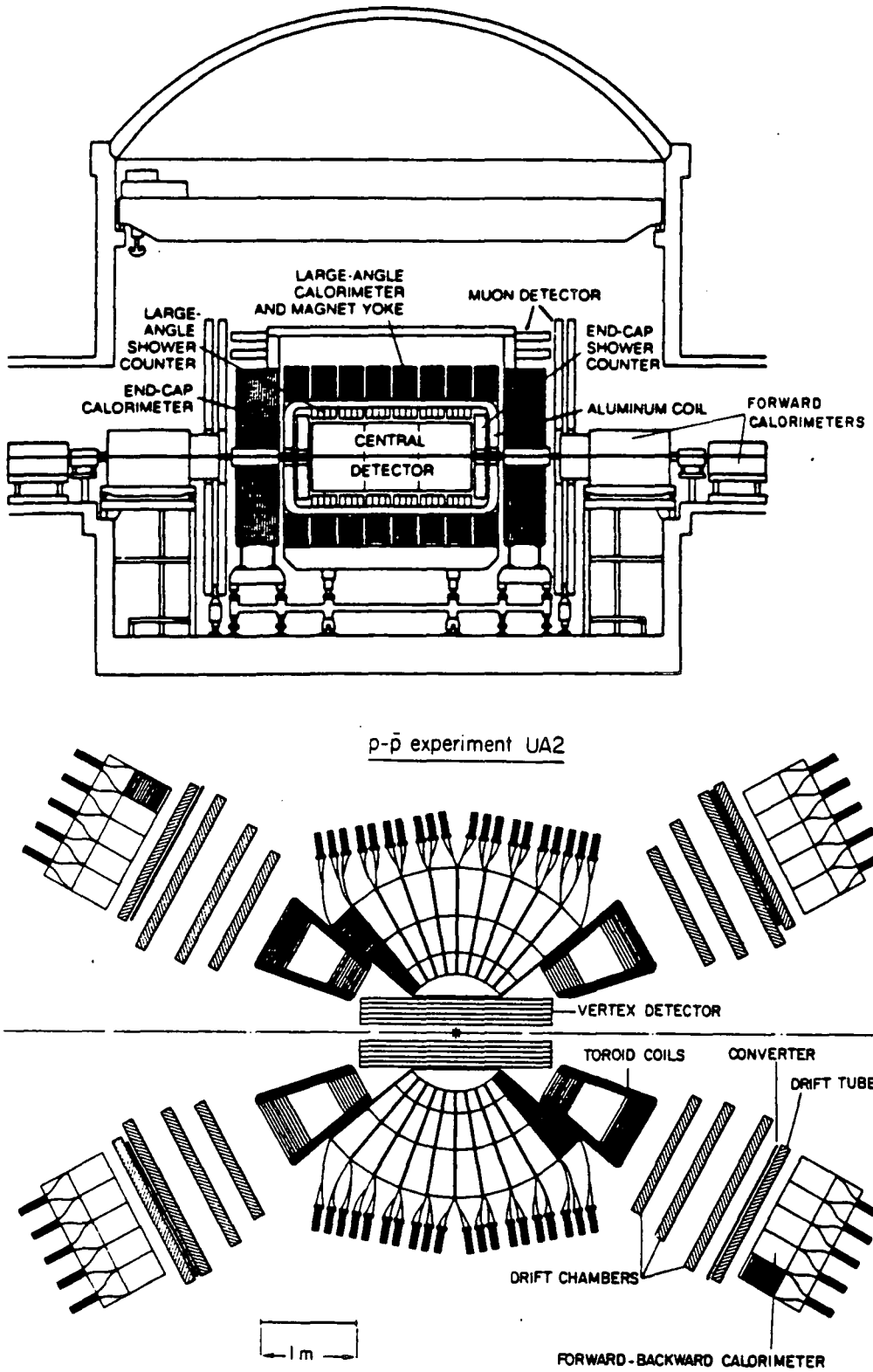

Figure 2.2
(a) The UA1 detector: side view
(b) The UA2 detector: schematic cross-section

structure of nucleons is probed with high energy leptons, have indicated that nucleons are composite objects of point-like constituents.[9] The extremely successful parton model[10] describes these constituent partons (now firmly identified with the quarks and gluons of QCD) as quasi-free particles within hadrons.

The main assumptions of the parton model are:

- At short distances (~ high momenta) hadrons look as if they are made of nearly-free (α_s(large Q^2) is small) partons (quarks, gluons) which share its momentum.
- At larger distances the partons are confined by colour forces; hence, struck partons must fragment into colour-singlet hadrons ("hadronisation"), at a scale μ such that $\alpha_s(\mu^2) \sim 1$.
- If the scattering process is characterised by a sufficiently high energy, the scattering of the nearly free partons occurs at times much shorter than the time required for hadronization to occur; thus the scattering and hadronisation processes may be considered to be independant.

To compute hadronic cross-sections in the parton model, two ingredients are necessary:

1) subprocess cross-sections, calculated using perturbation theory, and
2) parton distributions, measured in deep inelastic lepton-hadron scattering and evolved to higher momentum scales using a perturbative QCD approach.

The cross-section for a typical hadronic reaction (see

Fig. 2.3)

$$A + B \longrightarrow c + d + X \qquad (2.1)$$

(where X represents hadronic debris) is naïvely given by

$$\sigma(A+B\rightarrow c+d+X) = \sum f_i^A \, f_j^B \, \hat{\sigma}(i+j->c+d) \qquad (2.2)$$

where the summation is over all the parton constituents i, j of A and B. f_i^A is the probability of finding parton i in hadron A, and $\hat{\sigma}$ is the cross-section of the elementary subprocess leading to the required final state. This calculation can be improved by considering the parton kinematics. Each parton i carries a longitudinal momentum fraction x_i of the parent hadron's momentum; i.e. for a parental momentum $\vec{P}$, the parton has momentum $\vec{p} = x_i \vec{P}$. Clearly, to conserve (longitudinal) momentum these x_i must satisfy

$$0 < x_i < 1 \qquad (2.3)$$

and

$$\sum_i x_i = 1 \, . \qquad (2.4)$$

Since the partons are confined to a small spatial region, they will possess a small Fermi motion, thus allowing a transverse momentum of O(0.4) GeV. In nearly all of the calculations in $\bar{p}p$ collisions here, we consider only large-p_T processes, so this Fermi momentum can be neglected.

We can rewrite (2.2) to include these kinematics, viz:

$$\sigma(s; A+B\rightarrow c+d) = \int \sum_{ij} f_i^A(x_i) \, f_j^B(x_j) \, \hat{\sigma}(\hat{s}; i+j->c+d) \, dx_i \, dx_j \, . \qquad (2.5)$$

The summation runs over all the contributing parton configurations, and the integration in x_i, x_j extends only over the kinematically allowed region, $(m_c+m_d)^2 \leqslant (\hat{s} = x_i x_j s) \leqslant s$; $\sqrt{s}$ is the hadron c.m. energy and m_c, m_d the masses of the produced

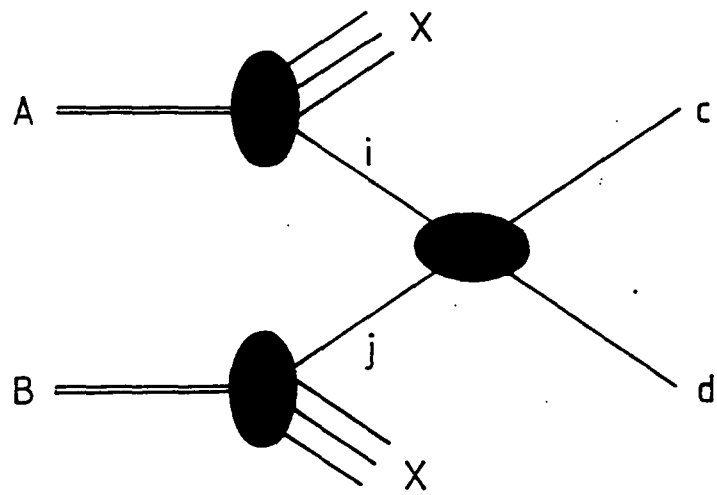

Figure 2.3
A schematic diagram of a typical hadronic reaction (Eq.(2.1)). ij $\longrightarrow$ cd is the elementary subprocess leading to the required final state; c and d may be partons (i.e. quarks and, or, gluons, which will subsequently hadronise), leptons, photons, &c. The other partons within the hadrons A, B form "debris," X.

particles. The structure function, $f_i^A(x_i)$, is the probability of finding parton i in hadron A with momentum fraction x_i.

A useful change of variables is

$$\begin{aligned} \tau &= x_i x_j = \hat{s}/s \ , \\ x_F &= x_i - x_j \ , \end{aligned} \tag{2.6}$$

such that

$$x_{i,j} = (\sqrt{(x_F^2 + 4\tau)} \pm x_F)/2 \tag{2.7}$$

and

$$dx_i \, dx_j = dx_F \, d\tau \ / \sqrt{(xF^2 + 4\tau)} \ . \tag{2.8}$$

If the threshold s for some process is M^2 at some hadron c.m. energy $\sqrt{s}$ then the limits on τ and x_F are

$$\begin{aligned} M^2/s < \tau < 1 \ , \\ |x_F| < (1 - \tau) \ . \end{aligned} \tag{2.9}$$

The corresponding limits on x_i, x_j are

$$\begin{aligned} M^2/s < x_i < 1 \\ M^2/x_i s < x_j < 1 \end{aligned} \tag{2.10}$$

Hence, for a typical process such as (2.1) the total cross-section is given by

$$\begin{aligned} \sigma(s;\ A+B\rightarrow c+d+X) &= \int \sum_{ij} dx_i \, dx_j \ (\ldots)\ \hat{\sigma}(\hat{s};\ i+j\rightarrow c+d) \\ &= \int \sum_{ij} \frac{dx_F \, d\tau}{\sqrt{(x_F+4\tau)}} \ (\ldots)\ \hat{\sigma}(\hat{s};\ i+j\rightarrow c+d) \end{aligned} \tag{2.11}$$

where

$$(\ldots) = \quad (f_i^A(x_i).f_j^B(x_j) + A \longleftrightarrow B \ )$$

Since the partons are coloured, they may radiate partons; this introduces a correction to the naive parton model described above. In the leading logarithm approximation[11] these modifications are independent of the subprocess $i + j \longrightarrow c + d$

and can be incorporated into the structure functions, viz:

$$f_i^A(x_i) \longrightarrow f_i^A(x_i, Q^2) \qquad (2.12)$$

where Q^2 is some scale of the interaction (such as $\hat{s}$ or p_T^2).

Similarly, the strong coupling constant acquires a correction from higher order Feynman diagrams; these can be summed to give a running coupling constant

$$\alpha_s(Q^2) = 4\pi / \beta_0 \ln(Q^2/\Lambda^2) \qquad (2.13)$$

where β_0 is the coefficient of the logarithms generated by the one-loop diagrams, and is given by

$$\beta_0 = 11 - 2N_f/3 \qquad (2.14)$$

with N_f the number of active quark flavours; i.e. the number that give rise to fermion loops. Λ is the QCD scale, and may be extracted from data from deep inelastic scattering experiments;[12] it lies in the range

$$0.1 \text{ GeV} < \Lambda < 0.5 \text{ GeV} \qquad (2.15)$$

There is some uncertainty in the choice of Q^2, Λ and N_f, and these choices affect the overall normalisations of cross-sections. For example, increasing N_f or Λ, or decreasing Q^2, causes α_s to rise. The choices used in calculations here are given when appropriate.

By absorbing first-order corrections into α_s and the structure functions, the use of lowest order hard scattering subprocesses (the Born approximation) is quite valid. Higher order corrections lead to a multiplicative factor, K, in the cross-section normalisations. This K-factor is energy and subprocess dependent; it may be as large as 2 at low $\sqrt{s}$, but is

taken to be 1 here, unless otherwise stated.

2.1.3 *More about Parton Densities and Differential Luminosities*

Many sets of parton densities have been presented in the literature.[14-17] The data from deep inelastic scattering experiments is used to generate structure functions at some Q_0^2 and these are evolved in Q^2 using the Altarelli-Parisi equation of perturbative QCD.[18] Typically, structure functions are measured at $Q_0^2 \sim 4$ GeV^2 and a parameterisation which follows the predicted evolution extracted. Small errors in the input distributions can lead to large errors at large Q^2, and, furthermore, the low x values are not well determined at low Q^2; the region in which any particular parameterisation is valid must not be exceeded.

For a $\bar{p}p$ collider operating at $\sqrt{s}$ = 540 GeV and producing c.m. energies from, say, $2m_b$ (~ the $\bar{b}b$ production threshold) to M_ω (O(100) GeV), the appropriate region in x is, approximately,

$$2m_b/\sqrt{s}\ (\sim 0.02) < x < M_\omega/\sqrt{s}\ (\sim 0.2) \qquad (2.16)$$

for 10 GeV $\lesssim Q \lesssim$ 100 GeV. Several parameterisations valid in this region exist, e.g. those of Glück et al.[15] (GHR) and Duke and Owens[16] (DO1 and DO2). Sample distributions are shown in Fig. 2.4 for different Q^2.

All distributions show a decrease in the mean value of x as Q^2 increases; this reflects the fact that as each hadron is probed to higher momenta the clouds of coloured objects screening the colour charge of the quarks are resolved and the number of partons

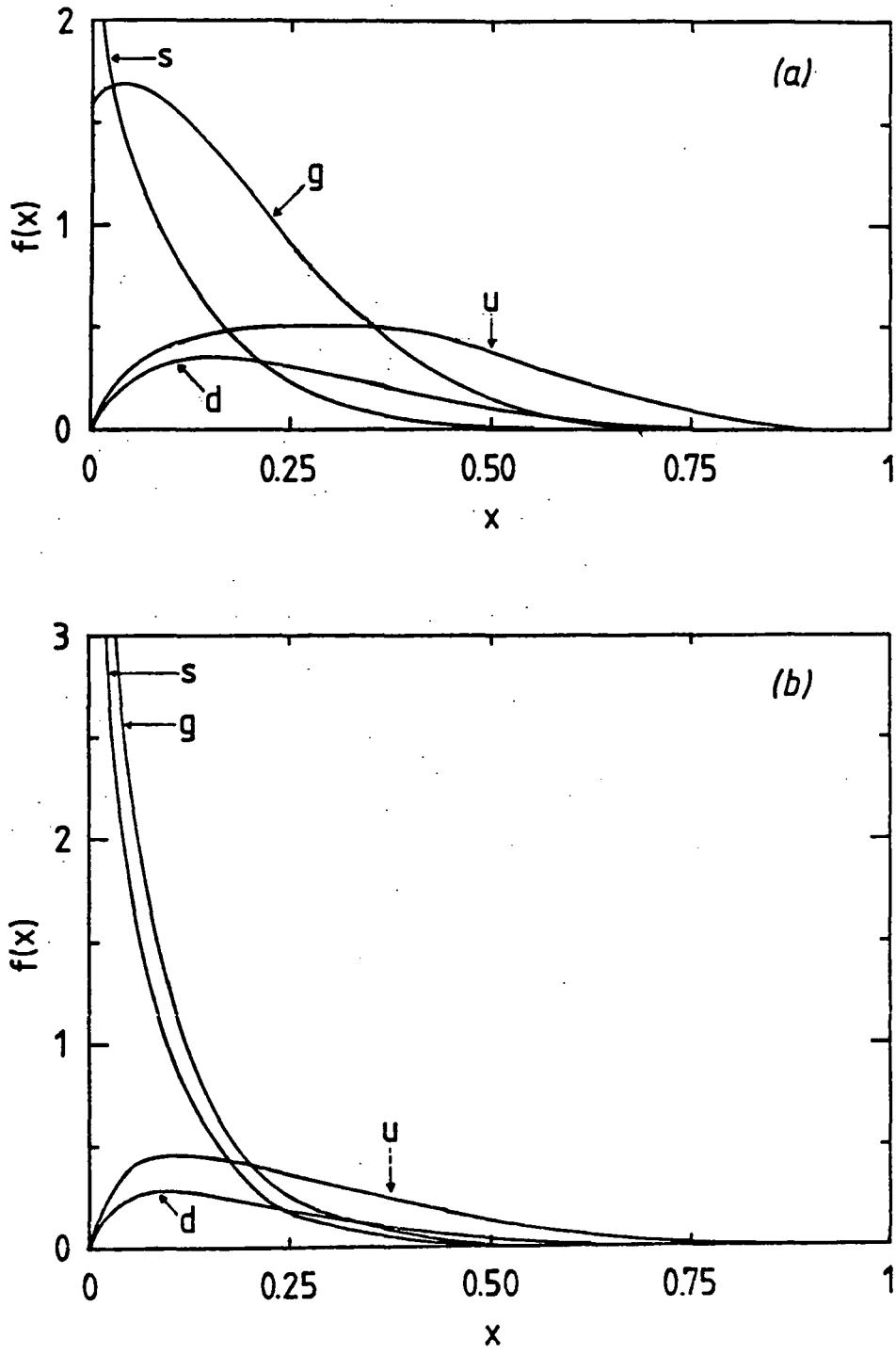

Figure 2.4
The parton densities of Ref. (16) (DO1) for gluons (g), valence up (u) & down (d) and sea (s) quarks, evaluated at
(a) $Q^2 = 4\ GeV^2$,
(b) $Q^2 = M_W^2$.

sharing the hadron's momentum is thereby increased. There is a larger probabilty of finding a particular parton at small x than at high x since high energy partons will lose energy by radiating other partons.

The differential cross-section for a process such as (2.1) can be written

$$\frac{d\sigma(A+B\rightarrow c+d+X)}{d\tau} = \sum_{ij} \frac{dL_{ij}}{d\tau}\,\hat{\sigma}(i+j\rightarrow c+d) \qquad (2.17)$$

where dL_{ij} is the "differential luminosity" of the partons i, j. The x_i, x_j integrations of (2.11) have been replaced by an integration over τ and an integration over x at fixed τ. The differential luminosity is defined as

$$\frac{dL_{ij}}{d\tau} = \frac{1}{1+\delta_{ij}} \int_\tau^1 \frac{dx}{x} \left(f_i^A(x,Q^2)\cdot f_j^B(\tau/x,Q^2) + i \longleftrightarrow j\right), \qquad (2.18)$$

and gives the probability of finding the partons i, j with a particular value of τ in the colliding beams. The differential luminosities are definite functions of τ at particular values of $\sqrt{s}$, and are common to many $\bar{p}p$ calculations.

Differential luminosities for various parton combinations are shown in Fig. 2.5 as a function of $M = \sqrt{s\tau}$. From the figure, it can be seen that for small M processes involving gluons dominate; as M increases the rapid fall of the gluon structure function with x allows the quark subprocesses to dominate, and at large M the gluon subrocesses are the weakest channels.

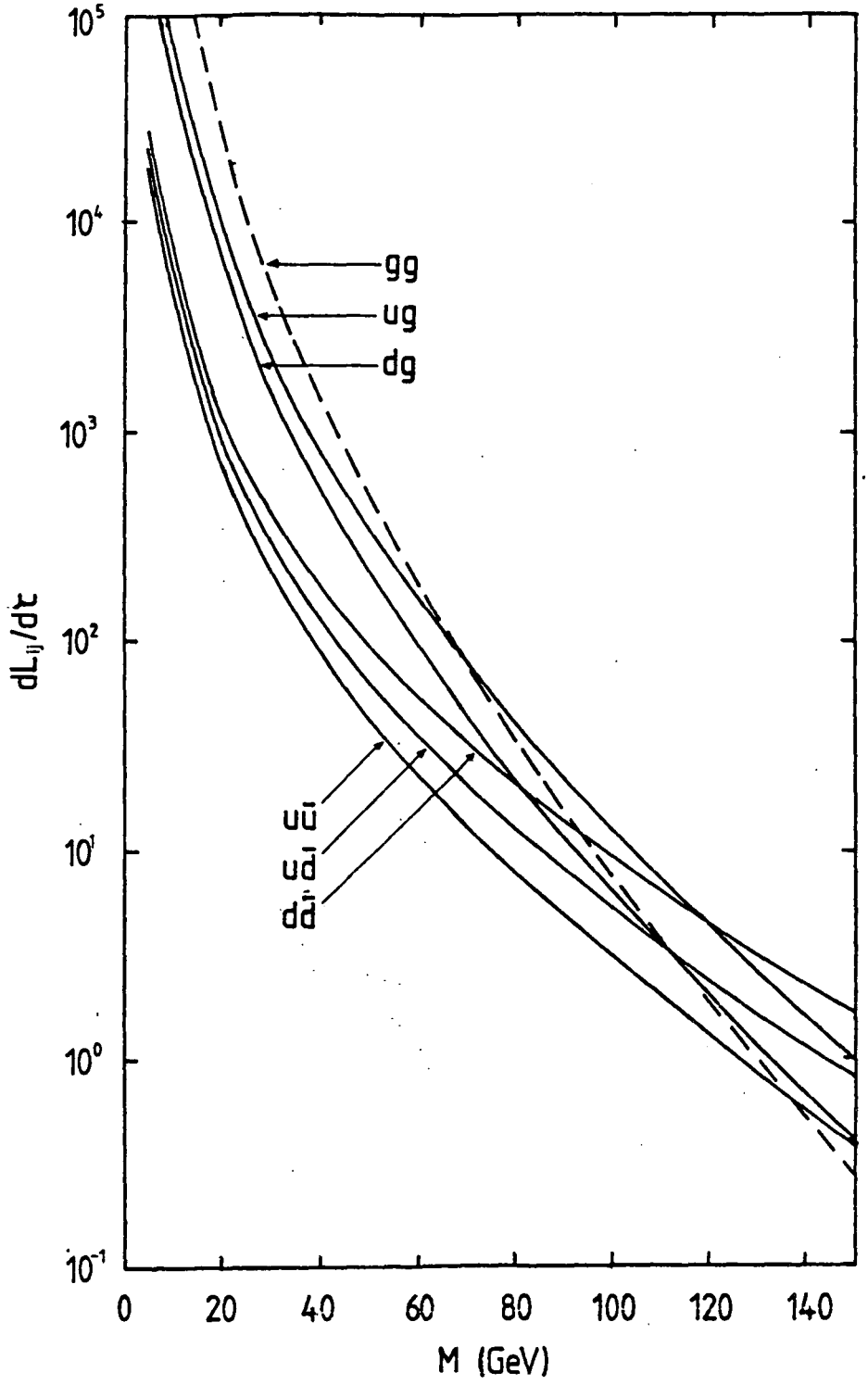

Figure 2.5
The differential luminosities, $dL_{ij}/d\tau$, as a function of $M = \sqrt{\hat{s}}$, at $\sqrt{s}$ = 540 GeV, for the DO1 parton densities evaluated at $Q^2 = M^2$, where $\tau = M^2/s$. The six principal parton-parton channels are shown.

2.2 e^+e^- Colliders

The success of the CERN $\bar{p}p$ project in the experimental observation of the electroweak gauge bosons cannot be underrated; however, because it is essentially a parton collider, the $\bar{p}p$ Collider is not the ideal machine for the study of electroweak phenomena, which have to be seen against a background of strong interaction events (QCD jets &c.). Furthermore, as mentioned above (§2.1.1), since the beam energy is shared amongst the partons in the proton and antiproton, the machine energy is necessarily much greater than the desired subprocess c.m. energy, whereas, since (at current energies, at least) leptons have no substructure, all the beam energy of an e^+e^- collider is available for the interaction. Lepton colliders also have the advantage that the laboratory and interaction c.m. frames coincide, so kinematic distributions can be determined directly.

However, the major disadvantage of e^+e^- collider is that, for a given interaction energy, the annular radius must be much larger than that of a $\bar{p}p$ machine (even though the beam energy of the hadron machine must be so much higher). The reason for this lies in energy loss due to synchrotron radiation, which effectively limits the radius of curvature of the particle beams; as the loss is inversly proportional to the particle's mass[4],[19] the losses in e^+e^- machines of given beam energy dictate a more gentle curvature, and hence a larger radius, than required in $\bar{p}p$ colliders. A minor disadvantage is that only neutral intermediate states may be formed; i.e. at $\sqrt{s} \sim M_Z$ Z^o's can be produced copiously but W's, which must be pair-produced and so cannot

(both) be on-shell, are rare.

In the near future, the construction of two e^+e^- colliders designed to operate at total c.m. energies in the region of the Z^o resonance will be completed and experiments begun. The first of these is the SLAC Linear Colider (SLC) at Stanford, a modification of the linear accelerator in which, one after the other, bunches of e^+'s and e^-'s are injected into two arms of a "horseshoe" to intersect at its midpoint. This is a small (but technically complex) construction project and will be completed shortly (c. 1987). However, its major disadvantage is that it is essentially a "one-pass" machine and, hence, high luminosities cannot be achieved.

Slightly further in the future (1988/89) lies the Large Electron-Positron collider (LEP) at CERN. This is a huge construction, with an annular beam tube about 7km across; interestingly, provision has been made for the constructon at a later date of a 10-20 TeV large pp or $\bar{p}p$ collider (the LHC) in the same tunnel. In the first instance, LEP will run at $\sqrt{s} \sim M_Z$, but in the future will be upgraded (LEP-II) to run at $\sqrt{s}$ = 200 GeV, so that pair production of (on-shell) W's can be studied. LEP-I, running on the Z^o resonance and with high luminosity, will produce Z^o's in abundance. Four experiments have been approved for LEP:[<20] DELPHI, a hermetic detector array with a high resolution; ALEPH, another "fine-grain" detector covering the complete available solid angle; OPAL, a powerful general purpose detector; and L3, designed to investigate the standard electroweak sector including a search for the Higgs boson.

Chapter 3

HIGGS BOSON PRODUCTION VIA BREMSSTRAHLUNG FROM WEAK GAUGE BOSONS

"Where - is - Higgs? Perhaps he's dead at last, or trapped in a lift somewhere, or succumbed to amnesia, wandering the land with his turn-ups stuffed with ticket-stubbs."
- from The Real Inspector Hound *by Tom Stoppard*

3.1 Introduction

The Standard Model[1] of electroweak interactions due to Weinberg and Salam (see Chapter 1) has proven to be very successful in describing the low energy data. Moreover, vindication of the gauge structure and the symmetry breaking mechanism of the model has been provided by the experimental discovery[2] of the W and Z bosons at the CERN $\bar{p}p$ Collider, with about the masses predicted by the theory. However, the minimal Standard Model also predicts the existence of a physical Higgs scalar boson; this particle has not yet been observed experimentally.

The experimental search for the Higgs boson is hampered by the fact that its mass is not predicted uniquely by the theory, and so we do not have a clear idea of the energy regime in which to look for it. However, the mass is not a completely free parameter; the Higgs boson cannot be arbitrarily light or heavy. In the minimal Standard Model , the mass is bound from below by cosmological constraints and radiative corrections,[3] $m_H \gtrsim 10.4$ GeV; and from above by perturbative constraints,[4] $m_H < 175$ GeV; these limits are discussed in Chapter 1, and in detail in Ref. (5). The range of allowed masses suggests that the Higgs boson, if it does indeed exist, may be produced

experimentally in current or near-future $\bar{p}p$ and e^+e^- colliders. Extended Standard Models with more than one Higgs doublet[5] and supersymmetric models[6] predict several physical Higgs bosons with a wide spectrum of masses.

Even though the mass of the Higgs boson is unkown (within the theoretical limits), the strengths of the couplings of the Higgs to fermions and gauge bosons are, in fact, described by the theory, and are proportional to the particle masses (see Chapter 1). These couplings are therefore determined, up to our knowledge of the particle masses. (Of course, since photons and gluons are massless, their couplings to Higgs bosons are non-zero only in higher orders in α, α_s.) Since only light fermions are experimentally abundant and the couplings of these particles are small, Higgs boson production will have small cross-sections and the low event rate will make experimental identification of the Higgs boson very difficult.

Because of the nature of the couplings, the Higgs bosons will decay predominantly to the heaviest particle pair that is kinematically allowed. For example, for m_H = O(10-100) GeV it will decay into heavy quark (c,b,t,...) or lepton (τ,...) pairs,[7] and for m_H > O(200) GeV it will decay into W or Z pairs, giving rise to four-fermion final states. (Decays into gg ($\gamma\gamma$) via heavy quark (fermion) loops are possible, but the branching ratio is always small (< 10^{-1} (< 10^{-2})).)

In Section 3.2 we briefly review four possible mechanisms for HIggs boson production at $\bar{p}p$ or e^+e^- colliders which have been

proposed and discussed in the literature. In Sections 3.3 and 3.4 we examine in some detail a fifth, Higgs boson production via Bremsstrahlung from a W or Z boson in $\bar{p}p$ collisions. Our conclusions are presented in Section 3.5.

3.2 Higgs boson production via ...

3.2.1 *Toponium radiative decay*

The mechanism for Higgs boson production in toponium ($|\mathfrak{T}\rangle = |\bar{t}t\rangle$) decay was proposed by Wilzcek.[9] The decay rate for $\mathfrak{T} \longrightarrow H\gamma$ (Fig. 3.1(a)) can be calculated in the non-relativistic bound state approximation; it is found

$$\frac{\Gamma(\mathfrak{T} \longrightarrow H\gamma)}{\Gamma(\mathfrak{T} \longrightarrow \mu\mu)} = \frac{G_F\, m_{\mathfrak{T}}^2}{4\sqrt{2}\,\pi\alpha}\left(1 - \frac{m_H^2}{m_{\mathfrak{T}}^2}\right). \qquad (3.1)$$

The branching ratio $\Gamma(\mathfrak{T} \longrightarrow H\ )/\Gamma(\mathfrak{T} \longrightarrow \text{all})$ is estimated to be about 0.01 for $m_{\mathfrak{T}} = 40$ GeV and $m_H = 10$ GeV, more for a heavier toponium (which is now indicated),[9] less for a heavier Higgs boson.

In an e^+e^- collider, with $\sqrt{s}$ at the toponium resonance, the monochromatic energy of the photon would serve to identify clearly the presence ot the Higgs boson. In a $\bar{p}p$ collider the photon would have a high transverse momentum (p_T), but would no longer be monochromatic. The event rate has been estimated to be $\sigma(\bar{p}p \rightarrow H\gamma X) \sim 0.5$ pb for $\sqrt{s} = 540$ GeV. Comparable backgrounds from ordinary prompt photon production would easily obscure the signal, unless the Higgs boson could be clearly identified from a

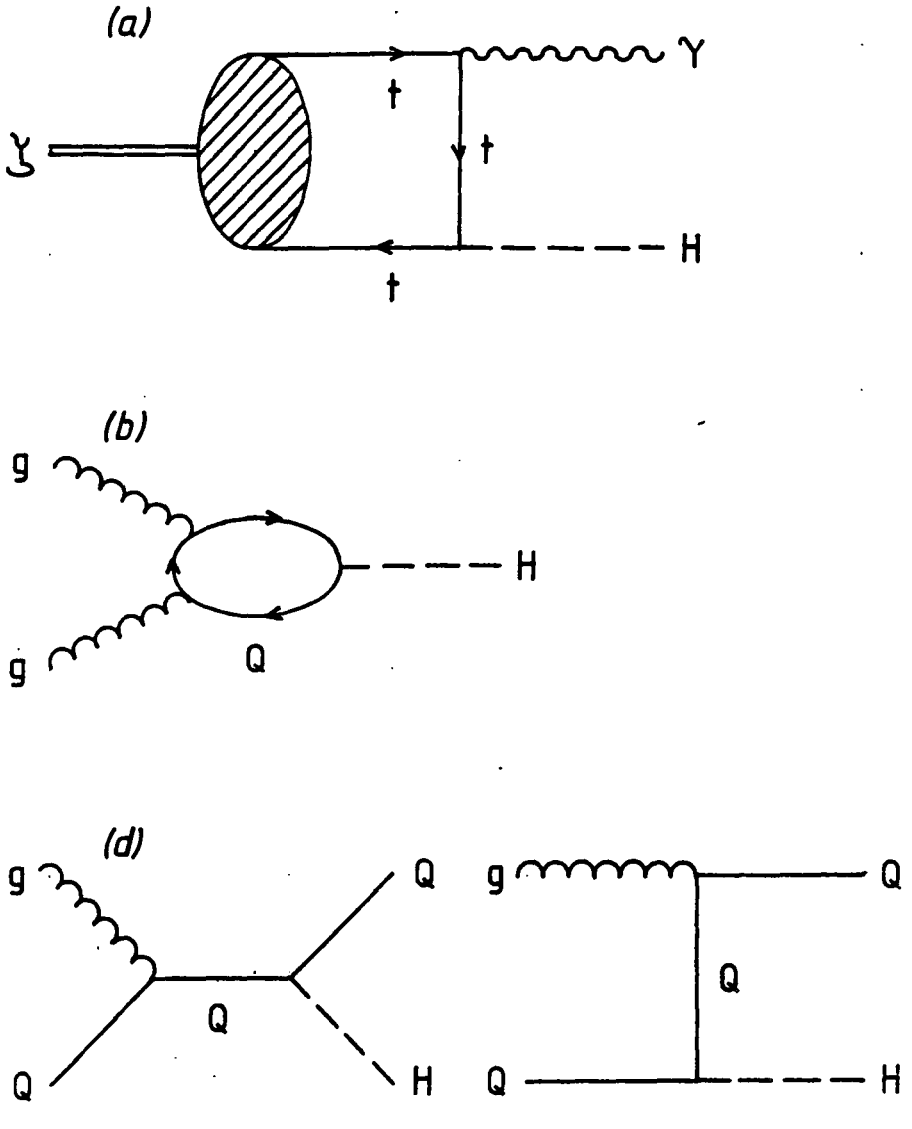

Figure 3.1
The lowest-order diagrams for the Higgs production mechanisms discussed in Section 3.2.
(a) Toponium radiative decay: $\Upsilon \longrightarrow H\gamma$
(b) Gluon-gluon fusion: g g $\longrightarrow$ H
(c) (see next page) Conjoined production with heavy quark flavours: (q $\bar{q}$ or g g) $\longrightarrow$ H Q $\bar{Q}$
(d) Diffractive heavy quark production: g Q $\longrightarrow$ H Q

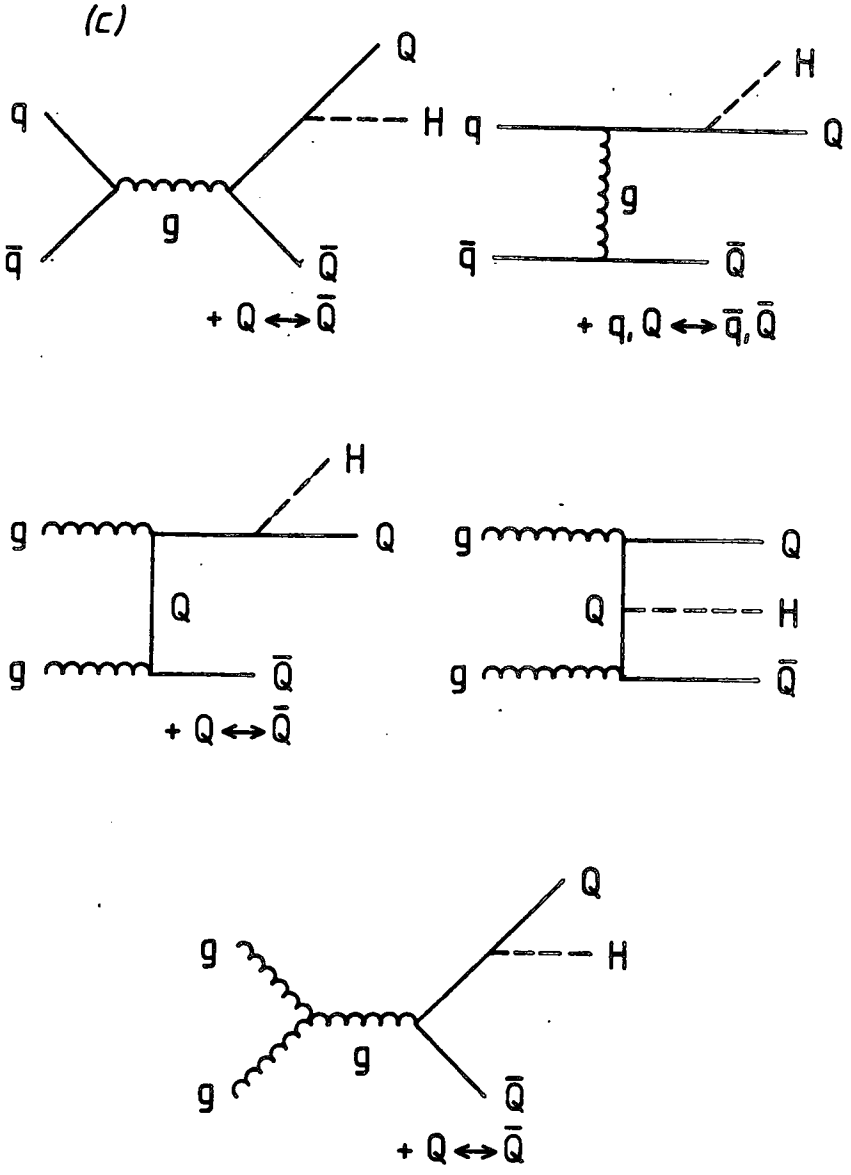

Figure 3.1 (c)
(see previous page)

particularly characteristic decay, such as $H \longrightarrow e^+e^-$.

3.2.2 *Gluon-gluon fusion*

Higgs boson production in gluon-gluon fusion[10] proceeds via a heavy quark loop (Fig. 3.1(b)). The strong coupling to the heavy quark compensates somewhat for the α_s^2 suppression relative to direct production. In contrast, the direct production of the Higgs boson via (valance) $\bar{q}q$ fusion is small because of the small quark mass.

For a Higgs boson of mass m_H = 10 GeV, this process gives a cross-section of $\sigma(pp \longrightarrow ggX \longrightarrow HX)$ = 40 pb at $\sqrt{s}$ = 540 GeV. This process may be identified only by detecting the heavy fermions from the Higgs boson decay; however, it appears that such a signal would be obscured by a large background from Drell-Yan $\bar{q}q, gg \longrightarrow \bar{c}c, \bar{b}b, \ldots$ and $\bar{q}q \longrightarrow e^+e^-, \ldots$ production.

3.2.3 *Conjoined production with heavy quark flavours*

Some authors[11,12] have considered the associated production of Higgs bosons and heavy quarks in $\bar{p}p$ collisions, via the subprocess (Fig. 3.1(c))

($\bar{q}q$ or gg) --> $\bar{Q}QH$ --> 4 (or more) jets . (3.2)

An advantage of this conjoined production is that it suppresses the Drell-Yan background. Sequential weak decays will lead to final states with many observed fermions (or jets), such as up to twenty c quark jets, or four c quark jets plus eight charged leptons, for Q = t.

The authors of Ref. (11) find a total cross-section of about 5 pb at $\sqrt{s}$ =540 GeV for m_b = 40 GeV and m_H = 10 GeV (and ~ 200 pb at $\sqrt{s}$ = 2 TeV for the same values of the masses).

3.2.4 *Diffractive heavy quark production*

There is evidence that heavy quark flavours are produced in $\bar{p}p$ collisions predominantly via diffractive production.[13] The mechanism of diffractive heavy quark production is not well understood, but it may be naively interpreted[14] as the Compton scattering Qg --> Qg, where the initial heavy (sea) quark, Q, is intrinsic to the proton. This suggests another mechanism for Higgs boson production, in association with a "diffractive" heavy quark (Fig. 3.1(d))

$$(Q \text{ or } \bar{Q})\ g \longrightarrow (Q \text{ or } \bar{Q})\ H\ . \qquad (3.3)$$

Barger et al.[15] considered Higgs boson production via this subprocess, for Q = c, in $\bar{p}p$ collisions at $\sqrt{s}$ = 540 GeV. They found a total cross-section of $\sigma(\bar{p}p \longrightarrow HcX)$ = 0.6 pb, for m_H = 10 GeV. Despite this rather low yield, they claim that the signal is unusually distinctive, such that identification of a Higgs boson should be possible with just a few events. The longtitudinal scaling distribution ($d\sigma/dx_L$, where $x_L = 2p_L/\sqrt{s}$ and p_L is the longtitudinal momentum) of the Higgs boson is characteristically diffractive, in contrast to the central production of the Higgs boson in gluon-gluon fusion. The background from electromagnetic pair-production was shown to be well below the signal.

We also considered Higgs boson production via subprocess (3.3), but for $Q = t$. Naively, we expect that the subprocess cross-section would be increased by a factor of $m_t^2/m_c^2 \sim 500$, due to the stronger coupling of the Higgs boson to the top quark, but this gain is diminished by about one order of magnitude because of phase space effects (for $\sqrt{s}_{threshold} < \sqrt{s} <$ few 100 GeV). However, the calculation of the total cross-section for $\bar{p}p \longrightarrow HtX$ is fraught with uncertainty as the structure functions for diffractive top production are not well known. We must bear in mind that there are, in the literature, several distinct models of diffractive production,[13] and it is probably inappropriate to use other momentum distributions as input for Higgs boson production via subprocess (3.2), which derives from the model of Barger et al.[15]

To make any realistic estimates of the cross-section for Higgs boson production in $\bar{p}p$ collisions via a Compton-like (or similar) subprocess, we must have a better understanding of the mechanism for the diffractive production of heavy quark flavours.

3.3. Higgs boson production via electroweak gauge bosons

A further potentially useful mechanism for Higgs boson production is via Bremsstrahlung from electroweak gauge bosons,[7,16-18] since the couplings to these heavy particles are large. W and Z bosons have been produced in abundance at the CERN $\bar{p}p$ Collider, and Z bosons will be produced copiously at future

e^+e^- colliders (SLC and LEP; see Chapter 2); thus this mechanism for Higgs boson production is relevant to both experimental scenarios. In this and the following ection, we investigate this production mechanism in $\bar{p}p$ collisions in particular, though much is also relevant to e^+e^- annihilation experiments.

Figure 3.2 shows the first-order Feynman diagrams for

$$\bar{q}_i\, q_j \longrightarrow H\, \bar{f}_i\, f_j \ . \tag{3.4}$$

In the first instance we simplify the calculation by considering only on-shell gauge boson decays

$$W \longrightarrow H\, W^* \longrightarrow H\, \bar{f}_1\, f_2 \ , \tag{3.5a}$$

$$Z \longrightarrow H\, Z^* \longrightarrow H\, \bar{f}_1\, f_1 \ . \tag{3.5b}$$

The calculation of the three-body decay is straightforward; we use the well known Feynman rules for Standard Model interactions, and take the final state fermions to be massless. We find (for $U = W,Z$)

$$\Gamma(U\longrightarrow H\bar{f}_i f_j) = \frac{g_U{}^4(c_V{}^2+c_A{}^2)}{3\ 2^8\ \pi^3} \int_{a_1}^{b_1} ds_1\ \frac{s_1\ \lambda^{1/2}(M_U{}^2,m_H{}^2,s_1)}{M_U\ [(s_1-M_U{}^2)^2 + M_U{}^2\Gamma_U{}^2]} \ , \tag{3.6}$$

where $g_W = g$, $g_Z = g/\cos\theta_W$, c_V and c_A are the fermionic vector and axial couplings ($c_V, c_A = 1/\sqrt{2}$ for $U = W$), and s_1 is the off-shell gauge boson (4-momentum)^2. The limits on the s_1 integration are $a_1 = 0$ and $b_1 = (M_U - m_H)^2$. (λ is the usual triangle function: $\lambda(a,b,c) = a^2+b^2+c^2-2ab-2bc-2ca$.) It is useful to consider the ratio of widths, $R_U = \Gamma(U\longrightarrow H\bar{f}_i f_j)/\ \Gamma(U\longrightarrow \bar{f}_i f_j)$,

$$R_U = \frac{g_U{}^2}{16\ \pi^2\ M_U{}^2} \int_{a_1}^{b_1} ds_1\ \frac{s_1\ \lambda^{1/2}(M_U{}^2,m_H{}^2,s_1)}{[(s_1-M_U{}^2)^2 + M_U{}^2\Gamma_U{}^2]} \ , \tag{3.7}$$

which suppresses the dependance on the gauge boson-fermion couplings.

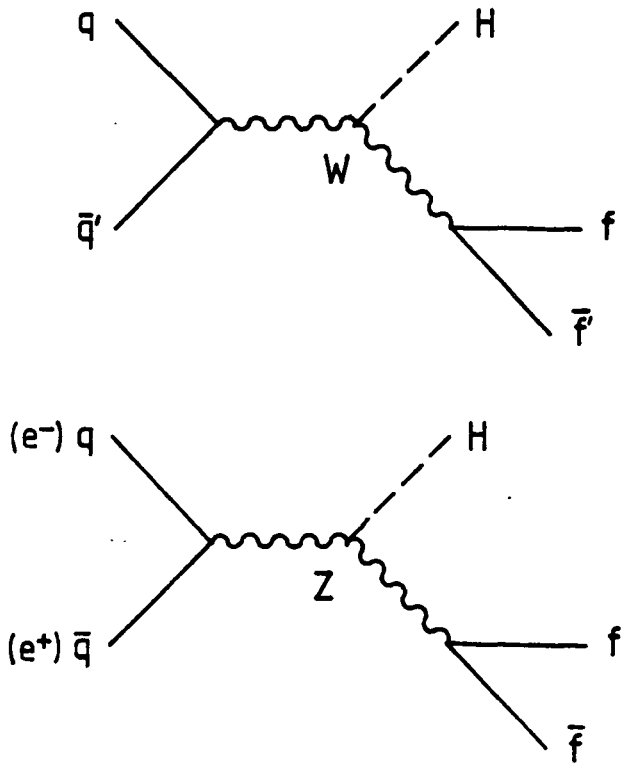

Figure 3.2
The lowest-order diagrams for Higgs boson production via Bremsstrahlung from electroweak gauge bosons in pp collisions (and, in the case of the Z, in e^+e^- annihilation).

Figure 3.3(a) shows this ratio, R_U, as a function of the Higgs boson mass, in the range $5\ \text{GeV} < m_H < 70\ \text{GeV}$, for $U = W, Z$ with masses $M_W = 81\ \text{GeV}$ and $M_Z = 93\ \text{GeV}$. We see from the figure that, for any value of m_H in this range, R_Z is greater than R_W; this is due to a simple factor of $1/\cos\theta_W$ in g_U, and to kinematic (phase space) factors. For definiteness we also show, in Fig. 3.3(b), the widths for $W \longrightarrow He\bar{\nu}_e$ and $Z \longrightarrow He^+e^-$. We see here that the different $(c_V^2+c_A^2)_U$ suppresses the Z width over most of the range of m_H, such that the rates are roughly equal; it is only for large values of m_H that $\Gamma(Z\longrightarrow Hee)$ is significantly greater than $\Gamma(W\longrightarrow He\nu)$, due to phase space factors.

We also consider the (invariant mass)^2 distribution of the fermion pair. This can be got trivially from Eq. (3.6), since the gauge boson (4-momentum)^2, s_1, is identically equal to the fermion pair (invariant mass)^2, viz

$$\frac{d\Gamma_U}{ds_1} = \frac{g_U^4(c_V^2+c_A^2)}{3\ 2^8\ \pi^3} \frac{s_1\ \lambda^{1/2}(M_U^2, m_H^2, s_1)}{M_U\left[(s_1-M_U^2)2 + M_U^2\Gamma_U^2\right]} \ . \qquad (3.8)$$

This distribution is shown for $\Gamma_U = \Gamma(Z\longrightarrow Hee)$ in Fig. 3.4, for five values of the Higgs boson mass. The distribution peaks towards the high s_1 end, due to the presence of the Z propagator. This distribution would be useful to distinguish between the production of Higgs bosons and that of other scalar (or pseudoscalar) particles.[18]

The cross-section for the production[16] of Higgs bosons via Z Bremsstrahlung in e^+e^- annihilation at the Z resonance can be found by a straightforward extension of the above calculation. In fact it is simply given by

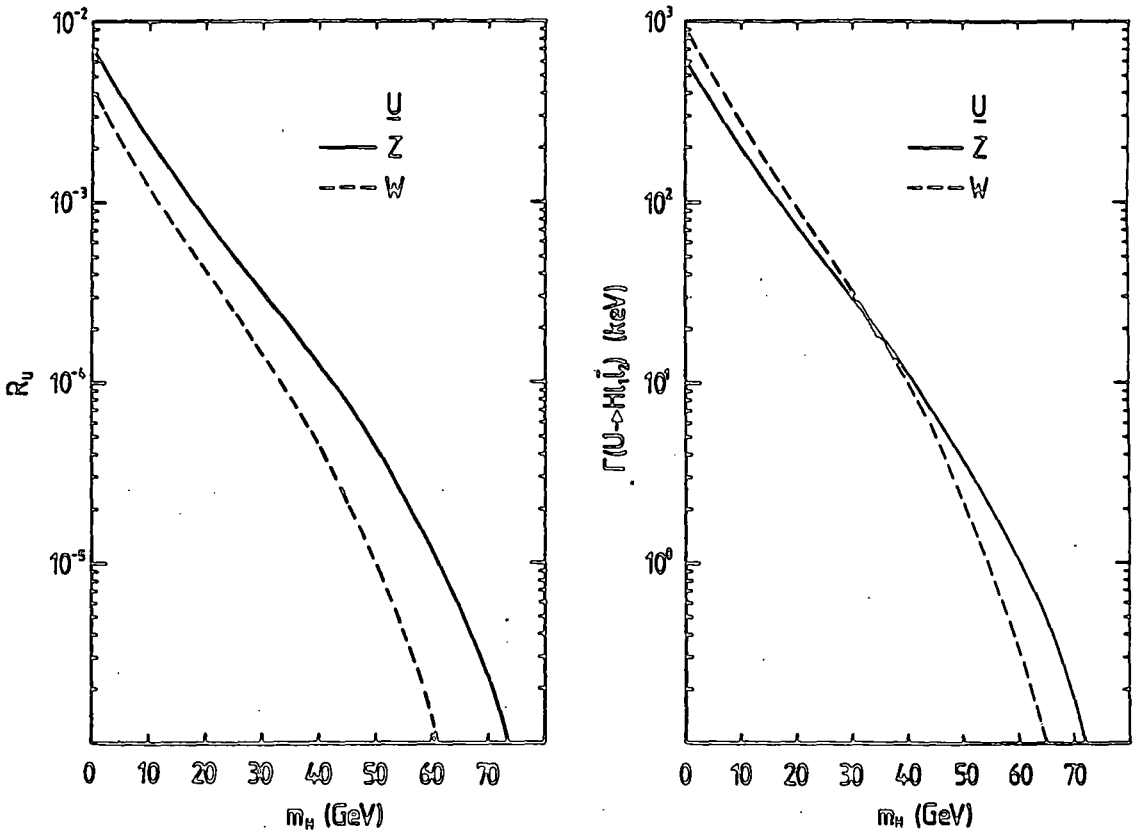

Figure 3.3
(a) The ratio of the decay widths, $R_U = \Gamma(U \longrightarrow H f_1 f_2) / \Gamma(U \longrightarrow f_1 f_2)$ (Eq. (3.7)) as a function of the Higgs boson mass, for $U = W, Z$ with masses $M_W = 81$ GeV, $M_Z = 93$ GeV. We take f_1, f_2 to be massless.
(b) The decay widths $\Gamma(W \longrightarrow He\bar{\nu}_e)$ and $\Gamma(Z \longrightarrow He^+e^-)$ as a function of the Higgs boson mass, with M_W, M_Z as in (a).

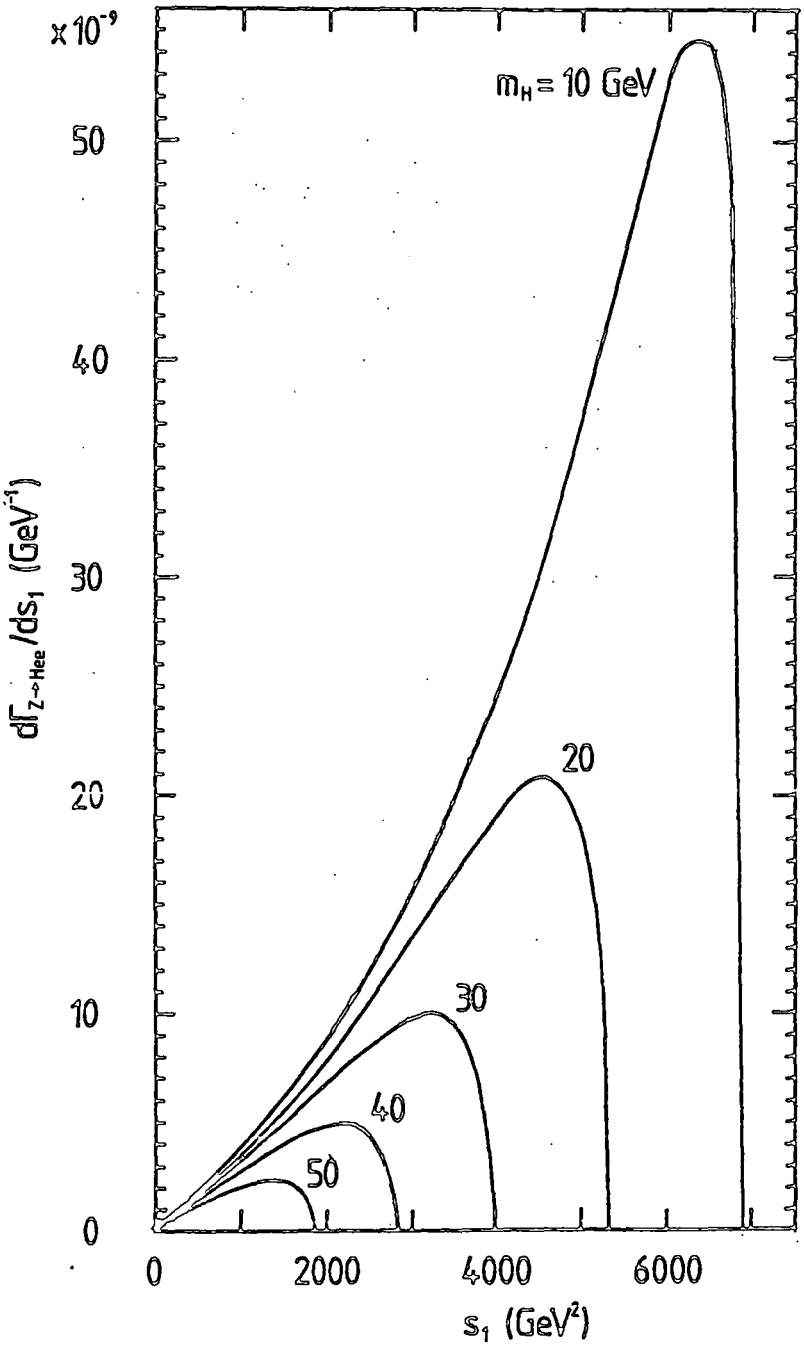

Figure 3.4
The (invariant mass)^2 (s_1) distribution of the electron pair in the decay $Z \longrightarrow H\, e^+ e^-$, for five values of the Higgs boson mass: m_H = 10, 20, 30, 40, 50 GeV, with M_Z = 93 GeV.

$$\sigma(e^+e^-\longrightarrow He^+e^-) = \frac{\Gamma(Z\longrightarrow He^+e^-)}{\Gamma(Z\longrightarrow e^+e^-)}\ \sigma(e^+e^-\longrightarrow e^+e^-)\ , \qquad (3.9a)$$

and the differential cross-section with respect to the (invariant mass)^2, s_1, of the fermion pair is similarly given by

$$\frac{d\sigma}{ds_1} = \frac{\sigma(e^+e^-\longrightarrow e^+e^-)}{\Gamma(Z\longrightarrow e^+e^-)}\ \frac{d\Gamma\ (Z\longrightarrow He^+e^-)}{ds_1}\ . \qquad (3.9b)$$

However, the calculation of cross-sections for Higgs boson production via gauge boson Bremsstrahlung in $\bar{p}p$ collisions is not so straightforward; this is discussed in the next section.

3.4 Higgs boson production via e/w gauge bosons in $\bar{p}p$ collisions

In the previous section we found that the rates $W \longrightarrow He\bar{\nu}_e$ (or $H\mu\bar{\nu}_\mu$) and $Z \longrightarrow Hee$ (or $H\mu\mu$) are comparable for most Higgs boson masses less than ~ 70 GeV. At the CERN $\bar{p}p$ Collider, the UA1 and UA2 collaborations have found about 200 $W \longrightarrow e\bar{\nu}_e$ events and only 20 $Z \longrightarrow e^+e^-$ events, a preponderance of W's by about one order of magnitude, in agreement with Standard Model calculations. Hence, it would seem that W Bremsstrahlung would give the better signal for Higgs boson production in $\bar{p}p$ collisions. However, this is not necessarily the case. The event rate is indeed higher, but we must require a semi-leptonic process like $W \longrightarrow He\bar{\nu}_e$ (with subsequent decay of the Higgs boson to the heaviest available fermionic species, $\bar{F}F$, which are seen as jets) to identify the signal against the QCD jet-production background, mindful that the ν_e can be identified only as missing transverse momentum (see Chapter 2). In spite of the fact that missing transverse momentum events were used reliably in the experimental discovery of the W

boson, we feel that the $e\bar{\nu}\bar{F}F$ ($\longrightarrow$ e jet jet missing p_T) signature will not be as clean a signal as the $ee\bar{F}F$ ($\longrightarrow$ e e jet jet) signature from $Z \longrightarrow Hee$, since what may be the most valuable signature for Higgs boson production requires the accurate measurement of the (invariant mass)^2 of the electron pair (see below).

The calculation of the differential cross-section for the subprocess $\bar{q}q \longrightarrow Hee$ (Eq. (3.4), with f = e) is straightforward. We find, for each quark flavour,

$$\sigma_q = \frac{G_F^3 M_Z^6}{\sqrt{2}\ 96\pi^5} \int ds_1\ d\Omega_H\ d\Omega_Z\ \frac{\lambda^{1/2}(\hat{s},s_1,m_H^2)}{s^2}\ S_q(q_1,p_1,\hat{s},s_1)\ , \tag{3.10a}$$

with

$$S_q = \frac{C_1(q)\ p_1\cdot q_2\ p_2\cdot q_1 + C_2(q)\ p_1\cdot q_1\ p_2\cdot q_2}{|D_Z(s)|^2\ |D_Z(s_1)|^2}\ , \tag{3.10b}$$

where s_1 has the same meaning as previously, $\hat{s}$ is the $\bar{q}q$ (c.m. energy)^2, q_i and p_i are the quark and electron momenta, $C_{1,2}(q)$ are functions of the fermionic couplings:

$$C_{1,2}(q) = (c_V^2(e)+c_A^2(e))(c_V^2(q)+c_A^2(q)) + 4\cdot c_V(e)\cdot c_A(e)\cdot c_V(q)\cdot c_A(q) \tag{3.10c}$$

(numerically we find, for $\sin^2\theta_W = 0.23$, $C_1(u) = 0.0775$, $C_2(u) = 0.0661$, $C_1(d) = 0.102$, and $C_2(d) = 0.0815$), and $D_Z(Q^2)$ is the Z propagator, $D_Z(Q^2) = (Q^2-M_Z^2) + iM_Z\Gamma_Z$. The double-propagator structure of the cross-section reflects the two dominant interaction pathways, viz: $\bar{q}q \longrightarrow Z \longrightarrow (Z^*\rightarrow ee)\ H$, and $\bar{q}q \longrightarrow Z^* \longrightarrow (Z\rightarrow ee)\ H$. The total cross-section for Higgs boson production in $\bar{p}p$ collisions, $\sigma(\bar{p}p\text{-->}HeeX)$, is given by

$$\sigma = \int_0^1 d\tau \int_{-1+\tau}^{1-\tau} dx_F \frac{1}{\sqrt{(x_F^2+4\tau)}} \sum_{q=u,d} \sigma_q \, q(x_1) \, q(x_2) \, , \qquad (3.11)$$

where x_1 and x_2 are the momentum fractions of the quarks ($x_{1,2} = (\pm x_F + \sqrt{(x_F^2+4\tau)})/2$), and $q(x)$ the momentum distributions (see Chapter 2). The total cross-section was calculated using Monte Carlo simulations of $O(10^6)$ events.

Figure 3.5 shows the differential cross-section with respect to the invariant mass of the e^+e^- pair from the decay of the Z for two different Higgs boson masses. The double peak in this distribution is a clear signature for the Bremsstrahlung of a Higgs boson. The narrow peak occurs at $M_{ee} = M_Z$ and corresponds to the resonance at $s_1 = M_Z^2$; the broader peak occurs at $M_{ee} \sim (M_Z - m_H)$ and corresponds to the resonance at $\hat{s} = M_Z^2$. Measurement of these two peaks can yield a value for m_H. This would, of course, be in addition to the measurment of the invariant mass of the $\bar{F}F$ pair from the Higgs boson decay, which would give m_H directly; however, for a light Higgs boson ($m_H < 25$ GeV) there are experimental difficulties involved in identifying the jets from the $b\bar{b}, \tau^+\tau^-, \ldots$ decays, and such direct measurement of m_H may not be possible.

None of the other kinematic distributions provide as striking a signature as the invariant mass distribution. The only other that is characteristic of the Z Bremsstrahlung is the e^+e^- acolinearity distribution (Fig. 3.6) which reflects the recoil momentum of the Z against the Higgs boson. The acolinearity peaks at $\alpha = 0$ (i.e. e^+e^- back-to-back); the peaking is steeper for low m_H (i.e. most events are approximately colinear). For larger m_H,

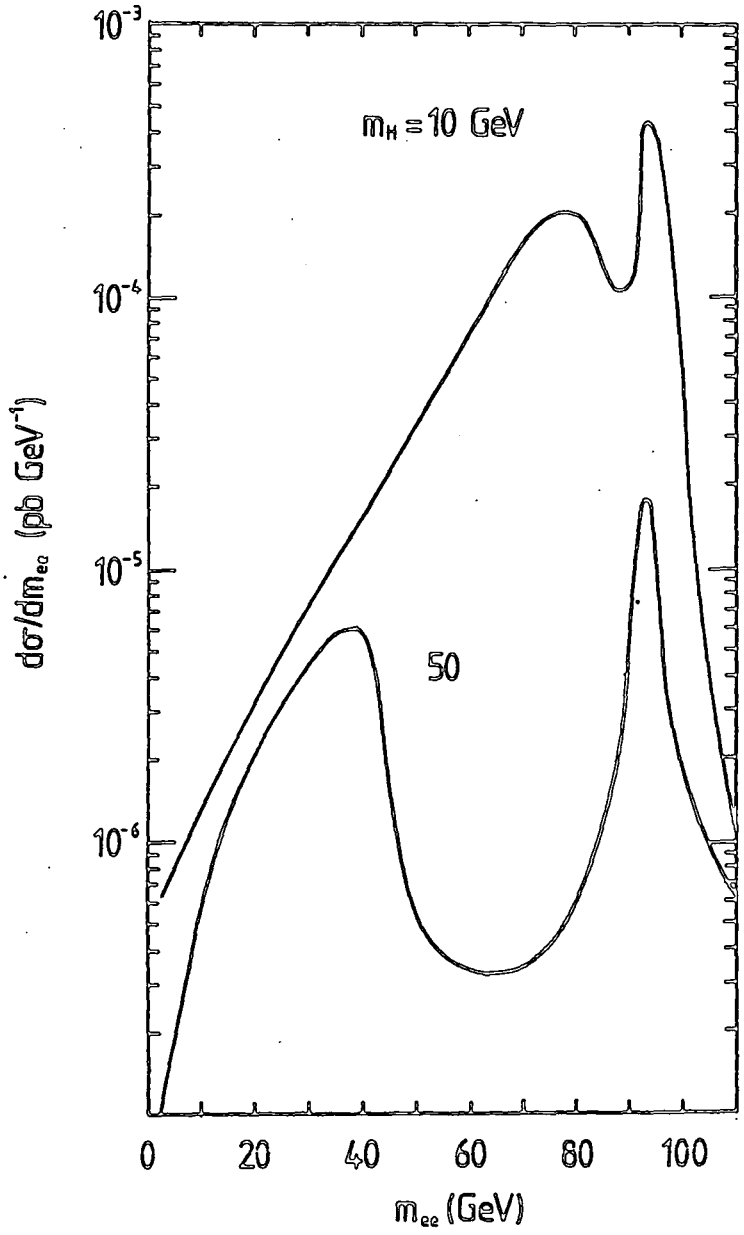

Figure 3.5
The differential cross-section for $p\bar{p} \longrightarrow X\,(Z \longrightarrow H\,e^+\,e^-)$ with respect to the invariant mass (m_{ee}) of the electron pair from the decay of the Z, for Higgs boson masses m_H = 10, 50 GeV, with M_Z = 93 GeV.

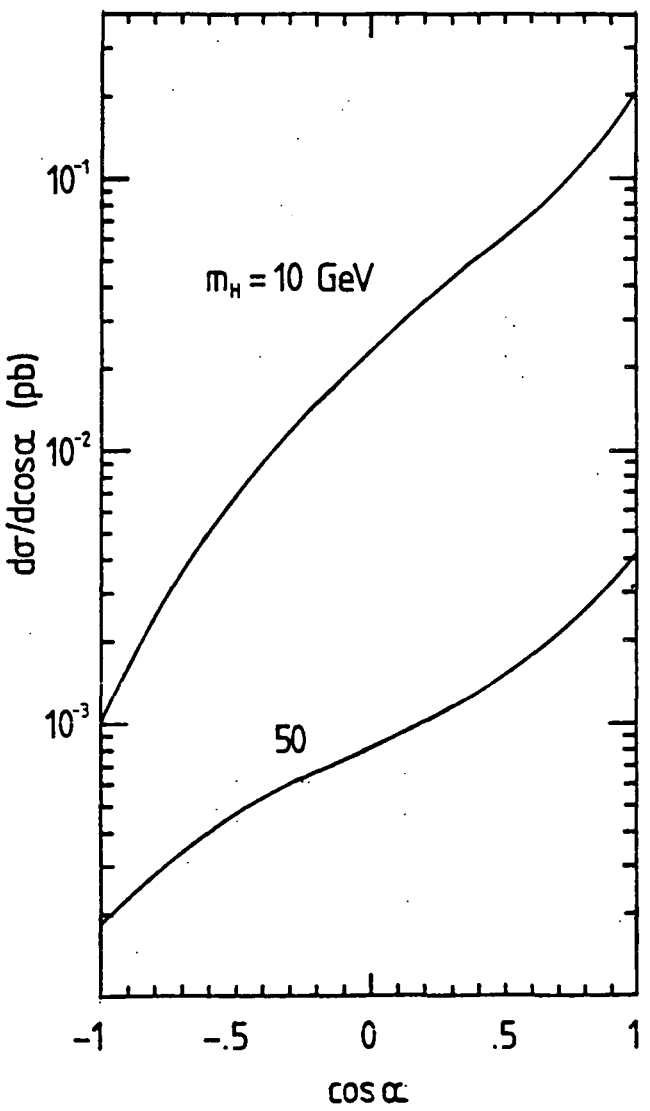

Figure 3.6
The differential cross-section for $p\bar{p} \longrightarrow X\ (Z \longrightarrow H\ e^+\ e^-)$ with respect to the acolinearity ($\alpha = \pi - \theta_{ee}$) of the electron pair from the decay of the Z, for Higgs boson masses m_H = 10, 50 GeV, with M_Z = 93 GeV.

the larger recoil momentum of the Z tends to collimate the e^+e^- pair such that a higher proportion of the events are acolinear.

Despite the clear signatures for the production of a scalar Higgs boson via Z Bremsstrahlung in $\bar{p}p$ collisions, the process may not, in fact, be observable as the total cross-section is small and, hence, will not yield a large event rate. Given these potentially low statistics for candidate Higgs boson events, construction of useful kinematic distributions will not be possible. It may be that the Collider data already contains Higgs boson events with nearly colinear e^+e^- which have been misidentified as ordinary $Z \longrightarrow e^+e^-$ events (if the Higgs boson is light such that the jets from the decay have not been seen). Identification of Higgs boson decay products may prove possible in the future with the introduction at the Collider of microvertex detectors.

3.5 Conclusions

We have reviewed some production mechanisms for Higgs boson production which have been discussed in the literature. Toponium (Υ) radiative decay will give a clear signal for Higgs boson production in e^+e^- annihilation, but the signal is likely to be obscured by ordinary prompt photon production in $\bar{p}p$ collisions. Production of the Higgs boson via gg fusion in $\bar{p}p$ collisions is likely to be obscured by the QCD Drell-Yan background; the background may be suppressed by considering conjoined production of Higgs bosons and heavy quark flavours, but here the signal is

small. Diffractive production of Higgs bosons and heavy quarks in $\bar{p}p$ collisions can give a clear signal, such that identification is possible with just a few events. However, the mechanism of diffractive heavy quark production is not well understood, and so calculations of the cross-sections for "diffractive" Higgs boson production (particularly with very heavy quark flavours (b,t,...)) are fraught with uncertainty.

We have studied one mechanism - the production of Higgs bosons via Bremsstrahlung from electroweak gauge bosons (in particular from Z bosons), in both e^+e^- annihilation and $\bar{p}p$ collisions - in some detail. We find that the invariant mass distribution of the lepton pair from the Z decay gives a clear signature for Higgs boson production. In particular, we note that, in $\bar{p}p$ collisions, this distribution has a double resonance structure, characteristic of the Bremsstrahlung of a scalar particle, which can yield a value for the mass of the Higgs boson. This may be useful, as direct measurement of the mass of the Higgs boson from the invariant mass of its decay products is not always feasible, particularly if it is light ($m_H < 25$ GeV), as the jets are too soft to be clearly identified. However, the production cross-section is small, and the potentially low statistics may make construction of useful kinematic distributions not viable.

We also find that the electron pair from the Z decay is almost colinear, the acolinearity arising from the small collimating effect of the recoil of the Z boson against the Higgs boson. Thus, for light Higgs bosons, where the jets are soft

enough to escape detection, the Bremsstrahlung events may be misidentified as standard $Z \longrightarrow e^+e^-$ events. The introduction of microvertex detectors at the Collider will improve the ability to identify light Higgs bosons via their decays, even if the event rate is low.

Chapter 4

SIGNATURES FOR SCALAR QUARK PRODUCTION AT THE pp COLLIDER

"What is the sound of one hand clapping?"
- traditional Zen koan

4.1 Introduction

The UA1 and UA2 collaborations have demonstrated that it is possible to reliably use missing transverse momentum triggers to isolate W boson production.[1] They have subsequently reported a number of exotic events consisting of large missing p_T accompanied by one or more jets[2] or a lepton and a jet.[2,3] Although the statistics are poor, these events do not appear to be explicable in terms of the Standard Model.

Broken supersymmetry, with a light photino, is a natural candidate to explain events with large missing p_T (see Chapter 1). However, the occurence of unusually large missing p_T events with a single energetic jet (of low multiplicity) had not been anticipated.

If the photino is the lightest supersymetric particle and if $m_{\tilde{g}} > m_{\tilde{q}}$ then the dominant decay modes of the scalar quark and gluino are

$$\tilde{q} \longrightarrow q\,\tilde{\gamma} \ , \tag{4.1a}$$

$$\tilde{g} \longrightarrow (\tilde{q}\bar{q} \text{ or } \bar{\tilde{q}}q) \longrightarrow \bar{q}\,q\,\tilde{\gamma} \ , \tag{4.1b}$$

and so the relevant QCD fusion subprocesses are

$$(\bar{q} \text{ or } q)\ g \longrightarrow (\bar{\tilde{q}} \text{ or } \tilde{q})\,\tilde{\gamma} \longrightarrow (\bar{q} \text{ or } q)\,\tilde{\gamma}\,\tilde{\gamma} \ , \tag{4.2}$$

$$(\bar{q}q \text{ or } gg) \dashrightarrow \bar{\tilde{q}}\,\tilde{q} \dashrightarrow \bar{q}\,q\,\tilde{\gamma}\,\tilde{\gamma} \ , \tag{4.3}$$

$$(\bar{q} \text{ or } q)\ g \dashrightarrow (\bar{\tilde{q}} \text{ or } \tilde{q})\,\tilde{g} \dashrightarrow (\bar{q} \text{ or } q)\,\bar{q}\,q\,\tilde{\gamma}\,\tilde{\gamma} \ , \tag{4.4}$$

$$(\bar{q}q \text{ or } gg) \longrightarrow \tilde{g}\,\tilde{g} \longrightarrow \bar{q}\,\bar{q}\,q\,q\,\tilde{\gamma}\,\tilde{\gamma} \ . \qquad (4.5)$$

Just as ordinary heavy quarks may be produced both by QCD fusion and via W bosons at relative rates depending on the quark mass, so it is important to consider also $\tilde{q}\tilde{q}'$ production via

$$\bar{q}_L\,q_L' \longrightarrow W \longrightarrow \tilde{\bar{q}}_L\,\tilde{q}_L' \longrightarrow \bar{q}\,q'\,\tilde{\gamma}\,\tilde{\gamma} \ . \qquad (4.6)$$

Since the photinos are stable and interact weakly with matter, they escape from the experimental detector. However, if the detector is hermetic, then their combined effect can be identified as missing transverse momentum.

The experimental rates of the QCD subprocesses (and the relative numbers of visible 1-jet, 2-jet, ... events) depend mainly on the value of $m_{\tilde{q}}$ for subprocesses (4.2) (which can, in any case, only give rise to monojet events) and (4.3), of both $m_{\tilde{q}}$ and $m_{\tilde{g}}$ for subprocess (4.4), and of $m_{\tilde{g}}$ for subprocess (4.5). Moreover, the predictions are sensitive to the particular experimental cuts imposed on the data. The present missing p_T data[<2] have a trigger requirement that at least one jet is seen and that it has $p_T > 25$ GeV; other jets are identified if they have $p_T > 12$ GeV. Thus, most events will have fewer jets than is naïvely implied by the number of final state quarks in (4.2-5), particularly at large missing p_T.

In Section 4.2, we show that, taking into account the acceptance cuts, subprocess (4.3) can yield large missing p_T events at about the observed rate and which are dominantly accompanied by a single jet, provided that $m_{\tilde{q}}$ is about 30 GeV. In Section 4.3, we investigate the effects of subprocesses (4.1) and (4.6), both of which give rise to appreciable cross-sections for

small scalar quark masses, on the range of possible scalar quark masses from Section 4.2. Then, in Section 4.4, we make further use of the UA1 data to put a bound on the gluino mass in this scenario, by considering the event rate arising from the Compton-like subprocess (4.4). In Section 4.5 we briefly review other supersymmetry scenarios advanced to explain the UA1 jet-plus-large-missing-p_T events. Our results are summarised in Section 4.6.

4.2 UA1 monojets: A signature for scalar quark pair production?

We assume that $m_{\tilde{g}} > m_{\tilde{q}}$ and that $m_{\tilde{g}}$ is sufficiently large (> 100 GeV) such that subprocess (4.3) (see Fig. 4.1) is the dominant supersymmetric mechanism for large missing p_T events. Furthermore, we assume the existence of only one SU(2) doublet of scalar quarks degenerate in mass ($m_{\tilde{u}} = m_{\tilde{d}} = m_{\tilde{q}}$), and also that the right-handed singlet scalar quarks have the same mass as this left-handed doublet.

To calculate the $\bar{\tilde{q}}\tilde{q}$ production in $\bar{p}p$ collisions at $\sqrt{s}$ = 540 GeV we use expessions for the cross-sections for the $\bar{q}q$ and gg fusion mechanisms from Refs (4,5), viz, for quark-quark fusion,

$$\frac{d\hat{\sigma}(\bar{q}_a q_b \rightarrow \bar{\tilde{q}}_i \tilde{q}_j)}{d\hat{t}} = \frac{4\pi\alpha_s^2}{9\hat{s}^2}\left\{\frac{\hat{s}(m_{\tilde{g}}^2-\hat{t}) - (m_{\tilde{q}}^2-\hat{t})^2}{(m_{\tilde{g}}^2-\hat{t})^2}\right.$$

$$\left. + \delta_{ij}\left[\frac{(m_{\tilde{q}}^2-\hat{t})(\hat{u}-\hat{t}) + s\,(m_{\tilde{g}}^2+\hat{t})}{3\hat{s}\,(m_{\tilde{g}}^2-\hat{t})} + \frac{\hat{s}-4m_{\tilde{q}}^2}{\hat{s}} - \frac{(\hat{u}-\hat{t})^2}{\hat{s}}\right]\right\}, \quad (4.7a)$$

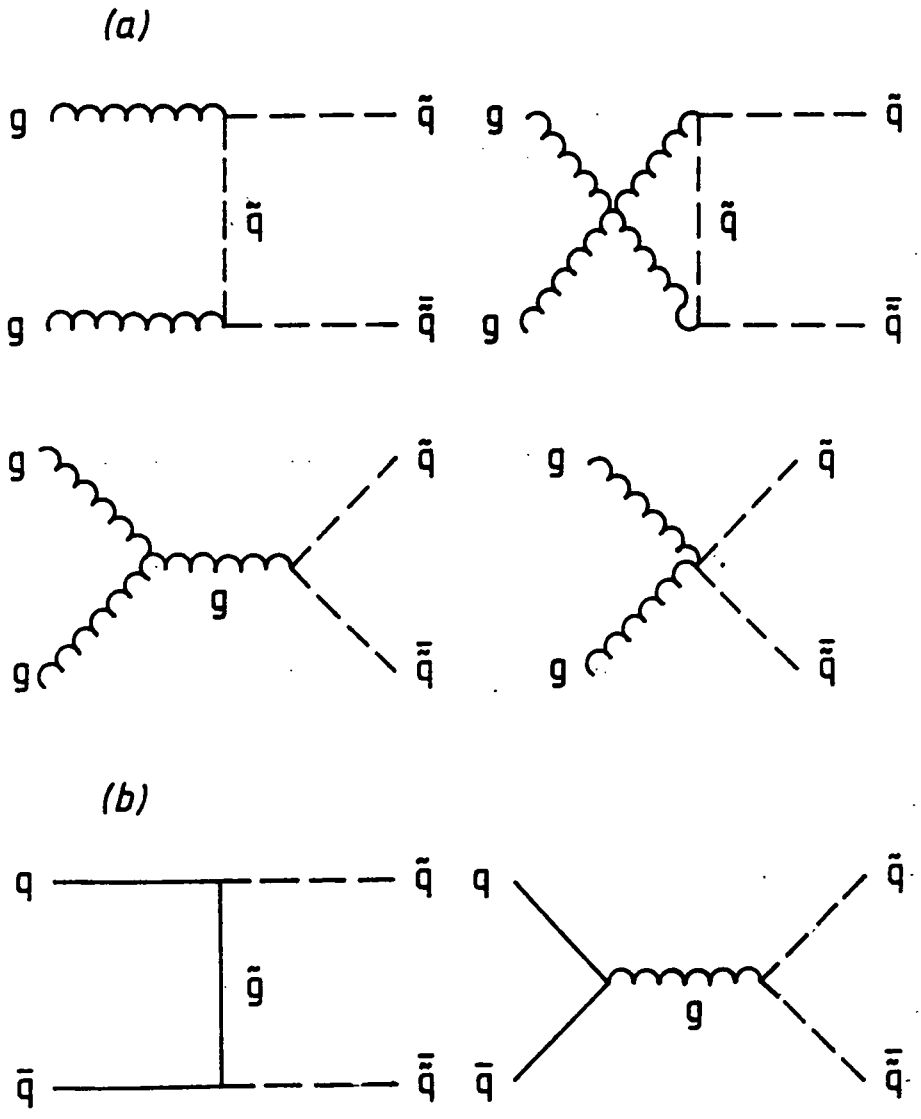

Figure 4.1
The first-order Feynman diagrams for scalar quark pair production:
(a) $g\,g \longrightarrow \tilde{q}\,\bar{\tilde{q}}$,
(b) $q\,\bar{q} \longrightarrow \tilde{q}\,\bar{\tilde{q}}$.

$$\hat{\sigma}(\bar{q}_a q_b \to \tilde{\bar{q}}_i \tilde{q}_j) = \frac{4\pi\alpha_s^2}{9\hat{s}^2}\left\{(\hat{s}+2\xi)\lambda - S\left(1+\frac{\xi^2}{\hat{s}m_{\tilde{q}}^2+\xi^2}\right)\right.$$

$$\left. + \delta_{ij}\left[\frac{2}{3}\left(\frac{\xi^2}{\hat{s}}+m_{\tilde{q}}^2\right)\lambda - S\left(1+\frac{2\xi}{3\hat{s}}-\frac{8m_{\tilde{q}}^2}{3\hat{s}}\right)\right]\right\}, \qquad (4.7b)$$

where $\tilde{q}_i$, $\tilde{q}_j$ = $\tilde{u}$ or $\tilde{d}$, $\xi = m_{\tilde{g}}^2 - m_{\tilde{q}}^2$, $\hat{s}$ is the subprocess (c.m. energy)^2, $S = \sqrt{\hat{s}}\sqrt{\hat{s}-4m_{\tilde{q}}^2}$, and $\lambda = \ln\{(\hat{s}+S+2\xi)/(\hat{s}-S+2\xi)\}$; and, for gluon-gluon fusion,

$$\sum_{q=u,d}\frac{d\hat{\sigma}(gg\to\tilde{\bar{q}}\tilde{q})}{d\hat{t}} = \frac{\pi\alpha_s^2}{4\hat{s}^2}\left(\frac{7}{3}+\frac{3(\hat{u}-\hat{t})^2}{\hat{s}^2}\right)\times$$

$$\left\{1+\frac{2m_{\tilde{q}}^2\hat{t}}{(\hat{t}-m_{\tilde{q}}^2)2}+\frac{2m_{\tilde{q}}^2\hat{u}}{(\hat{u}-m_{\tilde{q}}^2)^2}+\frac{4m_{\tilde{q}}^2}{(\hat{t}-m_{\tilde{q}}^2)(\hat{u}-m_{\tilde{q}}^2)}\right\}, \qquad (4.8a)$$

$$\sum_{q=u,d}\hat{\sigma}(gg\to\tilde{\bar{q}}\tilde{q}) = \frac{2\pi\alpha_s^2}{3\hat{s}^2}\left\{\left(\frac{5}{8}+\frac{31m_{\tilde{q}}^2}{4\hat{s}}\right)S+\left(4+\frac{m_{\tilde{q}}^2}{\hat{s}}\right)\frac{m_{\tilde{q}}^2}{\hat{s}}\ln\left[\frac{\hat{s}-S}{\hat{s}+S}\right]\right\}. \qquad (4.8b)$$

It has been assumed that it is not in practice possible to distinguish experimentally between left- or right-handed scalar quarks, nor between scalar quarks of different flavours, but that scalar quark and antiquark can be distinguished.[4] We use the structure functions of Ref. (6), and take $\alpha_s = 12\pi/\{b.\ln(s/\Lambda^2)\}$, with $b = 23$, and $\Lambda = .4$ GeV (as required by using these structure functions). Allowing for loop contributions[7] from active supersymmetric particles would give a smaller b, and hence a larger α_s. On the other hand, choosing a smaller value of would give a smaller α_s. These uncertainties, together with those of the structure functions, mean that there is an uncertainty of at least a factor of 2 in the cross-section predictions. We also take the branching ratio for the decay (4.1a) to be 100%; if the weak gauginos are lighter than the scalar quark then this branching ratio will be reduced, thus

giving an additional uncertainty in the normalisation of the cross-section.

In our Monte Carlo calculations, we simulate the UA1 experimental triggers and cuts, viz: a jet trigger of

$$p_T(\text{jet}) > 25 \text{ GeV} ; \tag{4.9a}$$

a jet recognition cut of

$$p_T(\text{jet}) > 12 \text{ GeV} ; \tag{4.9b}$$

quark jets are combined to form a single hadronic jet if $[(\Delta\phi)^2 + (\Delta y)^2]^{1/2} < 1$, where $\Delta\phi$ and Δy are the differences in azimuth and rapidity of the final state quarks, in accordance with the UA1 jet-finding algorithm. We note, however, that in the calculation below almost all single jet events have the jet coming from a single $\tilde{q}$ decay with the missing p_T coming dominantly from the accompanying $\bar{\tilde{q}}$ decay, or vice-versa.

The missing p_T is calculated by adding vectorially the $\vec{p}_T$ of the two photinos. The missing p_T distribution arising from $\bar{\tilde{q}}\tilde{q}$ production and decay (subprocess (4.3)) is shown in Fig. 4.2(a), for various values of $m_{\tilde{q}}$. To compare with the UA1 data [2], in addition to the requirement of (at least) one jet with $p_T > 25$ GeV, we also require that

$$p_T(\text{missing}) > 4\sigma , \tag{4.10}$$

with $\sigma = 0.7\sqrt{E_T}$, where $E_T = E_T(\bar{q}) + E_T(q) + 20$ GeV. The addition of 20 GeV represents the minimum bias E_T of the $\bar{p}$ and p debris at $\sqrt{s} = 540$ GeV. Imposing these cuts greatly suppresses the event rate, as is shown in Fig. 4.2(b). For the smaller values of $m_{\tilde{q}}$ the jet trigger (4.9a) requires the parent scalar quark to have large p_T; for instance, for $m_{\tilde{q}} = 25$ GeV we have

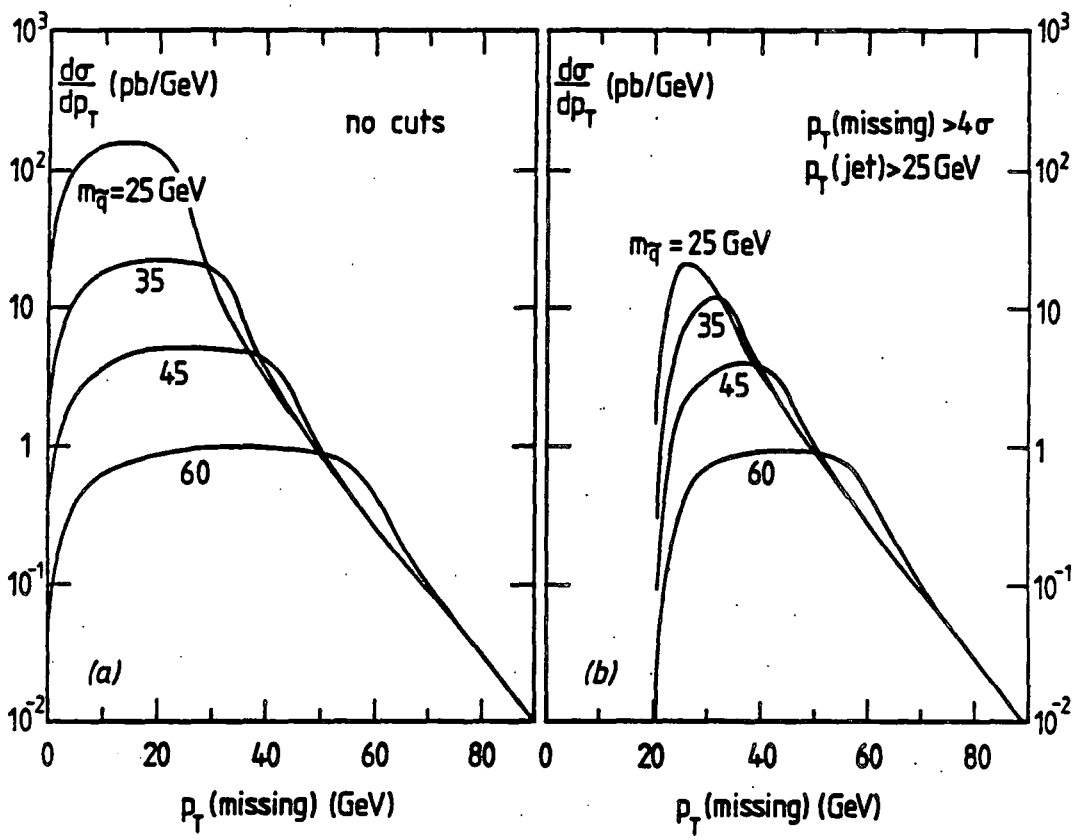

Figure 4.2

(a) The missing p_T distribution arising from $\tilde{q}\bar{\tilde{q}}$ production and decay in $p\bar{p}$ collisions at $\sqrt{s}$ = 540 GeV for four choices of the scalar quark mass.

(b) As (a), but showing the suppression which results from imposing the cuts of Eqs (4.9) and (4.10).

$\langle p_T(\tilde{q})\rangle \approx 30$ GeV. As the scalar quark mass increases this is of less importance, and a greater proportion of the events pass the trigger requirement.

The total $\tilde{q}\bar{\tilde{q}}$ cross-section is shown in Fig. 4.3 as a function of the scalar quark mass. The effect of imposing the UA1 acceptance cuts, (4.9) and (4.10), is also shown. The difference between the total and the 1-jet cross-sections is due to events with 2 visible jets (i.e. both jets have $p_T > 12$ GeV). For low scalar quark masses the requirement that the photino pair and one jet each have large p_T requires the second jet to be soft, resulting in the dominance of 1-jet events. On the other hand, for large values of $m_{\tilde{q}}$ two visible jets are expected. for scalar quark masses up to about 40 GeV, we see that the predicted event rate is consistent with the 16 1-jet and 5 2-jet events reported by UA1;[2] however, we must bear in mind the uncertainties in the theoretical prediction (due to the choice of α_s, Λ, the number of degenerate scalar quark flavours, $BR(\tilde{q}\text{-->}q\tilde{\gamma})$) and in the experimental rates (due to the possibility of confusing misidentified standard QCD jet events with the signal at low values of missing p_T).

If we now consider only the largest missing p_T events by increasing the cut (4.10) to

$$p_T(\text{missing}) > 35 \text{ GeV} , \qquad (4.11)$$

then the lower set of curves on Fig. 4.3 is obtained. We see that the 1-jet events dominate for a scalar quark mass in the range $20 \text{ GeV} < m_{\tilde{q}} < 30 \text{ GeV}$, and that for an integrated luminosity of $\sim 100\ nb^{-1}$ we would expect about 4 such events.

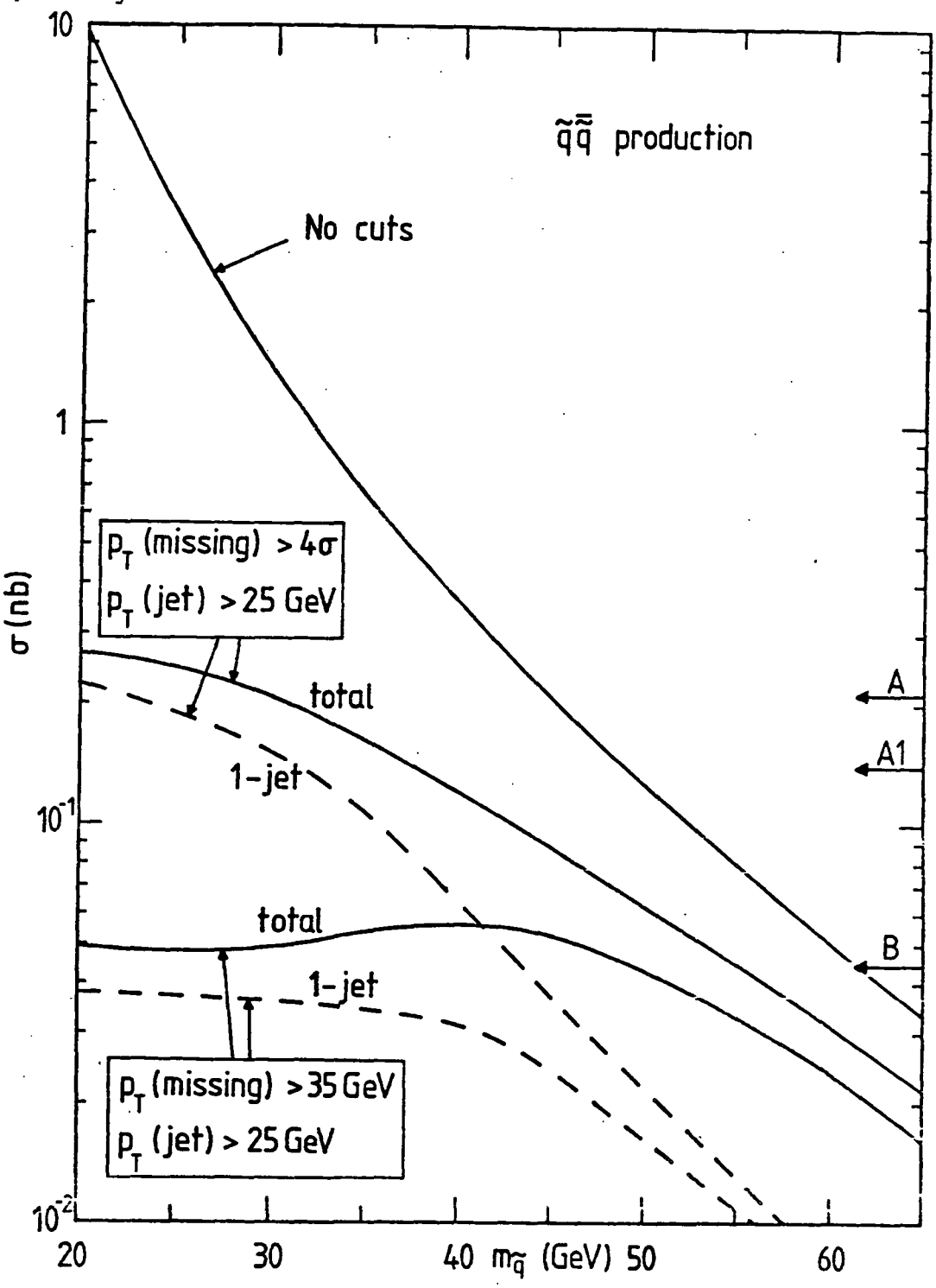

Figure 4.3

The $\tilde{q}\bar{\tilde{q}}$ production cross-section for subprocess (4.3) (Fig. 4.1) as a function of the scalar quark mass. The effect of imposing the cuts of Eqs (4.9) and (4.10) is also shown, where the dashed curve represents the fraction of the total events with a single visible jet. The lower pair of curves corresponds to the further requirement of Eq. (4.11). The UA1 event rates are shown to the right of the figure, corresponding to an integrated luminosity of 113 nb^{-1}: A) the 1- and 2-jet events with p_T(missing) > 4σ, A1) 1-jet events only, and B) 1-jet events with p_T(missing) > 35 GeV. We assume none of the UA1 events arise from misidentified standard QCD jets, and event A, which contains an energetic muon, is omitted.

To compare with the experimental p_T distributions, we take a scalar quark mass of 25 GeV. Figure 4.4(a) compares the missing p_T of the 24 observed events satisfying Eq. (4.10) with the model prediction. The experimental uncertainty on missing p_T is about ± 7 GeV, a little over the bin width chosen in the figure. Also, the experimental jet p_T distribution is known for the five 1-jet events with $p_T(\text{missing}) > 35$ GeV, and this is compared to our theoretical expectations in Fig. 4.4(b). Considering the low statistics and the theoretical uncertainties, there is good overall agreement with the observed UA1 rate and p_T distributions.

In order to assess the background to their 1-jet events with the largest missing p_T, UA1 relax their acceptance cut to[<2]

$$p_T(\text{missing}) > \max\{2\sigma,\ 15\ \text{GeV}\}\ , \qquad (4.12)$$

and studied how many events lie in the region $\cos\phi < -0.8$, where ϕ is the azimuthal angle between the jet and the residual visible p_T. Such events, which are approximately back-to-back in the transverse plane, are candidates for a background contribution from standard QCD jet events in which all but one jet is missed. About half the increased sample have $\cos\phi < -0.8$, although none of the six events with the largest missing p_T are in this region. Unfortunately, the proportion of the events with $\cos\phi < -0.8$ and $4\sigma < p_T(\text{missing}) < 35$ GeV is not given. For a scalar quark mass of 25 GeV, we find that none of the predicted 1-jet events with $p_T(\text{missing}) > 4\sigma$ (and $p_T(\text{jet}) > 25$ GeV) are in the region $\cos\phi < -0.8$.

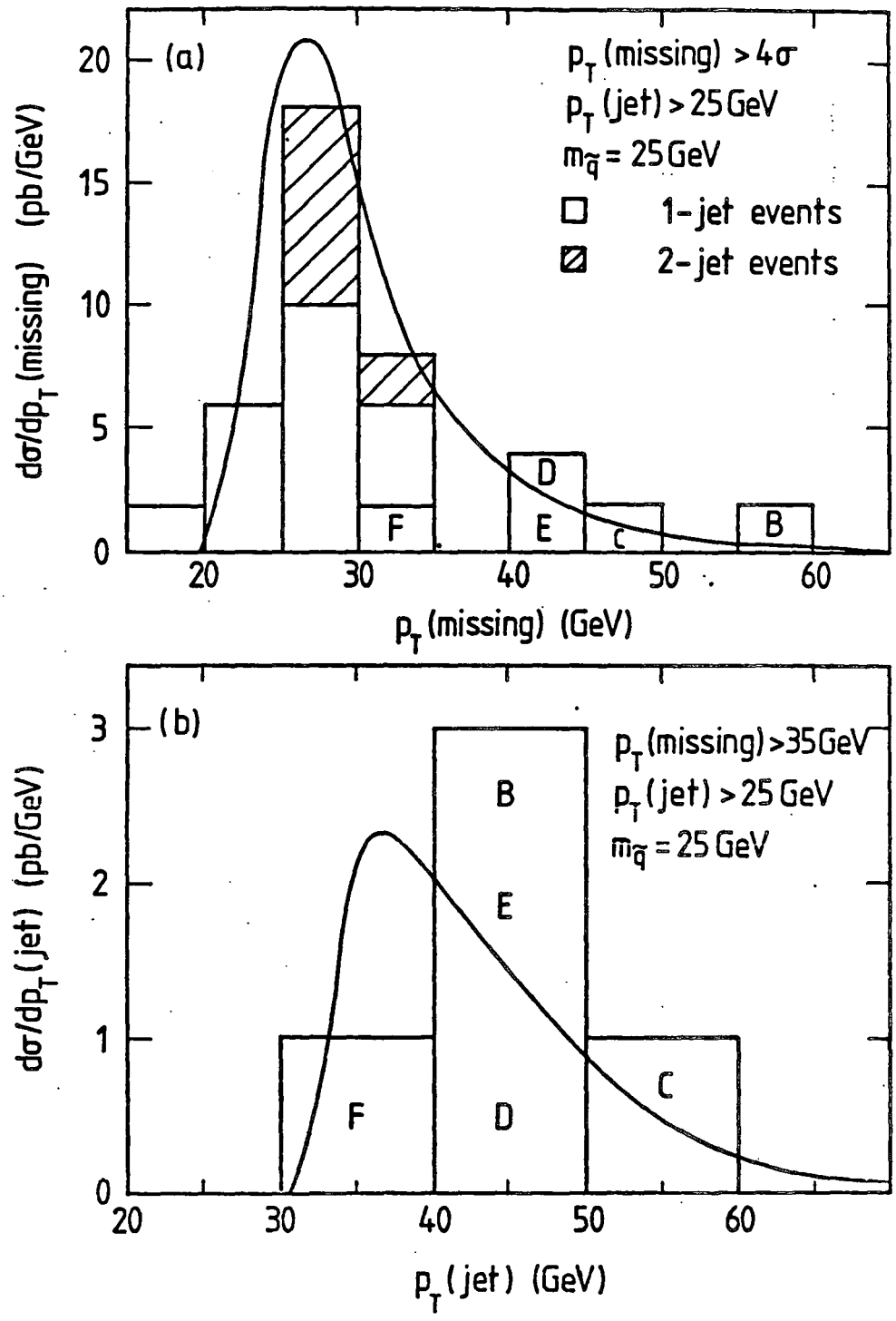

Figure 4.4
(a) The missing p_T distribution, and
(b) the jet p_T distribution (for 1-jet events with p_T(missing) > 35 GeV)
compared with the UA1 data, assuming no contribution from QCD jets. UA1 jets B-F are those with the largest p_T(missing); event A is omitted.

4.3 Further contributions to scalar quark production

In the previous Section we found that tha UA1 1- and 2-jet events could be explained in terms of QCD scalar quark pair production and decay (subprocess (4.3)); we fouund that the data constrained the scalar quark mass to be in the range 20 - 35 GeV. Here, we consider the effect of including scalar quark pair production via a W boson (see Fig. 4.5(a)),

$$\bar{q}_L\, q_L' \longrightarrow W \longrightarrow \tilde{\bar{q}}_L\, \tilde{q}_L' \longrightarrow \bar{q}\, q'\, \tilde{\gamma}\, \tilde{\gamma} \quad , \qquad (4.13)$$

and the Compton-like single scalar quark production (see Fig. 4.5(b)),

$$(\bar{q} \text{ or } q)\; g \longrightarrow (\tilde{\bar{q}} \text{ or } \tilde{q})\, \tilde{\gamma} \longrightarrow (\bar{q} \text{ or } q)\, \tilde{\gamma}\, \tilde{\gamma} \quad , \qquad (4.14)$$

on the possible range of values of scalar quark masses. (We neglect scalar quark pair production via a Z boson, as the total rate would be an order of magnitude down on that from subprocess (4.13) in $\bar{p}p$ collisions.)

Calculation of the cross-section for subprocess (4.13) involves the supersymmetric equivalent of the Kobyashi-Maskawa mixing matrix. Absence of flavour changing neutral currents require that this is equal to the Standard Model KM matrix[e] (i.e. $|U_{\tilde{u}\tilde{d}}|^2 = |U_{ud}|^2$). We find the differential cross-section for (4.13) to be

$$\frac{d\hat{\sigma}}{d\hat{t}} = \frac{e^4\, |U_{\tilde{u}\tilde{d}}|^4}{64\, \pi\, \hat{s}^2\, \sin^4\theta_W} \frac{\hat{t}\hat{u} - m_{\tilde{q}}^2\, m_{\tilde{q}'}^2}{(s-M_W^2)^2 + M_W^2\Gamma_W^2} \quad . \qquad (4.15)$$

We take $|U_{\tilde{u}\tilde{d}}|^2 = 1$, $M_W = 81$ GeV, $\Gamma_W = 3$ GeV, and normalise the cross-section to the experimentally observed $\sigma(W \longrightarrow e\bar{\nu}_e) = 0.53$ nb,[f] noting that

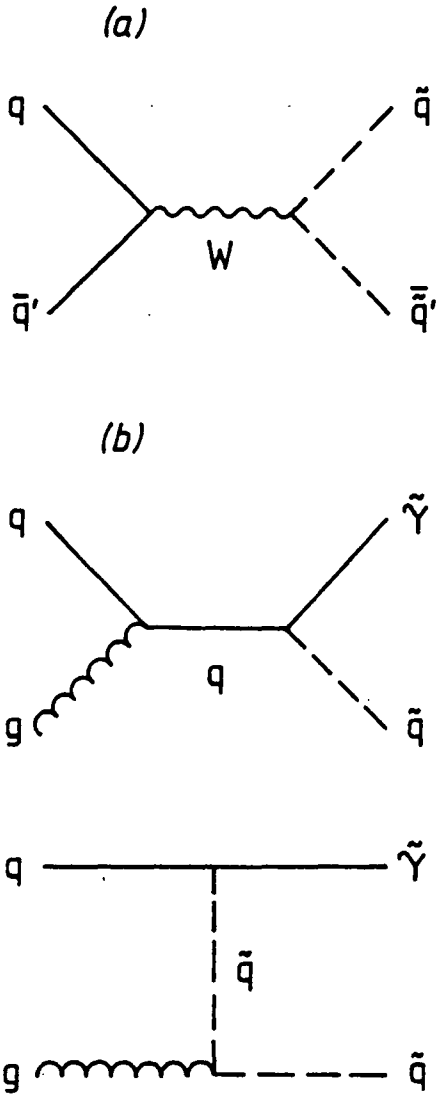

Figure 4.5
The first-order Feynman diagrams for
(a) $q_L \bar{q}_L' \longrightarrow W \longrightarrow \tilde{q}_L \bar{\tilde{q}}_L'$
(b) $q\, g \longrightarrow \tilde{q}\, \tilde{\gamma}$.

$$BR(W\longrightarrow\bar{\tilde{q}}\tilde{q}') = \frac{3}{2} BR(W\longrightarrow e\bar{\nu}_e)\ \lambda^{3/2}\left(1, \frac{m_{\tilde{q}}^2}{M_W^2}, \frac{m_{\tilde{q}'}^2}{M_W^2}\right) , \qquad (4.16)$$

where λ is the normal triangle function. The formula for the cross-section of subprocess (4.14) is[5,9]

$$\frac{d\hat{\sigma}(qg\longrightarrow\tilde{q}\tilde{\gamma})}{d\hat{t}} = \frac{\pi\alpha_s\,\alpha e_q^2}{3\hat{s}^2}$$

$$\times\left\{\frac{m_{\tilde{\gamma}}^2-\hat{t}}{\hat{s}} + \frac{(\hat{u}-m_{\tilde{\gamma}}^2)(\hat{u}+m_{\tilde{q}}^2)}{(\hat{u}-m_{\tilde{q}}^2)^2} - \frac{\hat{s}(\hat{u}+m_{\tilde{\gamma}}^2)+2\xi(m_{\tilde{\gamma}}^2-\hat{u})}{\hat{s}(\hat{u}-m_{\tilde{q}}^2)}\right\}, \qquad (4.17a)$$

$$\hat{\sigma}(qg\longrightarrow\tilde{q}\tilde{\gamma}) = \frac{\pi\alpha_s\,\alpha e_q^2}{3\hat{s}^2}\left\{\frac{S}{2}\left(1+\frac{7\xi}{\hat{s}}\right) + 2\left(m_{\tilde{q}}^2-m_{\tilde{\gamma}}^2+\frac{\xi^2}{\hat{s}}\right)\ln\left(\frac{\xi+\hat{s}-S}{\xi+\hat{s}+S}\right)\right\}, \qquad (4.17b)$$

where $\xi = m_{\tilde{q}}^2 - m_{\tilde{\gamma}}^2$, $S = \sqrt{\hat{s}}\,\sqrt{\hat{s}-4m_{\tilde{q}}^2}$.

In our Monte Carlo calculations we again simulate the UA1 experimental triggers and cuts, viz: a jet trigger of $p_T(\text{jet}) > 25$ GeV, a jet recognition cut of $p_T(\text{jet}) > 12$ GeV, quark jets coalesce to form a single jet if $[(\Delta\phi)^2 + (\Delta y)^2]^{1/2} < 1$, and a missing momentum cut of either 35 GeV or 4σ, with $\sigma = 0.7\sqrt{E_T}$ where $E_T = \sum E_T(\text{parton}) + 20$ GeV.

In Fig. 4.6 we show the cross-sections for subprocesses (4.13) and (4.14) as functions of the scalar quark mass. The effects of the experimental cuts are also shown. In Fig. 4.6(a), the dashed lines represent the 1-jet cross-section; the difference between this and the total cross-section is due to events with 2 visible jets. Although the total event rates for the two subprocesses are comparable, many more W events pass the cuts, due to the Jacobian peak in the transverse momentum in the scalar quark.

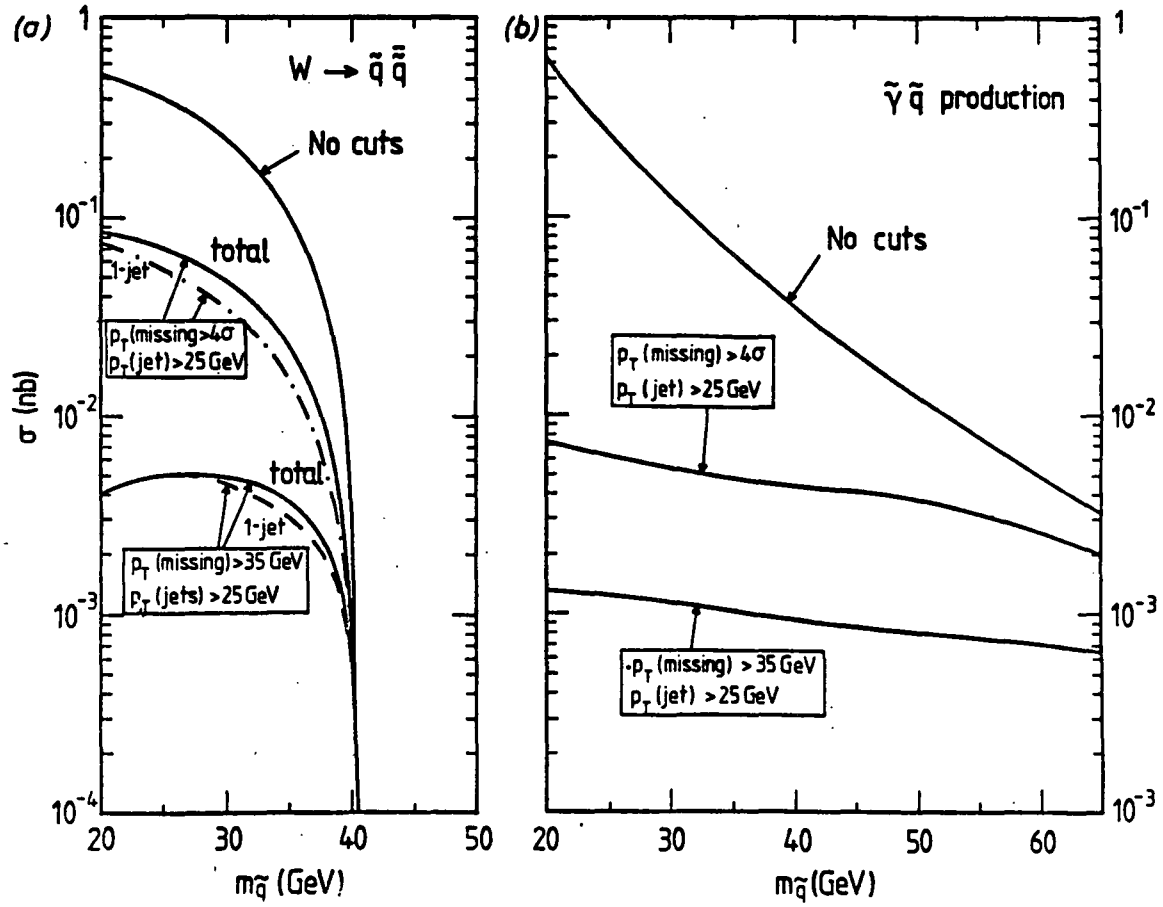

Figure 4.6
The cross-sections for
(a) $W \longrightarrow \tilde{q}_L \bar{\tilde{q}}_L'$
(b) $\tilde{q}\,\tilde{\gamma}$ production
as a function of the scalar quark mass. The effect of imposing the missing momemntum cuts p_T(missing) > 4σ or 35 GeV is also shown. The dashed lines in (a) represent the 1-jet cross-sections.

Figure 4.7 shows the total cross-section for both these subprocesses and the QCD fusion (subprocess (4.3)) of Section 4.2 as a function of the scalar quark mass. It can be seen from a comparison of Figs 4.3 and 4.7 that the largest contribution from the additional subprocesses is at low squark mass. However, the uncertainties inherent in the calculation are such that more restrictive bounds on the scalar quark mass than those given in Section 4.2 (20 GeV $< m_{\tilde{q}} <$ 35 GeV) are not justified.

In their analysis of the QCD background, UA1 introduce a second set of cuts:[12] $p_T(\text{missing}) > \max\{2\sigma, 15\ \text{GeV}\}$ and $\cos\phi > -0.8$, together with isolation cuts on $p_T(\text{missing})$. We find that all our events passing the 4σ cut survive this set of cuts.

4.4 Constraining the gluino mass

Having constrained the mass of the scalar quark, we now make further use of the UA1 data to place a lower bound on the gluino mass within our scenario. This we do by considering the Compton-like scalar quark-gluino production subprocess (see Fig. 4.8)

$$(\bar{q} \text{ or } q)\ g \longrightarrow (\bar{\tilde{q}} \text{ or } \tilde{q})\ \tilde{g} \longrightarrow (\bar{q} \text{ or } q)\ \bar{q}\ q\ \tilde{\gamma}\ \tilde{\gamma}\ , \qquad (4.18)$$

with a (most likely) scalar quark mass of 25 GeV. This mechanism can give rise to events with as many as 3 visible jets. The cross-section for this subprocess is[5,8]

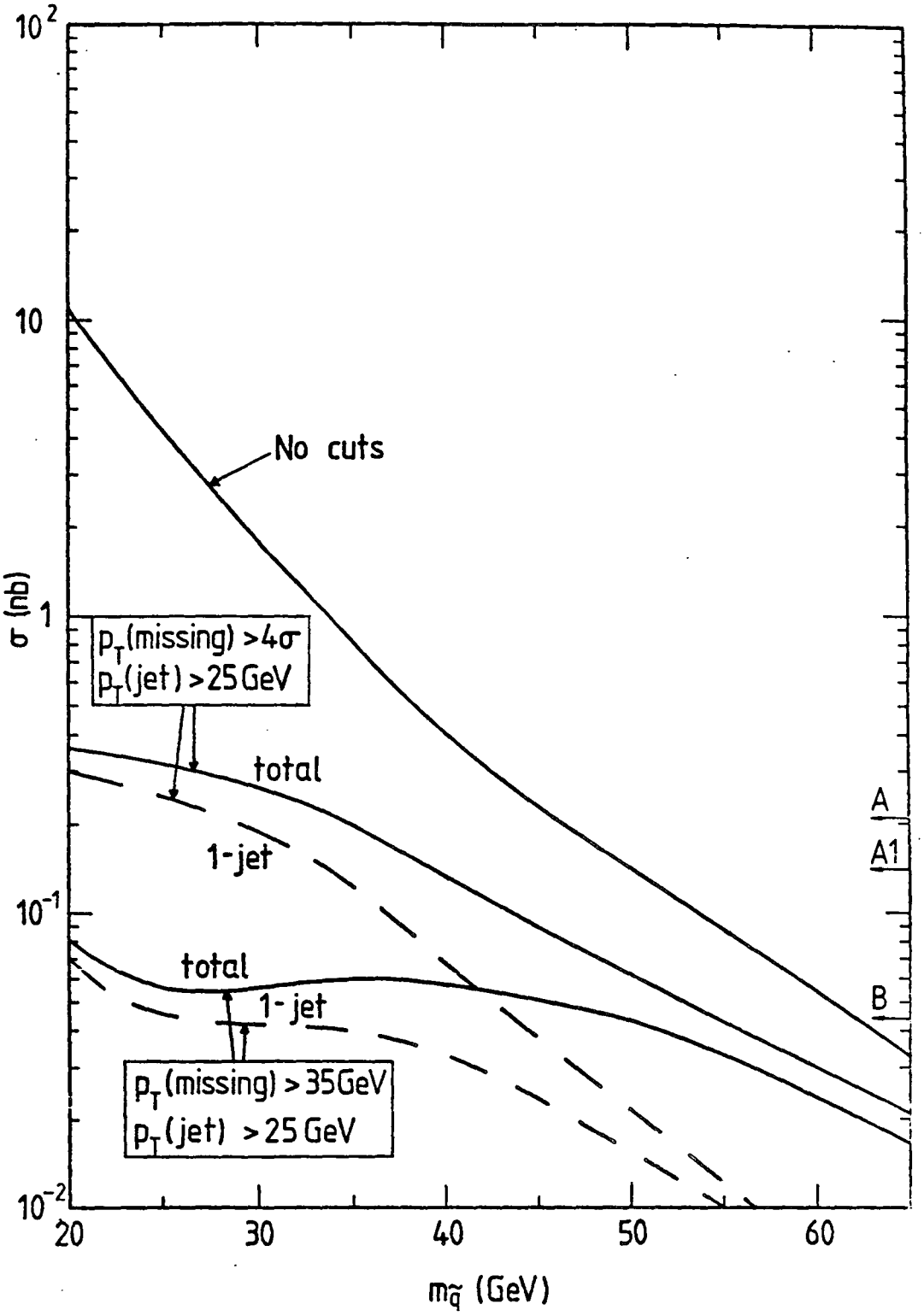

Figure 4.7
The combined cross-sections for processes (4.3) (Fig. 4.3), (4.13) (Fig. 4.6(a)), and (4.14) (Fig. 4.6(b)) as a function of the scalar quark mass at $\sqrt{s}$ = 540 GeV. The effect of imposing the missing momentum cuts is also shown, where the dashed curve represents the fraction of the total events with a single visible jet. The UA1 event rates are shown to the right of the figure, as in Fig. 4.3.

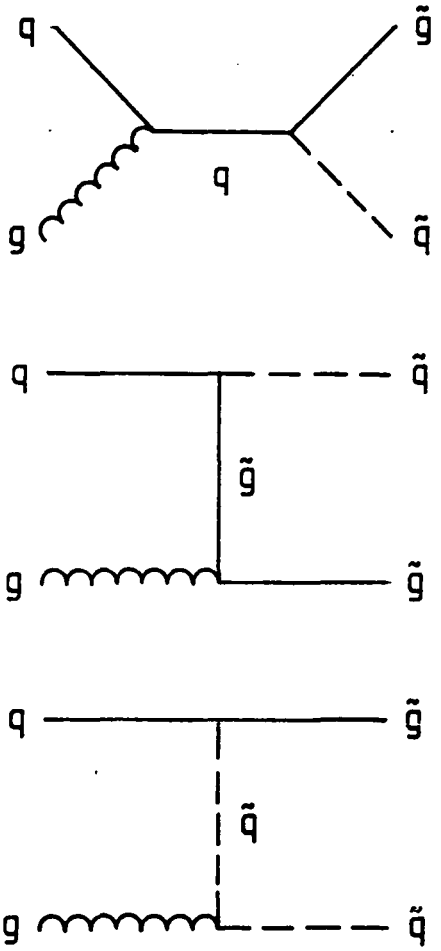

Figure 4.8
The first-order Feynman diagrams for $q\,g \longrightarrow \tilde{q}\,\tilde{g}$.

$$\frac{d\hat{\sigma}(qg\rightarrow\tilde{q}\tilde{q}\tilde{g})}{d\hat{t}} = \frac{\pi\alpha_s^2}{\hat{s}^2}\left\{\frac{4(m_{\tilde{g}}^2-\hat{t})}{9\hat{s}} + \frac{(m_{\tilde{g}}^2-\hat{t})\hat{s}+2m_{\tilde{g}}^2(m_{\tilde{q}}^2-\hat{t})}{(\hat{t}-m_{\tilde{g}}^2)^2}\right.$$

$$+\frac{4(\hat{u}-m_{\tilde{g}}^2)(\hat{u}+m_{\tilde{q}}^2)}{9(\hat{u}-m_{\tilde{q}}^2)^2} - \frac{(\hat{s}-\xi)(\hat{t}-m_{\tilde{q}}^2)-m_{\tilde{g}}^2\hat{s}}{\hat{s}(\hat{t}-m_{\tilde{g}}^2)} + \frac{\hat{s}(\hat{u}+m_{\tilde{g}}^2)+2\xi(m_{\tilde{g}}^2-\hat{u})}{18\hat{s}(\hat{u}-m_{\tilde{q}}^2)}$$

$$\left.+\frac{(m_{\tilde{q}}^2-\hat{t})(\hat{t}+2\hat{u}+m_{\tilde{g}}^2)+(\hat{t}-m_{\tilde{g}}^2)(\hat{s}+2\hat{t}-2m_{\tilde{q}}^2)+(\hat{u}-m_{\tilde{g}}^2)(\hat{t}+m_{\tilde{g}}^2+2m_{\tilde{q}}^2)}{4(\hat{t}-m_{\tilde{g}}^2)(\hat{u}-m_{\tilde{q}}^2)}\right\} \qquad (4.19a)$$

$$\hat{\sigma}(qg\rightarrow\tilde{q}\tilde{q}\tilde{g}) = \frac{\pi\alpha_s^2}{\hat{s}^2}\left\{\frac{S}{9}\left(\frac{32\xi}{\hat{s}}-7\right)+\left(\frac{8}{9}-\frac{\xi^2}{9\hat{s}}-\frac{\xi(m_{\tilde{q}}^2+m_{\tilde{g}}^2)}{\hat{s}}\right)\ln\left[\frac{\xi+\hat{s}-S}{\xi+\hat{s}+S}\right]\right.$$

$$\left.+\left(\hat{s}-2\xi+\frac{\xi^2}{\hat{s}}+\frac{\xi(m_{\tilde{q}}^2+m_{\tilde{g}}^2)}{\hat{s}}\right)\ln\left[\frac{\xi-\hat{s}-S}{\xi-\hat{s}+S}\right]\right\}, \qquad (4.19b)$$

where $\xi = m_{\tilde{q}}^2 - m_{\tilde{g}}^2$, $S = \sqrt{\hat{s}}\sqrt{\hat{s}-4m_{\tilde{q}}^2}$.

Figure 4.9 shows the cross-section for this subprocess as a function of the gluino mass before and after the missing momentum cuts. In this case the dashed curves represent the cross-sections for events with either 2 or 3 visible jets. For a gluino mass of 60 GeV or less, we see that at least O(20) 2- or 3-jet events pass the 4σ cut in p_T(missing) (in addition to the O(7) 2-jet events from scalar quark pair production). Even allowing for the uncertainties in the absolute normalisation of the calculation, this is excluded by the data. Thus, we put a lower bound of O(60) GeV on the gluino mass.

Although the curve shown is for a scalar quark mass of 25 GeV, varying the mass over the allowed range (20 - 35 GeV) does not change the conclusions. Unfortunately, the low statistics mean that the cleaner cut of p_T(missing) > 35 GeV does not give a more stringent bound. The experimental confirmation of 3-jet

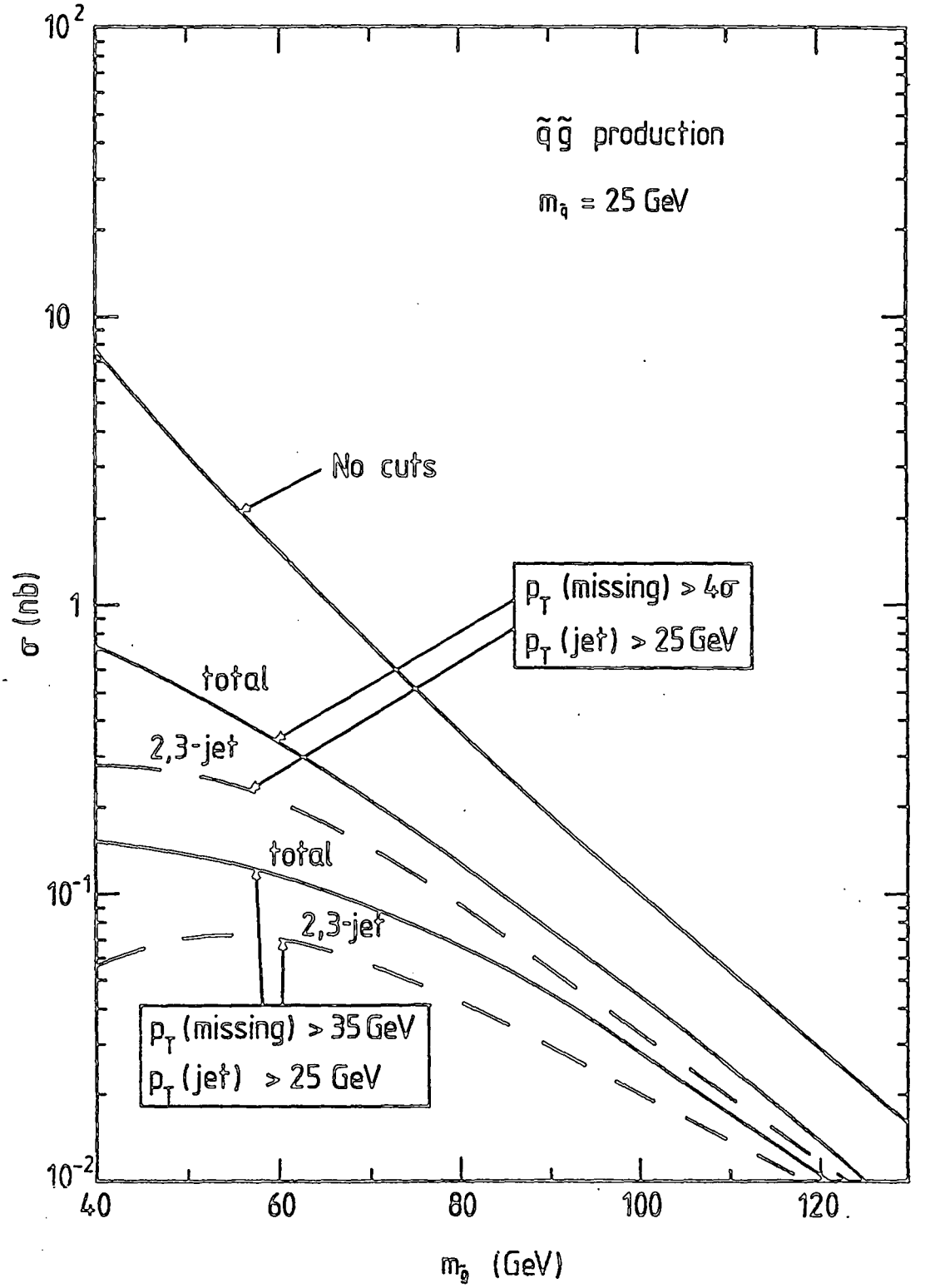

Figure 4.9
The $\tilde{q}\tilde{g}$ production cross-section as a function of the gluino mass at $\sqrt{s}$ = 540 GeV. The scalar quark mass is taken to be 25 GeV. The effect of imposing the missing p_T cuts is also shown, where the dashed curve represents the fraction of events with 2 or 3 visible jets.

events with p_T(missing) > 35 GeV would be very informative. We note, finally, that a gluino mass of O(60) GeV means that gluino pair production (subprocess (4.5))[10] would contribute 2 or 3 events at most to the UA1 data sample.

4.5 Other supersymmetric "monojet" scenarios

Apart from the work presented in this Chapter, a number of other supersymmetric scenarios have been proposed[10-14] to account for the UA1 monojet and multijet events with large missing p_T. These naturally fall into two classes characterised by the mass spectrum, which determines the dominant decay modes.

In those we group together as Class I, we have $m_{\tilde{g}} > m_{\tilde{q}}$ and the dominant decay modes are $\tilde{q} \longrightarrow q\tilde{\gamma}$ and $\tilde{g} \longrightarrow \bar{q}q\tilde{\gamma}$ (Eq. (4.1)); the scenario described in this chapter obviously falls into this class. The authors of Refs (10,11) have also attempted to describe the UA1 large missing p_T data in terms of scalar quark pair production

$$(\bar{q}q \text{ or } gg) \longrightarrow \tilde{q}\,\tilde{q} \longrightarrow \bar{q}\,q\,\tilde{\gamma}\,\tilde{\gamma} \quad . \qquad (4.20)$$

Barger et al.[11] assume five degenerate scalar quark flavours (and degenerate left- and right-handed partners), and use the calculated 1- and 2-jet cross-sections to put a lower bound on the scalar quark mass by comparison with the data. They obtain a bound of $m_{\tilde{q}} > O(40)$ GeV. Given the uncertainties inherent in any such QCD calculation, which are at least a factor of 2 in the cross-section, these bounds are at best approximate. The uncertainty in the number of degenerate scalar quarks is

approximately multiplicative; allowing for this, and for a different choice of α_s, the work of Barger et al. is comparable with that in this Chapter.

A similar bound is found by Ellis and Kowalski[10], who also assume five scalar quark flavours degenerate in mass. Their analysis depends on the accurate subtraction by UA1 of the QCD background which fakes missing p_T events in the region p_T^2(missing) < 1000 GeV2. The use of an astimate of a large background at lower values of p_T(missing) to rigorously exclude events produced from relatively low mass scalar quark pairs must necessarily involve large uncertainties.

In the Class II scenarios the mass spectrum is reversed, i.e. $m_{\tilde{g}} < m_{\tilde{q}}$, and the dominant decays are now

$$\tilde{q} \longrightarrow q\,\tilde{g}\ , \qquad (4.21a)$$

$$\tilde{g} \longrightarrow \bar{q}\,q\,\tilde{\gamma}\ . \qquad (4.21b)$$

Three mechanisms within this class have been considered.

First, Barger et al.[12] consider a light gluino nearly degenerate with the photino and a scalar quark of mass O(100) GeV, produced via the Compton-like subprocess

$$(\bar{q} \text{ or } q)\ g \longrightarrow (\bar{\tilde{q}} \text{ or } \tilde{q})\ \tilde{g} \longrightarrow (\bar{q} \text{ or } q)\ \tilde{\gamma}\ \tilde{g}\ . \qquad (4.22)$$

This explanation relies on a long gluino life-time in order to evade current experimental bounds on the gluino mass, but the necessary approximate degeneracy of $m_{\tilde{g}}$ and $m_{\tilde{\gamma}}$ seems rather contrived.

The second mechanism[10,13] is based on gluino pair

production (subprocess (4.5)), with $m_{\tilde{g}}$ = O(40) GeV. Monojet and 2-jet events from this mechanism contain a significant contribution from the coalescence of final state partons; such jets would be broader than seems to be the case in the UA1 data.

The third mechanism[14] involves the Compton-like scattering of light gluinos, intrinsic to the proton, off quarks to form heavy scalar quarks ($m_{\tilde{q}}$ = O(100) GeV),

$$(\bar{q} \text{ or } q)\ \tilde{g} \longrightarrow (\bar{\tilde{q}} \text{ or } \tilde{q}) \longrightarrow (\bar{q} \text{ or } q)\ \bar{q}\, q\, \tilde{\gamma}\ . \qquad (4.23)$$

This mechanism would give rise to events with up to 3 visible jets.

Supersymmetry scenarios belonging to Class I or II may be distinguished experimentally by relaxing the jet recognition criterion from 12 Gev to 8 GeV. In Class II gluino pair production leads to a four quark final state, giving more potential jets than in Class I, where scalar quark pair production has at most 2 quarks in the final state. The relaxed jet criterion increases the relative number of events with 2 or more visible jets; this is shown for scalar quark production (via subprocesses (4.3), (4.13), and (4.14)) in Table 4.1. There are experimental difficulties in recognising jets of low transverse momentum, but it may be possible to use such an analysis to distinguish between scalar quark and gluino pair production.

Table 4.1

Predictions for the numbers, N, of 1- and 2-jet events for subprocesses (4.3), (4.13), and (4.14) for an integrated luminosity of 113 nb^{-1} at $\sqrt{s}$ = 540 GeV. The effect of varying the jet recognition criterion is shown for missing p_T cuts of 4σ and 35 GeV (in brackets).

	$m_{\tilde{q}}$ = 25 GeV		$m_{\tilde{q}}$ = 35 GeV	
	p_T(jet) > 12	p_T(jet) > 8	p_T(jet) > 12	p_T(jet) > 8
N(1-jet)	27 (4.5)	20 (3.4)	14 (4.5)	10 (3.4)
N(2-jet)	8 (1.1)	15 (2.2)	8 (2.3)	12 (3.4)

4.6 Conclusions

We have found that, within theoretical and experimental uncertainties, the UA1 1- and 2-jet events with large missing p_T can be explained in terms of scalar quark QCD pair production and electromagnetic decay. The dominant configuration is that the harder jet comes from one $\tilde{q} \longrightarrow q\tilde{\gamma}$ decay and the bulk of the missing p_T is due to the photino from the other decay. Comparison with the data constrains the scalar quark mass to lie in the range 20 GeV $< m_{\tilde{q}} <$ 35 GeV, for two degenerate scalar quark flavours (and degenerate left- and right-handed partners), assuming that the gluino is sufficiently heavy to suppress $\tilde{q}\tilde{g}$ and $\tilde{g}\tilde{g}$ production.

We find that the additional contribution of scalar quark production from $W \longrightarrow \bar{\tilde{q}}\tilde{q}'$ and $\tilde{q}\tilde{\gamma}$ production is small, except for $m_{\tilde{q}} \sim 20$ GeV, and does not allow us to further constrain the scalar quark mass. Within our scenario, we used the UA1 data to constrain the gluino mass by considering qg production; we found a lower bound of $m_{\tilde{g}} = O(60)$ GeV.

There are several distinct supersymmetry scenarios for UA1 jet-plus-large-missing-p_T events. We note that by reducing the experimental jet recognition criterion it may be possible to distinguish between different scenarios.

Note

Since this work was completed, the emphasis has shifted from supersymmetric explanations of the UA1 jet-plus-large-missing-p_T events; it now appears that they may well be explicable in terms of Standard Model processes. Nevertheless, calculations such as those above may be used to put lower bounds on the masses of scalar quarks, gluinos, &c. Recently, de Rújula[115] has presented a comprehensive (and droll) review of the many different supersymmetric "monojet" scenarios, of which those discussed in Section 4.5 above are just a few, to which the interested reader is directed.

Chapter 5

SCALAR ELECTRON AND ZINO PRODUCTION

ON AND BEYOND THE Z RESONANCE IN $e^+ e^-$ ANNIHILATION

Deeper in the wood ...
who can tell what bizarre landscapes are to be found?
- from Mythago Wood *by Robert Holdstock*

5.1 Introduction

Recall from Chapter 1 that, if supersymmetry exists, both the left- and right-handed helicity states of the charged leptons (l_L^-, l_R^-) have scalar superpartners ($\tilde{l}_L^-$, $\tilde{l}_R^-$). In general, due to supersymmetry breaking, the mass eigenstates ($\tilde{l}_1^-$, $\tilde{l}_2^-$) are formed by (model dependant) linear combinations of the electroweak interaction states. There are constraints on the mass splitting, $m_{\tilde{l}} - m_{\tilde{\nu}}$, and in most models it is a good approximation to assume that the scalar electron mass eigenstates are degenerate.[1] Thus we assume that $\tilde{e}_1 = \tilde{e}_L$ and $\tilde{e}_2 = \tilde{e}_R$, and $m_{\tilde{e}} = m_{\tilde{e}_R} = m_{\tilde{\nu}}$.

Similarly, the mass eigenstates of the neutral gauginos (or netralinos), the superpartners of the netral gauge bosons, are also mixtures of the weak eigenstates: the photino, the zino and the higgsinos. Here we assume, for simplicity, that this mixing is minimal and, thus, the photino, $\tilde{\gamma}$, and zino, $\tilde{Z}$, are mass eigenstates. We take the photino to be light ($m_{\tilde{\gamma}}$ < few GeV) and investigate the effects of varying the mass of the zino.

Because scalar leptons interact electromagnetically, attention has focussed on their possible production in e^+e^- collisions.[2-7] For instance, if $m_{\tilde{\nu}}$ were less than the e beam

energies ($\sqrt{s}/2$) then

$$e^+ e^- \longrightarrow \tilde{e}^+ \tilde{e}^- \ , \qquad (5.1)$$

with subsequent electromagnetic decays of the scalar electrons, $\tilde{e} \longrightarrow e\tilde{\gamma}$, with a branching ratio which we will take to be 100%. (If the weak gauginos, $\tilde{W}$, $\tilde{Z}$, are lighter than the scalar electron, then the decays $\tilde{e} \longrightarrow \tilde{W} \nu_e$, $\tilde{e} \longrightarrow e \tilde{Z}$ can occur, and the e/m branching ratio will be reduced.) As stated in Chapter 1, we will assume that the photino is the lightest supersymmetric particle, and that it is stable. It interacts weakly with matter, and so will escape detection and appear as missing energy. Thus, the signature for process (5.1) is the production of acoplanar e^+e^- pairs in events where about half the energy is missing.

Several authors[3-7] have pointed out that the presence of scalar electrons with masses larger than the beam energy can be investigated, provided the photino is light. The first method is "single" scalar electron production,

$$e^+ e^- \longrightarrow \tilde{e}^{\pm} e^{\mp} \tilde{\gamma} . \qquad (5.2)$$

The second is

$$e^+ e^- \longrightarrow \tilde{\gamma} \tilde{\gamma} \gamma , \qquad (5.3)$$

where the extra photon is required to tag the event, just like the neutrino counting experiments, $e^+ e^- \longrightarrow \bar{\nu} \nu \gamma$. The cross section for process (5.3) involves a scalar electron propagator and so is sensitive to $m_{\tilde{e}}$. The most recent bounds on $m_{\tilde{e}}$ arising from the non-observation of these processes are $m_{\tilde{e}} > 26$ GeV from the search[8] for the direct production process, (5.2), and $m_{\tilde{e}} > 51$ GeV from the absence[9] of process (5.3). Both bounds assume a zero mass photino and that $\tilde{e}_L$ and $\tilde{e}_R$ are degenerate in mass.

In this Chapter we study the production of scalar electrons at e^+e^- colliders (SLC and LEP-I; see Chapter 2) designed to operate on or just above the Z resonance. In Section 5.2 we calculate the cross sections for on-shell scalar electron pair production, $e^+ e^- \longrightarrow \tilde{e}^+ \tilde{e}^-$, and off-shell production, $e^+ e^- \longrightarrow e^+ e^- \tilde{\gamma} \tilde{\gamma}$. We consider the relative importance of all the competing Feynman diagrams, particularly for the highest scalar electron masses experimentally accesible. In Section 5.3 we investigate the experimental signatures for scalar electrons and present the expected distributions for the process $e^+ e^- \dashrightarrow e^+ e^- \tilde{\gamma} \tilde{\gamma}$. We show how these distributions may reveal, not only the scalar electron, but also a zino of mass $m_{\tilde{z}} < \sqrt{s}$. Our results are summarised in Section 5.4.

5.2 Cross-sections for scalar electron production

The diagrams which are expected to dominate $e^+ e^- \longrightarrow \tilde{e}^+ \tilde{e}^-$ are shown in Fig. 5.1. Since the electron is essentially massless, the e-e-Higgs and e-$\tilde{e}$-higgsino couplings are vanishingly small, and so the Higgs and higgsino exchange contributions to the cross-section can be neglected.

Both s- and t-channel exchange diagrams contribute to

$$e^+ e^- \longrightarrow \tilde{e}_i^+ \tilde{e}_i^- \qquad (i = L \text{ or } R), \tag{5.4}$$

but only t-channel diagrams contribute to

$$e^+ e^- \longrightarrow \tilde{e}_i^+ \tilde{e}_j^- \qquad (i \neq j;\ i,j = L \text{ or } R). \tag{5.5}$$

Only the s-channel diagrams can contribute to $\tilde{\mu}$ ($\tilde{\tau}$, ...) pair

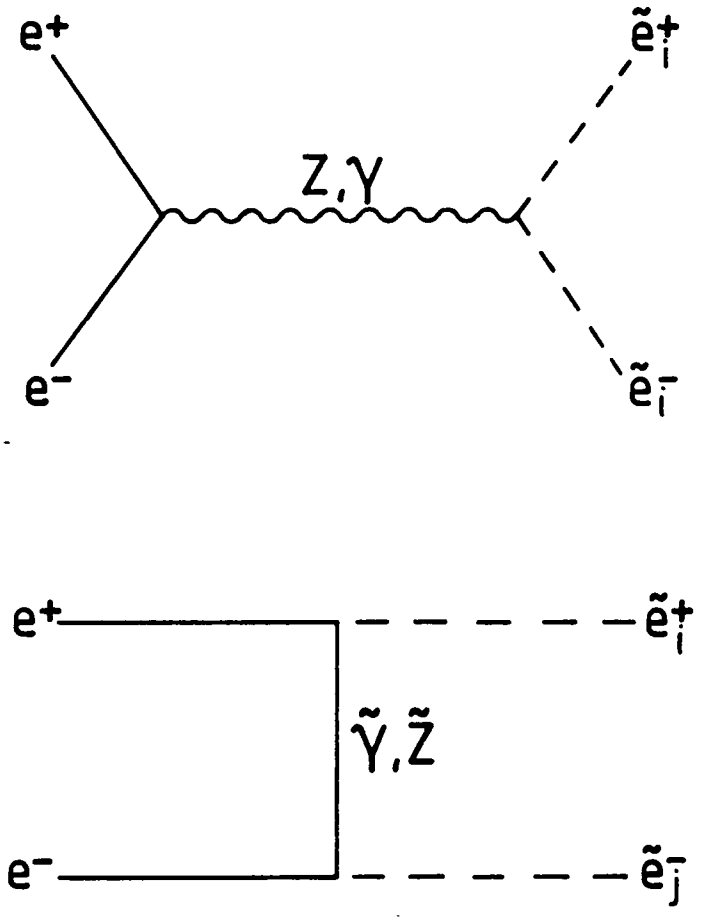

Figure 5.1
The dominant first-order Feynman diagrams for $e^+ e^- \longrightarrow \tilde{e}^+ \tilde{e}^-$.

production in e^+e^- annihilation, and hence only $e^+ e^- \longrightarrow \tilde{\mu}_i^+ \tilde{\mu}_i^-$ is possible.

The differential cross-sections for processes (5.4) and (5.5) were evaluated using Feynman rules given in Ref. (10). We find

$$\frac{d\sigma_{ii}}{dt} = \frac{\pi\alpha^2}{s^2} (ut - m_{\tilde{e}}^4)\, \rho_{ii}(s,t) \qquad (5.6a)$$

where

$$\rho_{ii}(s,t) = \frac{g^{\langle a\rangle}}{s^2} + \sum_{a=\tilde{\gamma},\tilde{z}} \left[\frac{g_a^{\langle x\rangle}}{s(t-m_a^2)} + \frac{g_a^{\langle t\rangle}}{(t-m_a^2)^2} \right] + \frac{g_{\tilde{\gamma}\tilde{z}}^{\langle t\rangle}}{(t-m_{\tilde{\gamma}}^2)(t-m_{\tilde{z}}^2)} , \qquad (5.6b)$$

and for process (5.5), with only , Z exchange,

$$\frac{d\sigma_{ij}}{dt} = \frac{\pi\alpha^2}{s} \left\{ \sum_{a=\tilde{\gamma},\tilde{z}} \left[\frac{f_a\, m_a^2}{(t-m_a^2)^2} \right] + \frac{f_{\tilde{\gamma}\tilde{z}}\, m_{\tilde{\gamma}}\, m_{\tilde{z}}}{(t-m_{\tilde{\gamma}}^2)(t-m_{\tilde{z}}^2)} \right\}. \qquad (5.7)$$

The coefficients $g_a^{\langle m\rangle}$ and f_a are given in Table 5.1. The total cross-sections are found by integration between the kinematic limits $t_{1,2} = m_{\tilde{e}}^2 - (s-S)/2$, where $S = \sqrt{s}\,\sqrt{s-4m_{\tilde{e}}^2}$, yielding

$$\sigma_{ii} = \frac{\pi\alpha^2}{s^2} \left\{ g^{\langle a\rangle} \frac{S^3}{6\,s^2} + \sum_{a=\tilde{\gamma},\tilde{z}} \left[\frac{g_a^{\langle x\rangle}}{s} [\eta_a \lambda_a - S(s/2 + \delta_a)] + g_a^{\langle t\rangle} [(s + 2\delta_a)\lambda_a - 2S] \right] + g_{\tilde{\gamma}\tilde{z}}^{\langle t\rangle} \frac{\eta_{\tilde{\gamma}} \lambda_{\tilde{\gamma}} - \eta_{\tilde{z}} \lambda_{\tilde{z}}}{m_{\tilde{\gamma}}^2 - m_{\tilde{z}}^2} \right\}, \qquad (5.8)$$

and

$$\sigma_{ij} = \frac{\pi\alpha^2}{s} \left\{ \sum_{a=\tilde{\gamma},\tilde{z}} \left[\frac{f_a\, m_a^2\, S}{\eta_a} \right] - f_{\tilde{\gamma}\tilde{z}} \frac{m_{\tilde{\gamma}}\, m_{\tilde{z}}}{m_{\tilde{\gamma}}^2 - m_{\tilde{z}}^2} (\lambda_{\tilde{\gamma}} - \lambda_{\tilde{z}}) \right\}, \qquad (5.9)$$

where $\delta_a = m_a^2 - m_{\tilde{e}}^2$, $\lambda_a = \ln[(s+S+2\delta_a)/(s-S+2\delta_a)]$, and $\eta_a = s\cdot m_a^2 + \delta_a^2$. These results agree with those of others.[11]

Table 5.1

The coefficient $g_\sigma^{(m)}$ and f_σ of Eqs (5.6) and (5.7). L and R are the left- and right-handed lepton couplings: $L = -1 + 2\sin^2\theta_W$, $R = 2\sin^2\theta_W$; $w = (\sin\theta_W \cdot \cos\theta_W)^{-1}$, and D_z is the Z-propagator: $D_z = (s - M_z^2) + iM_z\Gamma_z$. Note that if 1 = e only $g^{(*)}$ is non-zero.

$$g^{(*)} = 4 + {}^1/_2 \cdot w^2 \cdot (L+R)^2 \cdot \mathrm{Re}(s/D_z) + {}^1/_{16} \cdot w^4 \cdot (L^2+R^2)^2 \cdot s^2/|D_z|^2$$

$$g_\gamma^{(\times)} = 4 + {}^1/_2 \cdot w^2 \cdot (L^2+R^2) \cdot \mathrm{Re}(s/D_z)$$

$$g_Z^{(\times)} = {}^1/_2 \cdot w^2 \cdot (L^2+R^2) + {}^1/_8 \cdot w^4 \cdot (L^4+R^4) \cdot \mathrm{Re}(s/D_z)$$

$$g_\gamma^{(t)} = 2$$

$$g_{\gamma Z}^{(t)} = {}^1/_2 \cdot w^2 \cdot (L^2+R^2)$$

$$g_Z^{(t)} = {}^1/_{16} \cdot w^4 \cdot (L^4+R^4)$$

$$f_\gamma = 2$$

$$f_{\gamma Z} = w^2 \cdot L \cdot R$$

$$f_Z = {}^1/_8 \cdot w^2 \cdot L^2 \cdot R^2$$

Figure 5.2 shows σ_{ii} (summed over i=L,R) as a function of $\sqrt{s}$ for scalar leptons of mass 30 GeV, and for Γ_Z = 3 GeV. For the process $e^+ e^- \longrightarrow \tilde{e}_i^+ \tilde{e}_i^-$ we see that the s-channel contribution, equivalent to $\sigma(e^+e^- \longrightarrow \tilde{\mu}_i^+ \tilde{\mu}_i^-)$, is only dominant in the region of the Z resonance. Increasing the photino mass (to, say, 5 GeV) suppresses the t-channel contribution (by ~ 10 pb), whereas the cross-section is relatively insensitive to the value of $m_{\tilde{\gamma}}$. As may be expected, the Z exchange is the dominant s-channel process, and $\tilde{\gamma}$-exchange dominates the t-channel. The cross-section σ_{ij} is extremely small ($O(10^{-3})$ pb) for $m_{\tilde{\gamma}}$ = 0 and all $\sqrt{s}$ ($> 2m_{\tilde{e}}$), and rises to only ~ 1 pb for $m_{\tilde{\gamma}}$ = 5 GeV (c.f. the results of Ref. (12)). We will therefore neglect this process.

On the Z resonance (i.e. at $\sqrt{s}$ = 93 GeV) the t-channel and st-interference contribution to scalar electron pair production amounts to only ~ 40 pb or ~ 10% of the total. On the other hand, off-resonance the t-channel processes dominate, contributing (~ 80%) ~ 90% of the total cross-section at $\sqrt{s}$ = (102 GeV) 111 GeV. These energies should be attainable at SLC or LEP-I, and so pair production of scalar electrons with masses greater than $M_Z/2$ will be feasible at these machines. Since only the s-channel diagrams contribute to $\tilde{\mu}(\tilde{e}, \ldots)$ pair production, these cross-sections will be suppressed by about an order-of-magnitude away from the Z resonance, but the off-resonance cross-sections may still give an observable event rate.

We now consider the effect of allowing the scalar electrons to go off-shell in the process

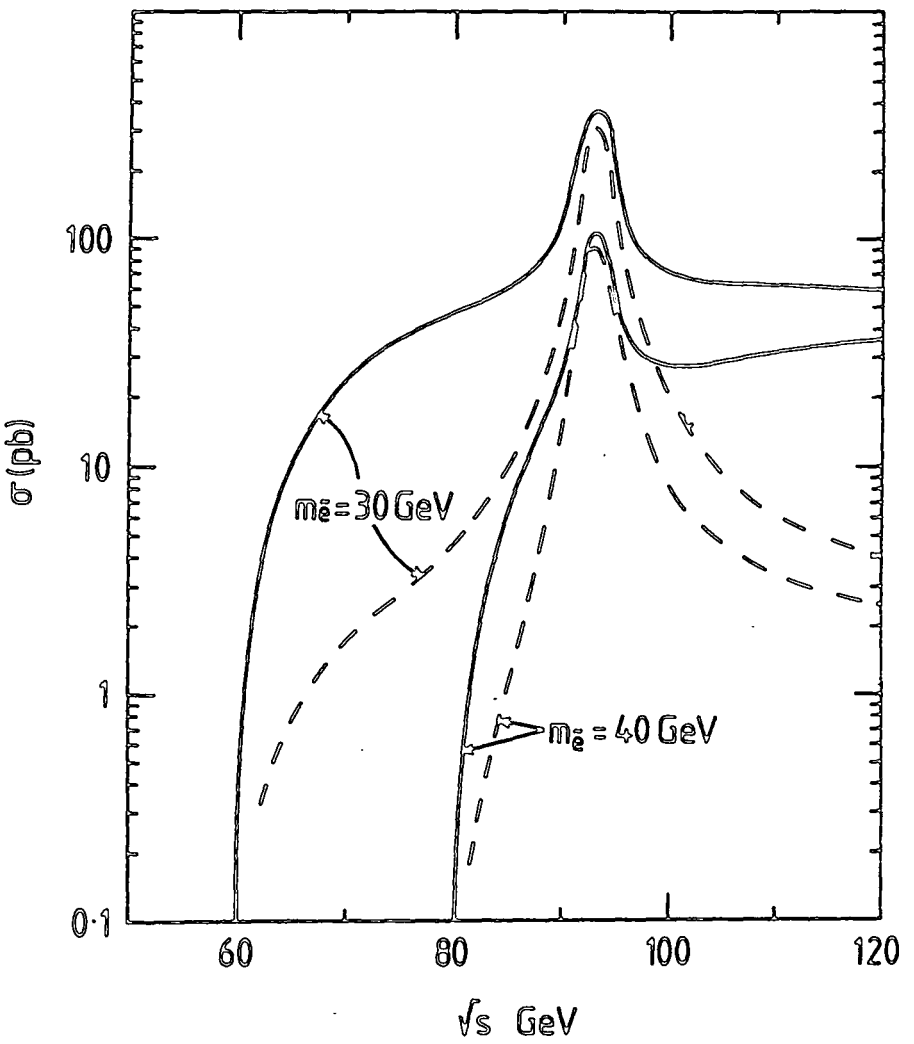

Figure 5.2
The cross-section for $e^+ e^- \longrightarrow \tilde{e}^+ \tilde{e}^-$ as a function of the total c.m. energy, $\sqrt{s}$, for $m_{\tilde{e}}$ = 30 GeV and 40 GeV. The dashed lines show the cross section for $e^+ e^- \longrightarrow \tilde{\mu}^+ \tilde{\mu}^-$ ($\tilde{\tau}^+ \tilde{\tau}^-$, ...), for which only the s-channel exchange diagrams of Fig. 5.1 contribute. Here, we take $m_{\tilde{z}}$ = 60 GeV.

$$e^+ e^- \longrightarrow e^+ e^- \tilde{\gamma} \tilde{\gamma} . \qquad (5.10)$$

In this case there are many more possible Feynman diagrams, as shown in Fig. 5.3; other diagrams with γ or $\tilde{\gamma}$ in the s-channel and Z or $\tilde{Z}$ in the t-channel give negligible contributions. The dominant contributions arise when one or other of the scalar electrons is (nearly) on shell; we omit diagrams such as (h) with two off-shell particles in the initial state.

The values of the cross-section, $\sigma(e^+e^- \to e^+e^-\tilde{\gamma}\tilde{\gamma})$, are obtained by carrying out the integrations using Monte Carlo techniques. The calculations are done in the conventional way of summing over the squared matrix elements of the individual diagrams and their interference terms; differential cross-sections for the dominant processes (see the discussion below) are given in Appendix A (§5.5.A). Part of the calculation (the contribution of the γ-exchange diagrams, 5.3(d) and (g)) have been checked[13] using a recent technique,[14] in which individual helicity amplitudes (which are just complex numbers) are calculated and their simple sum is squared.

The results for $\sigma(e^+e^- \to e^+e^-\tilde{\gamma}\tilde{\gamma})$ are shown in Fig. 5.4 for three different values of $m_{\tilde{\gamma}}$, and at two values of $\sqrt{s}$, on and just beyond the Z resonance, as a function of the electron mass. So that both the final e^+ and e^- are observable we require $|\cos\theta_{e^\pm}| < 0.9$, where $\theta_{e^\pm}$ is the $e^\pm$ scattering angle. Only the γ-exchange diagrams, 5.3(d) and (g), are very sensitive to these cuts. In their original paper, Gaillard et al.[13] considered (single) scalar electron production, where the spectator electron is scattered in the beam direction and so not detected, leading to

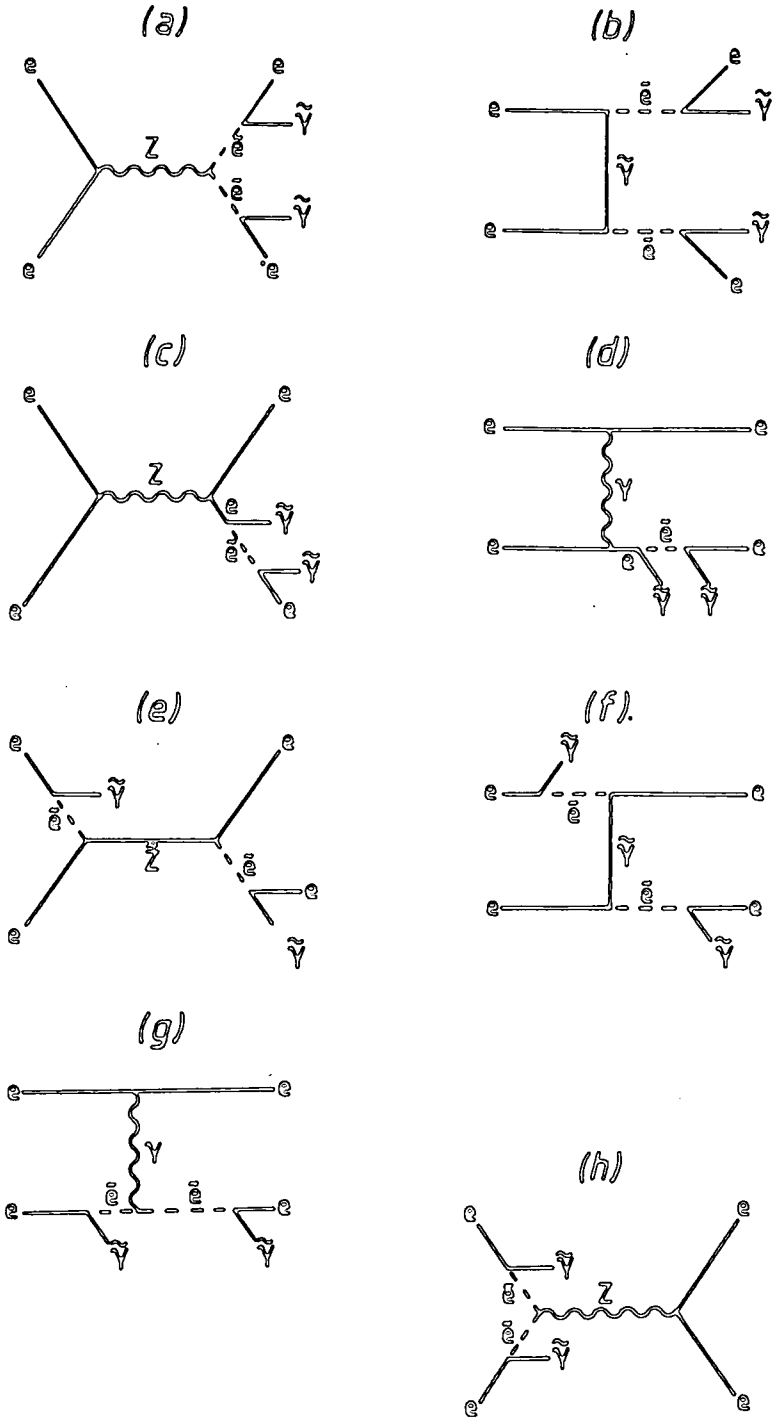

Figure 5.3
The dominant Feynman diagrams for $e^+ e^- \longrightarrow e^+ e^- \tilde{\gamma} \tilde{\gamma}$. All possible charge configurations are included in the calculation.

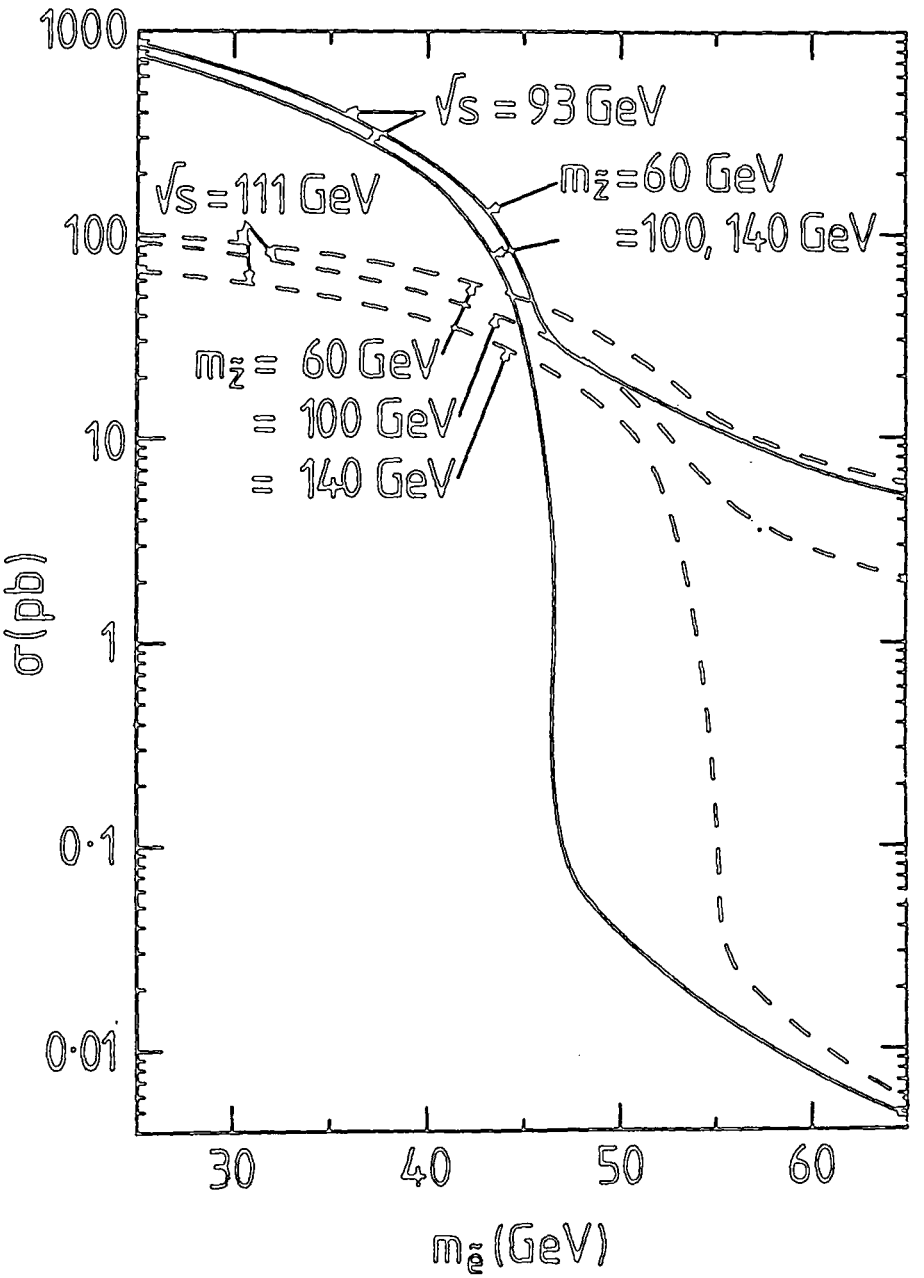

Figure 5.4
The cross-section for $e^+ e^- \longrightarrow e^+ e^- \tilde{\gamma}\tilde{\gamma}$ as a function of scalar electron mass for two different $e^+ e^-$ c.m. energies ($\sqrt{s} = M_Z$ (= 93 GeV) and $\sqrt{s}$ = 111 GeV) and three different choices of the zino mass ($m_{\tilde{z}}$ = 60, 100, 140 GeV). A cut of $|\cos\theta_{oo}| < 0.9$ is imposed, where θ_{oo} is the scattering angle between the initial and final state electron.

a final state with only one identified electron and with very large missing energy (resulting from the two photinos and the unobserved $e^{\pm}$). This give a very clean signature for scalar electron production when $m_{\tilde{e}} > \sqrt{s}/2$, which, in the absence of a light zino, has a larger cross-section than the case where both electrons are detected. We shall return to this later.

The sensitivity of the $e^+ e^- \longrightarrow e^+ e^- \tilde{\gamma} \tilde{\gamma}$ cross-section to the value of $m_{\tilde{Z}}$ is due to the s-channel diagram 5.3(e), where there is a possibility of the zino being on shell. We assume the width of the zino is given by the three-body decay $\tilde{Z} \dashrightarrow e^+ e^- \tilde{\gamma}$;

$$\Gamma_{\tilde{Z}} = \Gamma(\tilde{Z} \rightarrow e^+ e^- \tilde{\gamma}) = \frac{\alpha^2 w^2 (L^2+R^2)}{4\pi m_{\tilde{Z}}^3} \int_{m_{\tilde{\gamma}}^2}^{m_{\tilde{Z}}^2} ds \, \frac{(m_{\tilde{Z}}^2 - s)^2 \, (s - m_{\tilde{\gamma}}^2)^2}{s[(s-m_{\tilde{e}}^2)^2 + m_{\tilde{e}}^2 \Gamma_{\tilde{e}}^2]} \,, \qquad (5.11)$$

where w, L and R are defined in Table 5.1 and

$$\Gamma_{\tilde{e}} = \Gamma(\tilde{e} \rightarrow e \tilde{\gamma}) = \frac{\alpha}{2} m_{\tilde{e}} \left[1 - \frac{m_{\tilde{\gamma}}^2}{m_{\tilde{e}}^2} \right]^2 . \qquad (5.12)$$

If there are zino decay modes involving other possible light superparticles the width will be increased in a predictable fashion. From Fig. 5.5 we see that for a heavy zino ($m_{\tilde{Z}}$ = 100, 140 GeV) we have $\Gamma_{\tilde{Z}} \sim 1$ GeV for scalar electron masses in the range 25 to 70 GeV; for $m_{\tilde{Z}}$ = 60 GeV the width is very sensitive to $m_{\tilde{e}}$, varying from 0.4 GeV for $m_{\tilde{e}}$ = 25 GeV, to 0.4 MeV for $m_{\tilde{e}}$ = 60 GeV (the kinematic limit for $\tilde{Z} \longrightarrow \tilde{e}\, e$ decay), and to 90 keV for $m_{\tilde{e}}$ = 70 GeV.

Depending on the values of $\sqrt{s}$, $m_{\tilde{e}}$ and $m_{\tilde{Z}}$, different Feynman diagrams dominate $\sigma(e^+e^- \rightarrow e^+e^-\tilde{\gamma}\tilde{\gamma})$. For $m_{\tilde{e}} < \sqrt{s}/2$ the cross-section is dominated by the contributions of diagrams

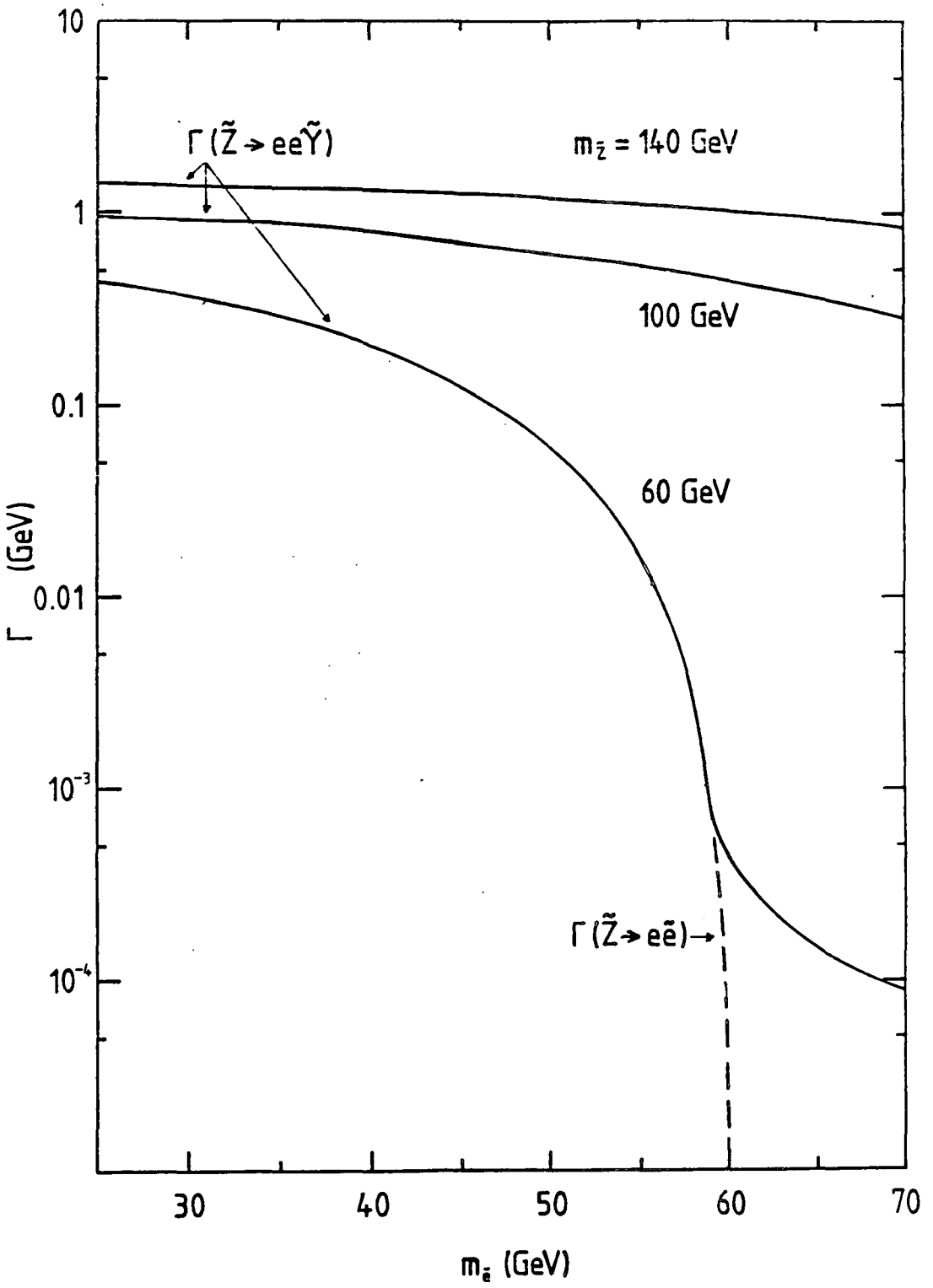

Figure 5.5
The decay width $\Gamma(\tilde{Z} \longrightarrow ee\tilde{\gamma})$ as a function of the scalar electron mass for three choices of the zino mass ($m_{\tilde{z}}$ = 60, 100, 140 GeV). The dashed line shows the decay width $\Gamma(\tilde{Z} \longrightarrow e\tilde{e})$ for $m_{\tilde{z}}$ =60 GeV. Here, we take $m_{\tilde{\gamma}}$ = 0.

5.3(a,b); as before, the s-channel Z exchange dominates at $\sqrt{s}$ = 93 GeV and the t-channel $\tilde{\gamma}$-exchange at $\sqrt{s}$ = 111 GeV. The only other appreciable contribution in this mass range comes from diagram 5.3(e), provided $m_{\tilde{Z}} < (\sqrt{s} - m_{\tilde{\gamma}})$ (in the case of Fig. 5.4, that is for $m_{\tilde{Z}}$ = 60 GeV at both energies, and for $m_{\tilde{Z}}$ = 100 GeV at $\sqrt{s}$ = 111 GeV). Essentially, this is zino production, $e^+ e^- \longrightarrow \tilde{Z}\,\tilde{\gamma}$, followed by the decay $\tilde{Z} \longrightarrow e\,e\,\tilde{\gamma}$. When $m_{\tilde{Z}} > (\sqrt{s} - m_{\tilde{\gamma}})$ this contribution is effectively "switched off", as can be seen from Fig. 5.4.

For $m_{\tilde{e}} > \sqrt{s}/2$ the cross-section is dominated by diagrams 5.3(c,d,e,f,g). In the absence of diagram 5.3(e) (that is, $m_{\tilde{Z}} > \sqrt{s}$) the largest contributions come from the photon-exchange diagrams, 5.3(d,g), which are sensitive to the θ_{ee} cut. To see this it is informative to compare our results with those obtained using the Weizsäcker-Williams approximation to calculate $e^+ e^- \longrightarrow \tilde{e}\,e\,\tilde{\gamma}$, via $\gamma e \longrightarrow \tilde{e}\,\tilde{\gamma}$,[13] where the spectator electron goes in the forward direction and escapes detection; the scalar electron subsequently decays, $\tilde{e} \longrightarrow e\,\tilde{\gamma}$, leading to a final state with a single observed electron and large missing energy ($> \sqrt{s}/2$). In Fig. 5.6 we compare the Weizsäcker-Williams approximation with our calculation of diagrams 5.3(d,g) at $\sqrt{s}$ = 93 GeV, taking the outgoing scalar electron on shell and with the $|\cos\theta_{ee}| < 0.9$ cut. We see that in the region $m_{\tilde{e}} > \sqrt{s}/2$ the "single electron signal" dominates the "two electron signal" by about an order-of-magnitude. Comparing this result with the values of the summed cross-section, we expect the "single electron signal" to dominate for $m_{\tilde{e}} > \sqrt{s}/2$ by, for example, a factor of 3 at $m_{\tilde{e}}$ = 60 GeV and a factor of 7 at $m_{\tilde{e}}$ = 60 GeV, provided $m_{\tilde{Z}} > \sqrt{s}$,

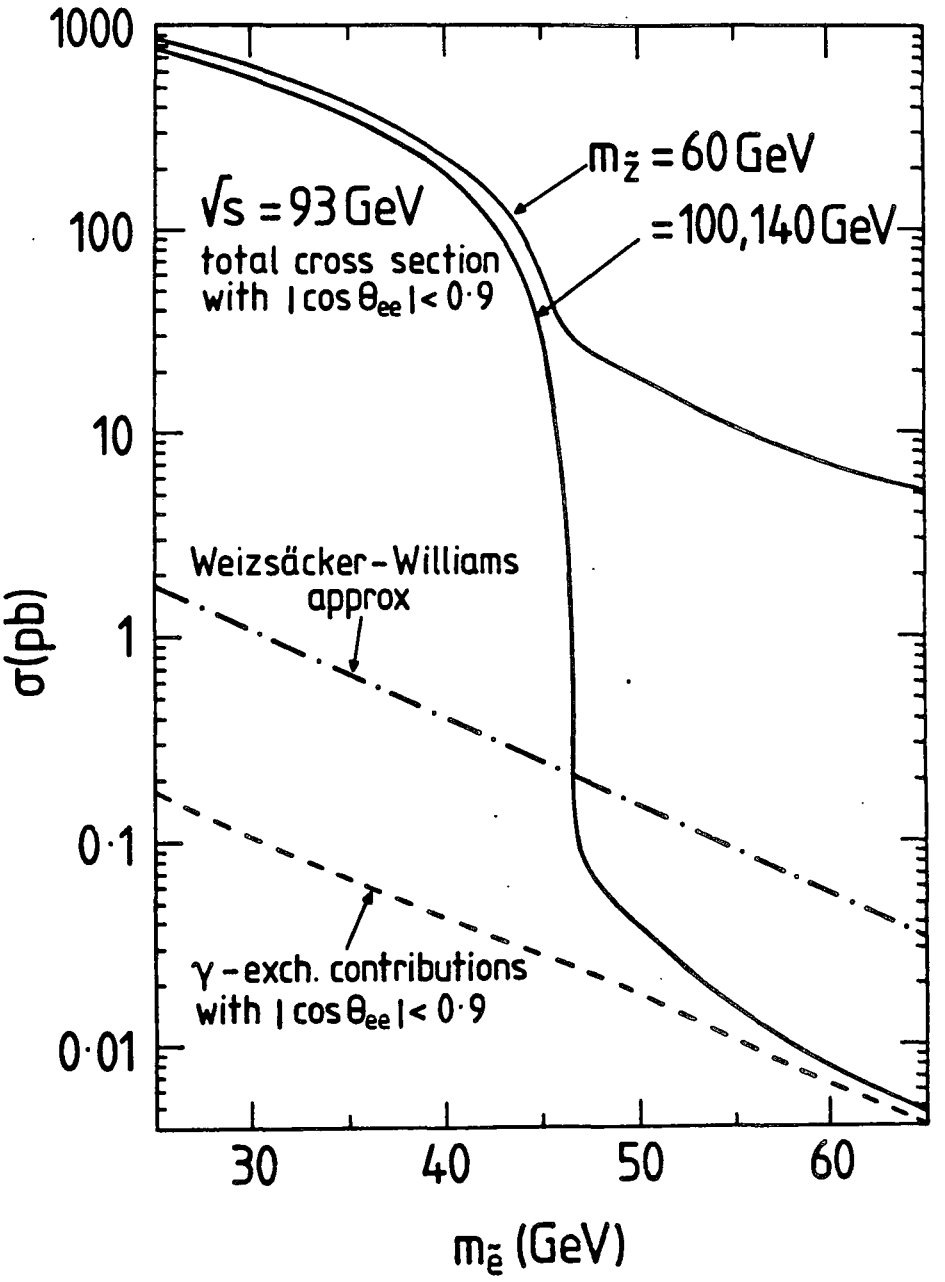

Figure 5.6
The contributions of the γ-exchange diagrams (Fig. 5.3(d,g)) to $\sigma(e^+ e^- \to e \tilde{e} \tilde{\gamma})$ at $\sqrt{s}$ = 93 GeV calculated (i) in the Weizsäcker-Williams approximation, and (ii) exactly, but with the $|\cos\theta_{ee}| < 0.9$ cut imposed. The curves for the total cross-section from Fig. 5.4 are also shown.

and to give a good observable scalar electron signal for masses considerably in excess of the beam energy, as originally emphasised by Gaillard et al.[13]

The case when $m_{\tilde{z}} < \sqrt{s}$ is particulaly interesting. Here $\sigma(e^+e^- \rightarrow e^+e^-\tilde{\gamma}\tilde{\gamma})$ depends critically on the value of the zino mass. If $m_{\tilde{z}} > M_z$ (e.g. $m_{\tilde{z}} = 100$ GeV), increasing the beam energy from M_z to $\sqrt{s} > (m_{\tilde{z}} + m_{\tilde{\gamma}})$ will "switch on" the zino contribution of diagram 5.3(e), enhancing the cross-section by more than two orders-of-magnitude, if $m_{\tilde{e}} > \sqrt{s}/2$. However, if $m_{\tilde{z}} < M_z$ then this enhancement is present for all $\sqrt{s} > M_z$. In either case, the "two electron signal", principally from this on-shell zino production and decay, will dominate the "single electron signal" by up to two orders-of-magnitude, which is the case at $\sqrt{s} = 93$ GeV shown in Fig. 5.5. (This result is only strictly valid if the zino width is given by Eq. (5.11); if there are other possible zino decay modes then the zino width may be substantially increased, and the contribution of process (e) to scalar electron production will be reduced by the branching ratio for the decay $\tilde{l} \longrightarrow e^+ e^- \tilde{\gamma}$. Nevertheless, it is unlikely that this branching ratio will be only ~ 1% such that the "two electron signal" from process (e) would fall below the "single electron signal.") In this case, the magnitude of the cross-section is relatively insensitive to increasing the total beam energy above $\sqrt{s} = m_{\tilde{z}}$.

The values of $\sigma(e^+e^- \rightarrow e^+e^-\tilde{\gamma}\tilde{\gamma})$ with $|\cos\theta_{e^-}| < 0.9$ are not particularly sensitive to the value of $m_{\tilde{\gamma}}$, except in the "switch-on" energy, $(m_{\tilde{z}} + m_{\tilde{\gamma}})$, of the zino contribution. Only the contribution of diagram 5.3(f), with a t-channel $\tilde{\gamma}$-propagator is

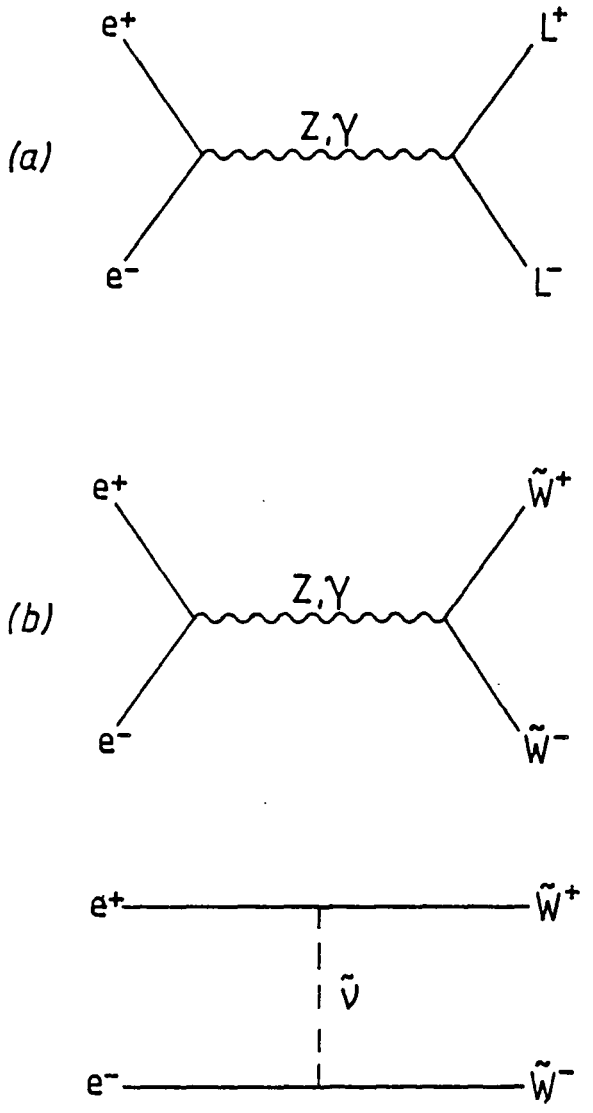

Figure 5.7
The first-order Feynman diagrams for
(a) $e^+ e^- \longrightarrow L^+ L^-$ ($L = \tau, \lambda$ (?));
(b) $e^+ e^- \longrightarrow \tilde{W}^+ \tilde{W}^-$.

process (see Appendix B (§5.5.B)). (The e^+e^- signature from $\tilde{W}$ pair production will be similarly suppressed.) However, the cross-section ($e^+e^- \longrightarrow e^+e^- \bar{\nu}_e \nu_e \bar{\nu}_e \nu_e$) is in fact comparable with or greater than that for $\tilde{e}$ pair production for $m_{\tilde{g}} > 45$ GeV at $\sqrt{s} = M_Z$, but may easily be distinguished by the different event topology, characterised by back-to-back electrons.

The final state electron distributions resulting from

$$e^+ e^- \longrightarrow e^+ e^- \tilde{\gamma} \tilde{\gamma} \qquad (5.15)$$

were calculated using Monte Carlo simulations of $O(10^5)$ events. Important kinematic distributions are shown in Figs 5.8-11 for $m_{\tilde{z}} = 60$, 100 GeV.

Figure 5.8 shows the electron (e^-) momentum distribution for two values of $m_{\tilde{g}}$ at each of two values of $\sqrt{s}$. At $\sqrt{s} = 93$ GeV, the presence of the zino, of either mass, is not apparent, and we see a distribution characteristic of the two-body decay of a spinless particle of unique energy (arising from diagram 5.2(a); see Appendix C (§5.5.C)). The limits on the plateau region are given by the kinematics of the on-shell $\tilde{e}$ two-body decay

$$p_{\pm} = (\sqrt{s} \pm \sqrt{s - 4m_{\tilde{e}}^2})/4 \ . \qquad (5.16)$$

The tail on either side of the plateau in the momentum distribution is due to off-shell $\tilde{e}$ decays. For $m_{\tilde{g}} > \sqrt{s}/2$ the plateau structure disappears; see, for example, the case $\sqrt{s} = 93$ GeV, $m_{\tilde{g}} = 55$ GeV and $m_{\tilde{z}} = 100$ GeV, which has an asymmetric distribution concentrated roughly about $\sqrt{s}/4$. However, for $m_{\tilde{z}} = 60$ GeV the distribution shows a striking double-peaked structure, arising almost entirely from zino production and decay. The tall, narrow peak is due to slow electrons from the decay

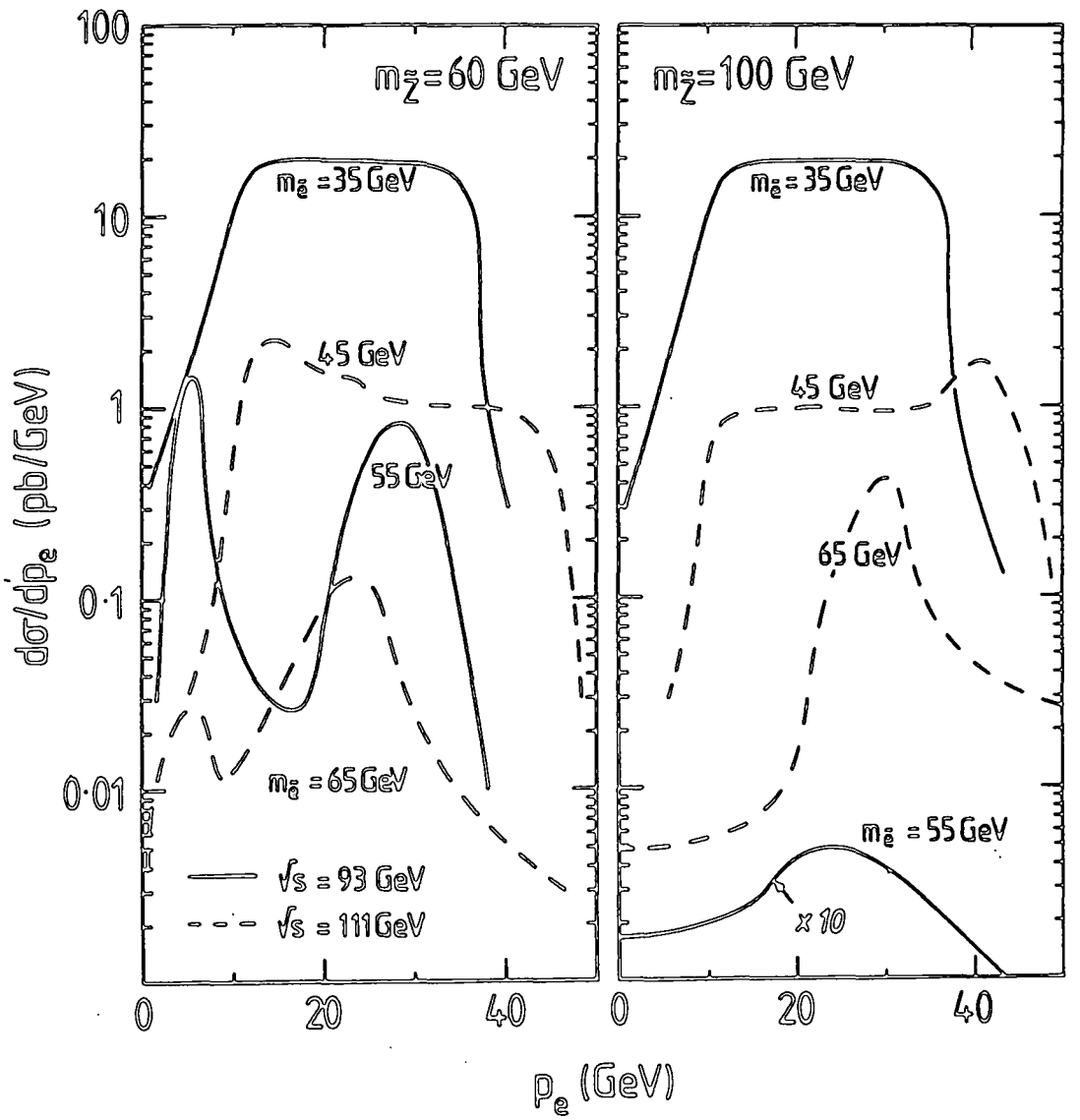

N.B. The differential cross-section for $m_{\tilde{z}} = 100$ GeV and $m_{\tilde{e}} = 55$ GeV has been multiplied by 10.

Figure 5.8
The electron momentum distribution in $e^+ e^- \longrightarrow e^+ e^- \tilde{\gamma}\tilde{\gamma}$, with the $|\cos\theta_{e^-}| < 0.9$ cut imposed.

$\tilde{Z} \longrightarrow \tilde{e}\ e$, where the zino is almost at rest; the broader, lower peak is due to fast electrons from the subsequent $\tilde{e} \longrightarrow e\tilde{\gamma}$ decay. The exact features of the distributions are sensitive to the values of $\sqrt{s}$, $m_{\tilde{e}}$ and $m_{\tilde{Z}}$, but the general features persist for other values of the parameters. For $\sqrt{s}$ = 111 GeV the presence of the zino can be seen in the distributions, even for the lighter scalar electron ($m_{\tilde{e}}$ = 45 GeV); the double-peak distribution is superimposed on the plateau distribution from $\tilde{e}$ pair production, though this is not very clear in the case of the heavier zino. For the heavier scalar electron ($m_{\tilde{e}}$ = 65 GeV) the double-peak distribution is seen again. However, for $m_{\tilde{Z}}$ = 60 GeV the e is forced off shell and the distribution is smeared out somewhat; for $m_{\tilde{Z}}$ = 100 GeV the peaks are superimposed at about the same value of p_o, a consequence of the particular choice of parameters.

Figure 5.9 shows the distribution with respect to $\cos\theta_{oo}$, where θ_{oo} is the angle between the ingoing and outgoing e^-. For $\sqrt{s}$ = 93 GeV and $m_{\tilde{e}}$ = 35 GeV this distribution is essentially flat; the isotropic scalar decay has washed out most of the $\sin^2\theta$ dependance of the parent scalar electron distribution. For the same $\sqrt{s}$, $m_{\tilde{e}}$ = 55 GeV and $m_{\tilde{Z}}$ = 100 GeV we see that the distribution is strongly peaked in the forward direction due to the dominance of the t-channel γ-exchange diagrams 5.3(d,g) and, to a lesser extent, 5.3(f). For all other values of the parameters shown, the underlying distribution shows the $(1-\cos\theta)^2$ dependance of the subprocess $\tilde{e}\ e \longrightarrow \tilde{Z} \longrightarrow \tilde{e}\ e$ which is superimposed on an essentially flat distribution arsisng from the other diagrams; the underlying $\sin^2\theta$ dependance of diagram 5.3(a) can still be seen for $m_{\tilde{e}}$ = 45 GeV at $\sqrt{s}$ = 111 GeV.

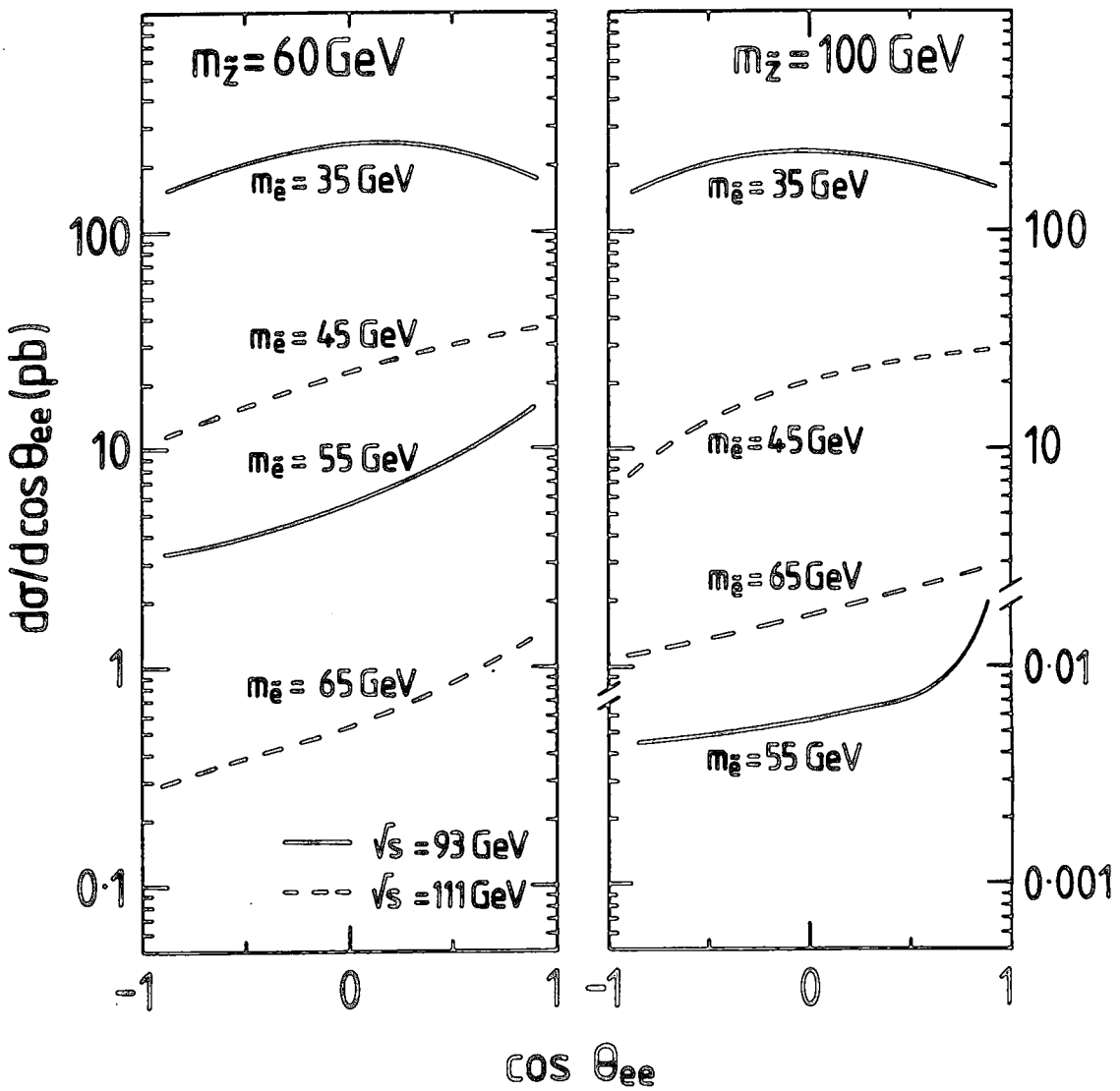

Figure 5.9
The electron angular distribution in $e^+ e^- \longrightarrow e^+ e^- \tilde{\gamma}\tilde{\gamma}$, for $|\cos\theta_{ee}| < 0.9$.

Figure 5.10 shows the distribution of the total missing energy, i.e. the sum of the photino energies. Naïvely, we would expect that this would peak at $\sqrt{s}/2$; indeed, this is the case for $\sqrt{s}$ = 93 GeV and $m_{\tilde{\gamma}}$ = 35 GeV where the cross-section is dominated by $\tilde{e}$ pair production, though the distribution is rather broad. However, where zino production dominates, the distribution is more sharply peaked, at ~ 60 GeV for $m_{\tilde{Z}}$ = 60 GeV; i.e. for a light zino about two thirds of the total energy is missing. For $\sqrt{s}$ = 111 GeV and both sample values of $m_{\tilde{Z}}$ we see a superposition of these two distributions (with the broad peak due to the zino just evident in the region of 30 GeV for $m_{\tilde{Z}}$ = 100 GeV).

Figure 5.11 shows the invariant mass distribution for the e^+e^- pair. Again, we see broad distributions for the cases where diagrams 5.3(a,b) dominate (e.g. $\sqrt{s}$ = 93 GeV, $m_{\tilde{\gamma}}$ = 35 GeV), more sharply peaked where the zino contribution (diagram 5.3(e)) dominates ($m_{\tilde{\gamma}} = \sqrt{s}/2$ and $m_{\tilde{Z}} > \sqrt{s}$), and a superposition of these for e.g. $\sqrt{s}$ = 111 GeV and $m_{\tilde{\gamma}}$ = 45 GeV.

The characteristic momentum distributions of Fig. 5.8 serves to distinguish the production of scalar electrons from either heavy lepton or wino production. Indeed, in the case where $m_{\tilde{Z}} < \sqrt{s}$ and $m_{\tilde{\gamma}} > \sqrt{s}/2$ the electron momentum distributions can give a striking signature for zino production. The angular and missing energy distributions are not so distinctive; for particular values of $\sqrt{s}$, $m_{\tilde{Z}}$ and $m_{\tilde{\gamma}}$ they can be similar to those from heavy lepton and wino production.[15,16]

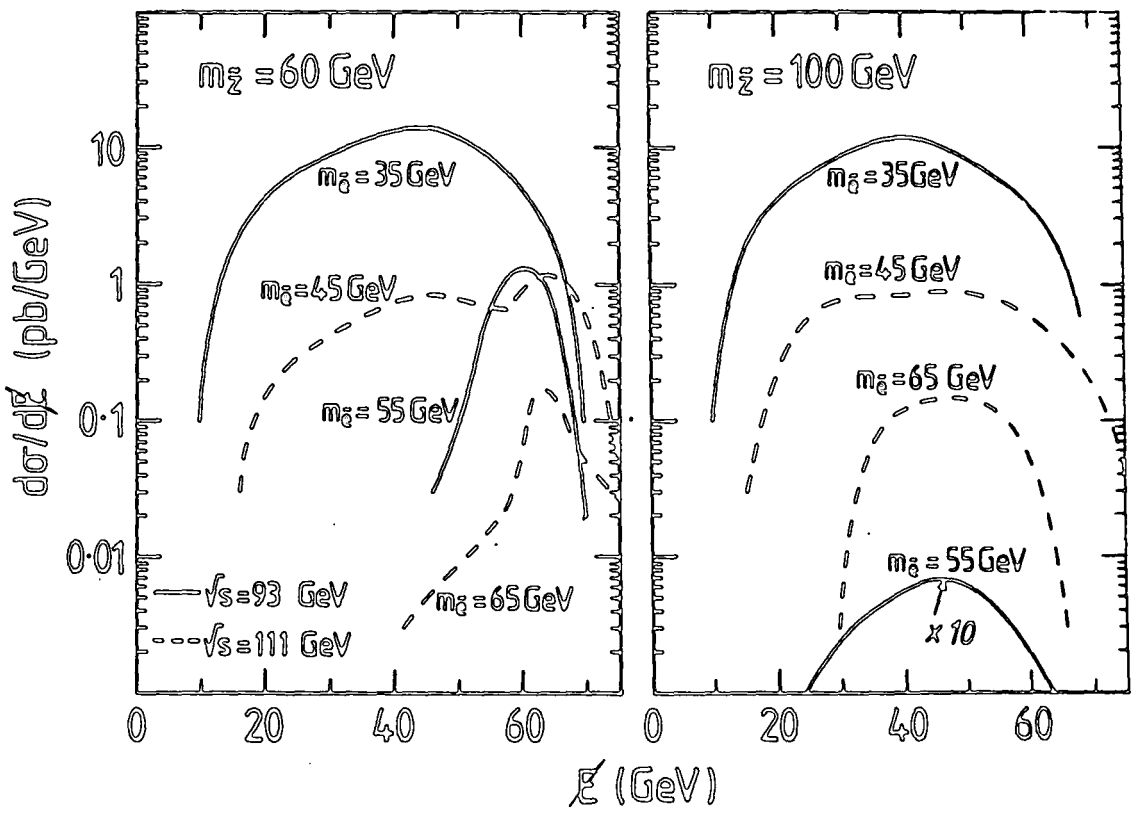

N.B. The differential cross-section for $m_{\tilde{e}} = 100$ GeV and $m_{\tilde{\gamma}} = 55$ GeV has been multiplied by 10.

Figure 5.10
The total missing energy ($\not{E} = \Sigma E_{\tilde{\gamma}}$) distribution in $e^+ e^- \longrightarrow e^+ e^- \tilde{\gamma}\tilde{\gamma}$, with the $|\cos\theta_{e^-}| < 0.9$ cut imposed.

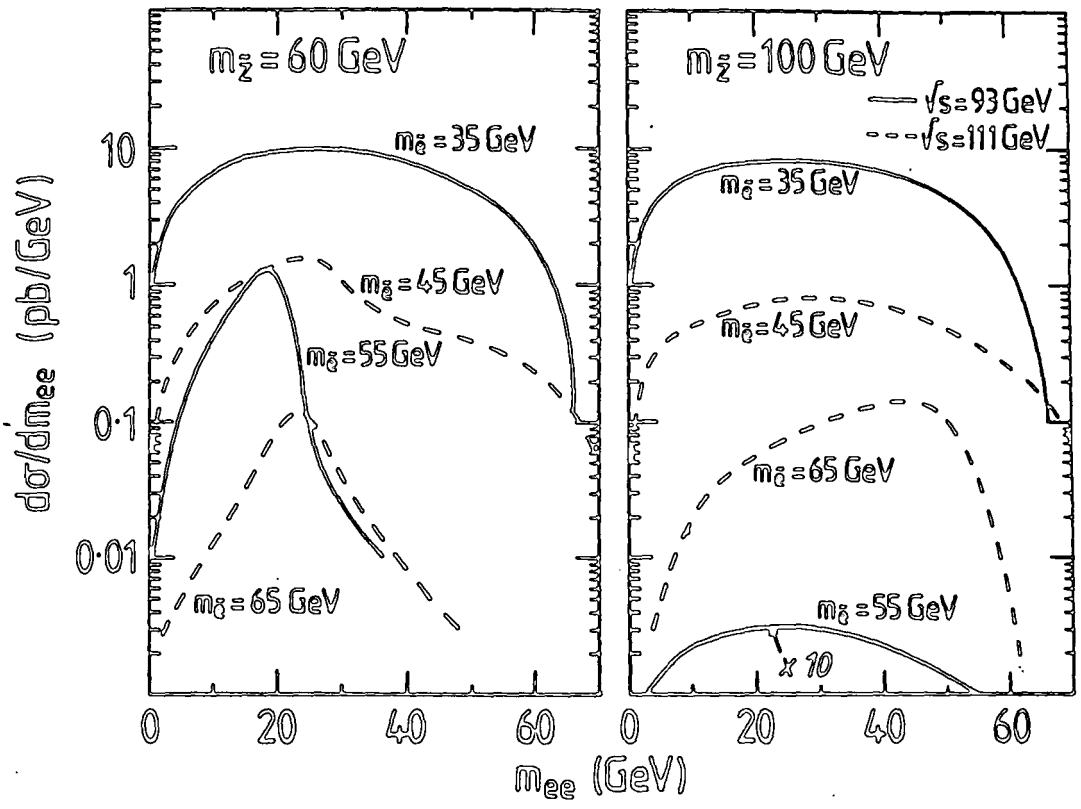

N.B. The differential cross-section for $m_{\tilde{z}} = 100$ GeV and $m_{\tilde{e}} = 55$ GeV has been multiplied by 10.

Figure 5.11
The invariant mass (m_{ee}) distribution of the outgoing electron pair in $e^+e^- \longrightarrow e^+ e^- \tilde{\gamma}\tilde{\gamma}$, with the $|\cos\theta_{ee}| < 0.9$ cut imposed.

5.4 Conclusions

We have calculated the cross-section and studied the signatures for the production of scalar electrons in e^+e^- annihilation on and beyond the Z resonance.

If $m_{\tilde{e}} < \sqrt{s}/2$ the cross-section is dominated by $\tilde{e}$ pair production; on the Z resonance s-channel Z-production dominates, whereas off resonance the t-channel $\tilde{\gamma}$-exchange contributes the bulk of the cross-section. The signature for $\tilde{e}$ pair production and decay, $e^+ e^- \longrightarrow \tilde{e}^+ \tilde{e}^- \longrightarrow e^+ e^- \tilde{\gamma} \tilde{\gamma}$, is an acolinear and uncorrelated e^+e^- pair, acoplanar with the incident beams, with about half the available energy missing. The electron momentum distribution is flat between the (on-shell) kinematic limits. The electron angular distribution is almost isotropic, reflecting the scalar $\tilde{e} \longrightarrow e \tilde{\gamma}$ decay.

If $m_{\tilde{e}} > \sqrt{s}/2$ the situation is quite different. When the contribution from zino production is negligible (i.e. when $m_{\tilde{z}} > (\sqrt{s} - m_{\tilde{\gamma}})$), the cross-section is dominated by "single" scalar electron production via t-channel photon exchange. These diagrams give rise to a final state with only one observed electron; the other is scattered in the forward direction and so escapes detection. Events with a single observed electron accompanied by large missing energy would be a very clean signature for scalar electron production.[13] However, if a zino exists with $m_{\tilde{z}} < \sqrt{s}$, $\tilde{e}$ production will be dominated by $\tilde{Z}$ production and decay ($e^+ e^- \longrightarrow \tilde{Z} \tilde{\gamma}$; $\tilde{Z} \longrightarrow e^+ e^- \tilde{\gamma}$), leading to a final state with

two observed electrons and missing energy. For particular values of $m_{\tilde{Z}}$ and $m_{\tilde{e}}$ at a given $\sqrt{s}$ the missing energy distribution may be quite different from that naively expected, peaked at $\sqrt{s}/2$. The electron angular distribution has a forward bias due to the contribution from the subprocess $\tilde{e}\ e \longrightarrow \tilde{Z} \longrightarrow \tilde{e}\ e$. The most striking signature for scalar electron via a zino is the electron momentum distribution, which may show a double peak as a consequence of the kinematics of the zino decay $\tilde{Z} \longrightarrow e\ \tilde{e} \longrightarrow e\ (\ e\ \tilde{\gamma}\ )$.

In summary, scalar electron production leading to a final state with two observed electrons and large missing energy may be the best way to observe scalar electrons experimentally if $m_{\tilde{e}} < \sqrt{s}/2$, and even in the case $m_{\tilde{e}} > \sqrt{s}/2$ if a zino exists with mass $m_{\tilde{Z}} > \sqrt{s}$. In this later case, the process $e^+\ e^- \longrightarrow e^+\ e^-\ \tilde{\gamma}\ \tilde{\gamma}$ may reveal the presence of both the $\tilde{e}$ and the $\tilde{Z}$ via a distinctive signature in the electron momentum distribution. If $m_{\tilde{e}} > \sqrt{s}/2$ and $m_{\tilde{Z}} > \sqrt{s}$, however, the most hopeful signature is events with a single observed electron and large missing energy.

5.5 Appendices

5.5.A *Cross-sections for (off-shell) scalar electron production*

In this Appendix, we present formulae for the cross-sections of the dominant processes contributing to $e^+ e^- \longrightarrow e^+ e^- \tilde{\gamma} \tilde{\gamma}$ (see the discussion in Section 5.2 above).

The contribution of diagrams (a,b) (see Fig. 5.3) is given by

$$\sigma^{*} = \int_{a_1}^{b_1} ds_1 \int_{a_2}^{b_2} ds_2 \int_{-1}^{1} dz \; \frac{\alpha^4}{4\pi} \frac{S'}{s^2} \, (ut - s_1 s_2) \, \rho_{11}(s,t) \sum_{k=1,2} \frac{(s_k - m_{\tilde{\gamma}}^2)^2}{s_k \, |D_{\tilde{e}}(s_k)|^2} \, , \tag{5.17}$$

where $S' = \lambda^{1/2}(s, s_1, s_2)$, $D_{\tilde{e}}(s)$ is the scalar electron propagator, $D_{\tilde{e}}(s) = (s - m_{\tilde{e}}^2) - i m_{\tilde{e}} \Gamma_{\tilde{e}}$ (with the scalar electron width, $\Gamma_{\tilde{e}}$, given by Eq. (5.12)), and $\rho_{11}(s,t)$ is given by Eq. (5.6b). The integration was performed numerically; the limits on the s_k integrations are $a_k = m_{\tilde{\gamma}}^2 \sim 0$, $b_1 = (\sqrt{s} - m_{\tilde{\gamma}})^2 \sim s$, and $b_2 = (\sqrt{s} - \sqrt{s_1})^2$; the Mandelstam variables t,u are functions of the integration variables: $t,u = (s_1 + s_2 - s \pm S' z)$, where $z = \cos\theta_{oo}$, the cosine of the angle between $e^-_{initial}$ and e^-. The contribution is largest when one (or both) of the scalar electrons is on shell (i.e. when $s_k = m_{\tilde{e}}$, and Eq. (5.17) $\longrightarrow$ Eq. (5.6)).

The γ-exchange contributions of diagrams (d,g) can be closely approximated by $\tilde{e}e\tilde{\gamma}$ production, followed by the decay $\tilde{e} \longrightarrow e\tilde{\gamma}$. The cross-section for $e^+ e^- \longrightarrow \tilde{e}^{\pm} e^{\mp} \tilde{\gamma}$ is given by

$$\sigma = \int_{-1}^{1} d\cos\theta_1 \int_{-1}^{1} d\cos\theta_2 \int_{-\pi}^{\pi} d\Omega_2 \int_{b_0}^{a_0} ds_0 \; \alpha^3 \, \rho(p_1) \, \frac{(s-s_0)^2 \, \lambda^{1/2}(s_0, m_{\tilde{e}}^2, m_{\tilde{\gamma}}^2)}{2\pi s^2 \, s_0} \,, \tag{5.18a}$$

where

$$\rho(p_1) = \frac{1}{t_0^2} \left(\left[\frac{2}{s_0^2} \{d\} \right] + \left[\frac{1}{|D_e(t_1)|^2} \{g\} \right] + \left[\frac{4}{s_0} \mathrm{Re} \left(\frac{1}{D_e(t_1)} \right) \{x\} \right] \right) , \tag{5.18b}$$

with

$$\{d\} = 2(m_{\tilde{\gamma}}^2 + p_4 \cdot p_5)(p_1 \cdot p_2 \; p_3 \cdot p_5 + p_1 \cdot p_3 \; p_2 \cdot p_5) - (m_{\tilde{e}}^2 - m_{\tilde{\gamma}}^2)(p_1 \cdot p_2 \; p_3 \cdot p_4 + p_1 \cdot p_3 \; p_2 \cdot p_4) \,, \tag{5.18c}$$

$$\{g\} = p_1 \cdot p_4 \, [2 \; p_2 \cdot (p_1 - p_4 + p_5) \; p_3 \cdot (p_1 - p_4 - p_5) - p_2 \cdot p_3 \, (m_{\tilde{\gamma}}^2 - m_{\tilde{e}}^2 - 2 \, (p_1 \cdot p_4 - p_1 \cdot p_5 + p_4 \cdot p_5)] \,, \tag{5.18d}$$

$$\begin{aligned} \{x\} = {} & [p_1 \cdot p_4 \; p_3 \cdot (p_4 + p_5) - p_1 \cdot (p_4 + p_5) \; p_3 \cdot p_4 \\ & + p_1 \cdot p_3 \, (m_{\tilde{\gamma}}^2 + p_4 \cdot p_5)] \, (p_1 \cdot p_2 - p_2 \cdot (p_4 - p_5)) \\ & + [p_1 \cdot p_4 \; p_2 \cdot (p_4 + p_5) - p_1 \cdot (p_4 + p_5) \; p_2 \cdot p_4 \\ & + p_1 \cdot p_2 \, (m_{\tilde{\gamma}}^2 + p_4 \cdot p_5)] \, (p_1 \cdot p_3 - p_3 \cdot (p_4 - p_5)) \\ & + [p_1 \cdot p_4 \, (m_{\tilde{e}}^2 - m_{\tilde{\gamma}}^2 + p_1 \cdot p_4 + p_1 \cdot p_5) \\ & - p_1 \cdot (p_4 + p_5)(p_1 \cdot p_4 - m_{\tilde{\gamma}}^2 + p_4 \cdot p_5) \\ & + p_1 \cdot (p_4 + p_5)(m_{\tilde{\gamma}}^2 + p_4 \cdot p_5)] \; p_2 \cdot p_3 \; ; \end{aligned} \tag{5.18e}$$

$p_{1,2}$ are the momenta of the initial e , p_3 the momentum of the spectator e, p_4 of the photino and p_5 of the scalar electron, and

$$\begin{aligned} s_0 &= (p_4+p_5)^2 \,, \\ t_0 &= (p_2-p_3)^2 \,, \\ t_1 &= (p_1-p_4)^2 \,. \end{aligned} \tag{5.18f}$$

The limits on the s_0 integration are $a_0 = (m_{\tilde{e}}+m_{\tilde{\gamma}})^2$ and $b_0 = s$.

The contribution from diagram (e) can be closely approximated as $\tilde{Z}$ production, followed by the decay $\tilde{Z} \longrightarrow e^+e^-\tilde{\gamma}$. The $e^+ e^- \longrightarrow \tilde{Z}\,\tilde{\gamma}$ production cross-section is

simply

$$\sigma = \int_{-1}^{1} \frac{16\pi\alpha^2 w^2 (L^2+R^2)}{|D_e(t)|^2} \frac{\lambda^{1/2}(s, m_{\tilde{\gamma}}^2, m_Z^2)}{s^2} p_1 \cdot p_3 \; p_2 \cdot p_4 \; d\cos\theta , \qquad (5.19)$$

where $p_{1,2}$ are the momenta of the initial e^-, p_3 is the photino momentum and p_4 that of the zino; $t = (p_1-p_3)^2$, and w, L, R are defined in Table 5.1.

5.5.B *Cross-sections for sequential heavy lepton pair production*

The diagrams which contribute to sequential heavy lepton pair production,

$$e^+ e^- \longrightarrow L^+ L^- \qquad (L = \tau, \lambda(?)) , \qquad (5.20)$$

are shown in Fig. 5.7(a). At $\sqrt{s} \sim M_Z$ the Z-exchange diagram will, of course, dominate. The differential cross-section was evaluated using the well known Feynman rules for electroweak interactions. We obtain

$$\frac{d\sigma}{dt} = \frac{\pi\alpha^2}{s^4} \{ k_s m_L^2 s + k_t (t-m_L^2)^2 + k_u (u-m_L^2)^2 \} . \qquad (5.21)$$

The coefficients k_m are given in Table 5.2(a). The total cross-section is found by integration between the limits $t_{1,2} = m_L^2 - (s \pm S)/2$, where $S = \sqrt{s}\sqrt{s-4m_L^2}$, yielding

$$\sigma = \frac{\pi\alpha^2}{s^4} \{ K_1 s^2 S + K_2 s(s-2m_L^2) S + K_3 (S_3 + 3[s^2 - 4(s-m_L^2)m_L^2]) S \} \qquad (5.22)$$

The coefficients K_i are given in Table 5.2(b).

Figure 5.12 shows $\sigma(e^+e^- \longrightarrow L^+L^-) \times BR^2(L \longrightarrow e \bar{\nu}_e \nu_L)$, for $m_\tau = 1.8$ GeV and as a function of m_λ; we have taken $BR(\tau \longrightarrow e \bar{\nu}_e \nu_\tau) = 1/6$ and $BR(\lambda \longrightarrow e \bar{\nu}_e \nu_\lambda) = 1/9$. We also show the cross-section for scalar electron pair production (process (5.1))

Table 5.2

(a) The coefficients k_m of Eq. (5.21). L, R, w and D_z have the same meanings as in Table 5.1.

$$k_s = 4 + w^2.(L+R)^2.Re(s/D_z) + 2.w^4.L.R.(L^2+R^2).s^2/|D_z|^2$$

$$k_t = 2 + 2.w^2.L.R.Re(s/D_z) + 2.w^2.L^2.R^2.s^2/|D_z|^2$$

$$k_u = 2 + w^2.(L^2+R^2).Re(s/D_z) + {}^1/_2.w^4.(L^4+R^4).s^2/|D_z|^2$$

(b) The coefficients K_i of Eq. (5.22). The k_m are as given above and $y = m_L^2/s$.

$$K_1 = k_s.y + k_t.y^2 + k_u.(1-y)^2$$

$$K_2 = k_t.y - k_u.(1-y)$$

$$k_3 = (k_t + k_u)/12$$

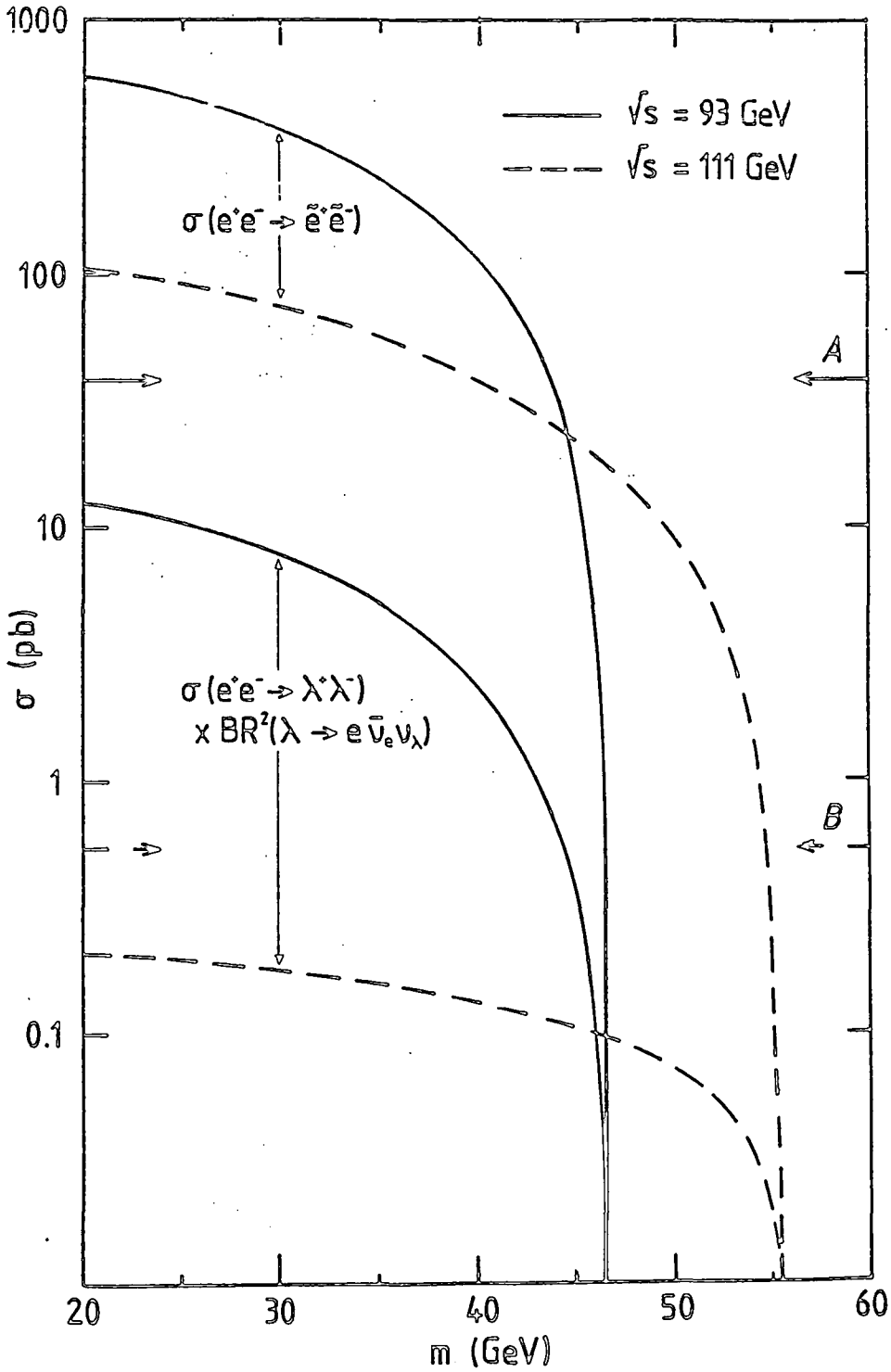

Figure 5.12
The cross-sections $\sigma(e^+e^- \longrightarrow \lambda^+\lambda^-) \times BR^2(\lambda \longrightarrow e\bar{\nu}_o \nu_\lambda)$ and $\sigma(e^+e^- \longrightarrow \tilde{e}^+\tilde{e}^-)$ as a function of the (scalar) lepton mass for $\sqrt{s}$ = 93 GeV (continuous curves) and $\sqrt{s}$ = 111 GeV (dashed curves). The arrows (A, B) indicate the cross-section $\sigma(e^+e^- \longrightarrow \tilde{e}^+\tilde{e}^-) \times BR^2(\tilde{e} \longrightarrow e\bar{\nu}_o \nu_e)$ for $m_{\tilde{e}}$ = 1.8 GeV for each value of $\sqrt{s}$.

for comparison (see Section 5.3).

5.5.C *The e momentum distribution from on-shell $\tilde{e}$ decay*

In this appendix we consider the c.m. momentum distribution of the electron produced in the two-body decay ($\tilde{e} \longrightarrow e\,\tilde{\gamma}$) of an on-shell scalar electron produced in e^+e^- annihilation.

Consider a scalar electron with energy $E_{\tilde{e}}$ ($= \sqrt{s}/2$) and momentum $p_{\tilde{e}}$ ($= \lambda^{1/2}(s,m_{\tilde{e}}^2,m_{\tilde{e}}^2)/(2\sqrt{s}) = \sqrt{s-4m_o^2}/2$) in the c.m. frame; let its direction of motion define the z'-axis. It decays electromagnetically into an electron and a photino. Since the scalar electron is a spinless particle the decay is isotropic, i.e. there is no angular dependance, and $d\Gamma/d\bar{\phi}$ or $d\Gamma/d\cos\bar{\theta}$ is flat. Also the electron momentum and energy are single valued:

$$\begin{aligned} \bar{p}_o &= \lambda^{1/2}(m_{\tilde{e}}^2,m_o^2,m_{\tilde{\gamma}}^2)/2m_{\tilde{e}} \ , \\ \bar{E}_o &= (m_{\tilde{e}}^2+m_o^2-m_{\tilde{\gamma}}^2)/2m_{\tilde{e}} \ ; \end{aligned} \tag{5.23}$$

note that if m_o, $m_{\tilde{\gamma}} = 0$ then $\bar{p}_o = \bar{E}_o = m_{\tilde{e}}/2$.

To find the electron momentum, p_o, in the c.m. frame we must boost along the z'-axis; only the z'-component (p_3) of the electron momentum changes: $p_3 = \gamma(\bar{p}_3+\beta\bar{E}_o)$, where $\gamma = E_{\tilde{e}}/m_{\tilde{e}}$ ($= \sqrt{s}/2m_{\tilde{e}}$), and $\beta\gamma = p_{\tilde{e}}/m_{\tilde{e}}$ ($= \sqrt{s-4m_{\tilde{e}}^2}/2m_{\tilde{e}}$). Hence (in the case m_o, $m_{\tilde{\gamma}} = 0$)

$$\begin{aligned} p_o &= \sqrt{(p_1^2 + p_2^2 + p_3^3)} \\ &= \sqrt{(\bar{p}_1^2 + \bar{p}_2^2 + \gamma^2(\bar{p}_3+\beta\bar{E}_o)^2)} \\ &= \sqrt{((1+\gamma^2\beta^2)\bar{p}_o^2 + (\gamma^2-1)\bar{p}_3^2 + 2\gamma^2\beta\bar{p}_3\bar{p}_o)} \ . \end{aligned} \tag{5.24}$$

Substituting $\bar{p}_3 = \bar{p}_o\cdot\cos\bar{\theta}$ gives

$$p_* = \sqrt{(\gamma^2(1+\beta^2\cos^2\bar{\theta})\bar{p}_*^2 + 2\gamma^2\beta\cos\bar{\theta}\bar{p}_*^2)}$$

$$= \gamma(1+\beta\cos\bar{\theta})\bar{p}_* \qquad (5.25)$$

$$= (\sqrt{s} + \sqrt{s-4m_{\tilde{e}}^2}\cos\bar{\theta})/4 \ .$$

Differentiation yields

$$dp_* = (\sqrt{s-4m_{\tilde{e}}^2}/4)\cdot d\cos\bar{\theta} \ . \qquad (5.26)$$

Hence, since the angular distribution in the $\tilde{e}$ rest frame is flat, so is the electron momentum distribution in the c.m. frame. The kinematic limits of the p_* distribution (Eq. (5.16)) follow trivially from Eq. (5.25).

Chapter 6

CONCLUSIONS

"Come listen, my men, while I tell you again
The five unmistakable marks
By which you may know, wheresoever you go,
The warranted genuine Snarks."
- from The Hunting of the Snark
by Lewis Carroll

6.1 Higgs boson production: Conclusions

In Chapter 3, we reviewed some production mechanisms for Higgs boson production which have been discussed in the literature. Toponium ($\Im$) radiative decay will give a clear signal for Higgs boson production in e^+e^- annihilation, but the signal is likely to be obscured by ordinary prompt photon production in $\bar{p}p$ collisions. Production of the Higgs boson via gg fusion in $\bar{p}p$ collisions is likely to be obscured by the QCD Drell-Yan background; the background may be suppressed by considering conjoined production of Higgs bosons and heavy quark flavours, but here the signal is small. Diffractive production of Higgs bosons and heavy quarks in $\bar{p}p$ collisions can give a clear signal, such that identification is possible with just a few events. However, the mechanism of diffractive heavy quark production is not well understood, and so calculations of the cross-sections for "diffractive" Higgs boson production (particularly with very heavy quark flavours (b,t,...)) are fraught with uncertainty.

We also studied one mechanism - the production of Higgs bosons via Bremsstrahlung from weak guage bosons (in particular from Z bosons), in both e^+e^- annihilation and pp collisions - in

some detail. We found that the invariant mass distribution of the lepton pair from the Z decay gives a clear signature for Higgs boson production. In particular, we noted that, in $\bar{p}p$ collisions, this distribution has a double resonance structure, characteristic of the Bremsstrahlung of a scalar particle, which can yield a value for the mass of the Higgs boson. This may be useful, as direct measurement of the mass of the Higgs boson from the invariant mass of its decay products is not always feasible, particularly if it is light ($m_H < 25$ GeV), as the jets are too soft to be clearly identified. However, the production cross-section is small, and the potentially low statistics may make construction of useful kinematic distributions not viable.

We also found that the electron pair from the Z decay is almost colinear, the acolinearity arising from the small collimating effect of the recoil of the Z boson against the Higgs boson. Thus, for light Higgs bosons, where the jets are soft enough to escape detection, the Bremsstrahlung events may be misidentified as standard $Z \longrightarrow e^+e^-$ events. The introduction of microvertex detectors at the Collider will improve the ability to identify light Higgs bosons via their decays, even if the event rate is low.

6.2 Signatures for scalar quark production: Conclusions

In Chapter 4,[1,2] we found that, within theoretical and experimental uncertainties, the UA1 1- and 2-jet events with large missing p_T can be explained in terms of scalar quark QCD pair

production and electromagnetic decay. The dominant configuration is that the harder jet comes from one $\tilde{q} \longrightarrow q\tilde{\gamma}$ decay and the bulk of the missing p_T is due to the photino from the other decay. Comparison with the data constrains the scalar quark mass to lie in the range 20 GeV $< m_{\tilde{q}} <$ 35 GeV, for two degenerate scalar quark flavours (and degenerate left- and right-handed partners), assuming that the gluino is sufficiently heavy to suppress qg and gg production.

We found that the additional contribution of scalar quark production from $W \longrightarrow \bar{\tilde{q}}\tilde{q}'$ and $\tilde{q}\tilde{\gamma}$ production is small, except for $m_{\tilde{q}} \sim 20$ GeV, and does not allow us to further constrain the scalar quark mass. Within our scenario, we used the UA1 data to constrain the gluino mass by considering qg production; we found a lower bound of $m_{\tilde{g}} = O(60)$ GeV.

There are several distinct supersymmetry scenarios for UA1 jet-plus-large-missing-p_T events. We noted that by reducing the experimental jet recognition criterion it may be possible to distinguish between different scenarios.

6.3 Scalar electron and zino production: Conclusions

In Chapter 5,[43] we calculated the cross-section and studied the signatures for the production of scalar electrons in e^+e^- annihilation on and beyond the Z resonance.

We found that, if $m_{\tilde{e}} < \sqrt{s}/2$ the cross-section is dominated

by $\tilde{e}$ pair production; on the Z resonance s-channel Z-production dominates, whereas off resonance the t-channel $\tilde{\gamma}$-exchange contributes the bulk of the cross-section. The signature for e pair production and decay, $e^+ e^- \longrightarrow \tilde{e}^+ \tilde{e}^- \longrightarrow e^+ e^- \tilde{\gamma} \tilde{\gamma}$, is an acolinear and uncorrelated e^+e^- pair, acoplanar with the incident beams, with about half the available energy missing. The electron momentum distribution is flat between the (on-shell) kinematic limits. The electron angular distribution is almost isotropic, reflecting the scalar $\tilde{e} \longrightarrow e \tilde{\gamma}$ decay.

If $m_{\tilde{e}} > \sqrt{s}/2$ the situation is quite different. When the contribution from zino production is negligible (i.e. when $m_{\tilde{z}} > (\sqrt{s} - m_{\tilde{\gamma}})$), the cross-section is dominated by "single" scalar electron production via t-channel photon exchange. These diagrams give rise to a final state with only one observed electron; the other is scattered in the forward direction and so escapes detection. Events with a single observed electron accompanied by large missing energy would be a very clean signature for scalar electron production. However, if a zino exists with $m_{\tilde{z}} < \sqrt{s}$, $\tilde{e}$ production will be dominated by $\tilde{Z}$ production and decay ($e^+ e^- \longrightarrow \tilde{Z} \tilde{\gamma}$; $\tilde{Z} \longrightarrow e^+ e^- \tilde{\gamma}$), leading to a final state with two observed electrons and missing energy. For particular values of $m_{\tilde{z}}$ and $m_{\tilde{e}}$ at a given $\sqrt{s}$ the missing energy distribution may be quite different from that naively expected, peaked at $\sqrt{s}/2$. The electron angular distribution has a forward bias due to the contribution from the subprocess $\tilde{e}\, e \longrightarrow Z \longrightarrow \tilde{e}\, e$. The most striking signature for scalar electron via a zino is the electron momentum distribution, which may show a double peak as a consequence of the kinematics of the zino decay

$\tilde{Z} \longrightarrow e\ \tilde{e} \longrightarrow e\ (\ e\ \tilde{\gamma}\ )$.

In summary, we concluded that scalar electron production leading to a final state with two observed electrons and large missing energy may be the best way to observe scalar electrons experimentally if $m_{\tilde{e}} < \sqrt{s}/2$, and even in the case $m_{\tilde{e}} > \sqrt{s}/2$ if a zino exists with mass $m_{\tilde{Z}} > \sqrt{s}$. In this later case, the process $e^+ e^- \longrightarrow e^+ e^- \tilde{\gamma}\ \tilde{\gamma}$ may reveal the presence of both the $\tilde{e}$ and the $\tilde{Z}$ via a distinctive signature in the electron momentum distribution. If $m_{\tilde{e}} > \sqrt{s}/2$ and $m_{\tilde{Z}} > \sqrt{s}$, however, the most hopeful signature is events with a single observed electron and large missing energy.

6.4 Some final remarks

The CERN $\bar{p}p$ Collider has achieved remarkable success with the discovery of the W and Z bosons, whose existence and masses were correctly predicted by the Weinberg-Salam model of electroweak interactions. This result seemed to vindicate the Standard Model; however, there is, as yet, no evidence of the production of Higgs bosons (discussed in Chapter 3), and which therefore remains the "grail" of SM physics. Other results (i.e. the jet-plus-large-missing-p_T events) suggested that we were seeing physics beyond the scope of the SM. A variety of explanations were proposed, many of which, such as the one presented here in Chapter 4, involved the production of supersymmetric particles. Nevertheless, the "monojet" events now seem to be explicable in terms of SM processes, and so, as yet,

there is no experimental evidence for supersymmetry.

In Chapter 5 we dicussed how, at the forthcoming e^+e^- colliders (SLC at Stanford and LEP at CERN) running on the Z resonance, we may identify particular supersymmetric particles (scalar electrons and zinos). There is no doubt that these machines will provide a superb opportunity for precise tests of the Standard Model; furthermore, the experiments approved for LEP (see Chapter 2) should also be able to reveal physics beyond the Standard Model, whether it be supersymmetry, compositeness or something entirely novel, should it manifest itself at such energies.

We point out that, although we have considered only a few specific cases, much of this work is generally relevant. For example, events with large missing p_T or missing energy are characteristic of the production of particles, such as neutrinos and photinos, that have very small interaction cross-sections; and "flat-topped" momentum distributions, such as those from scalar electron decay (Chapter 5), are characteristic of the decay products of any elementary scalar (e.g. the Higgs boson).

In summary, we remark that the $\bar{p}p$ Collider at CERN has been conspicuously successful, and fully expect similar success at SLC and LEP (and at the 1 TeV FNAL $\bar{p}p$ Collider); high energy collider phenomenology will continue to be an important and intriguing branch of particle physics.

Appendix

MONTE CARLO INTEGRATION AND EVENT SIMULATION

A.1 Introduction

Monte Carlo techniques are used to calculate many of the multi-dimensional integrals in this work. The technique is illustrated in the following example.

Consider the integral, I, of the function f(x), shown in Fig A.1(a), for [a,b]

$$I = \int_a^b f(x)\,dx \sim \frac{(b-a)}{N} \sum_{i=1}^{N} f(x_i). \qquad (A.1)$$

That is, the area under the curve is the average value of the function in the range multiplied by that range. In the Monte Carlo method the points x_i are picked randomly and uniformly in the range. Clearly, the larger the number of points, the closer $^1/_N$ $f(x_i)$ will be to the true average value of the function and the more acurate the numerical value of the integral.

As an explicit example, consider the function

$$f(x) = x \exp(x^2) \text{ on } x = [0,1] \qquad (A.2)$$

such that

$$I_1 = \int_0^1 f(x)\,dx = 0.859... \qquad (A.3)$$

A Monte Carlo estimate of the integral (generated using a Monte Carlo program on a BBC Microcomputer), for a set of N random x_i, is given in Table A.1. Note that, since the points are picked at

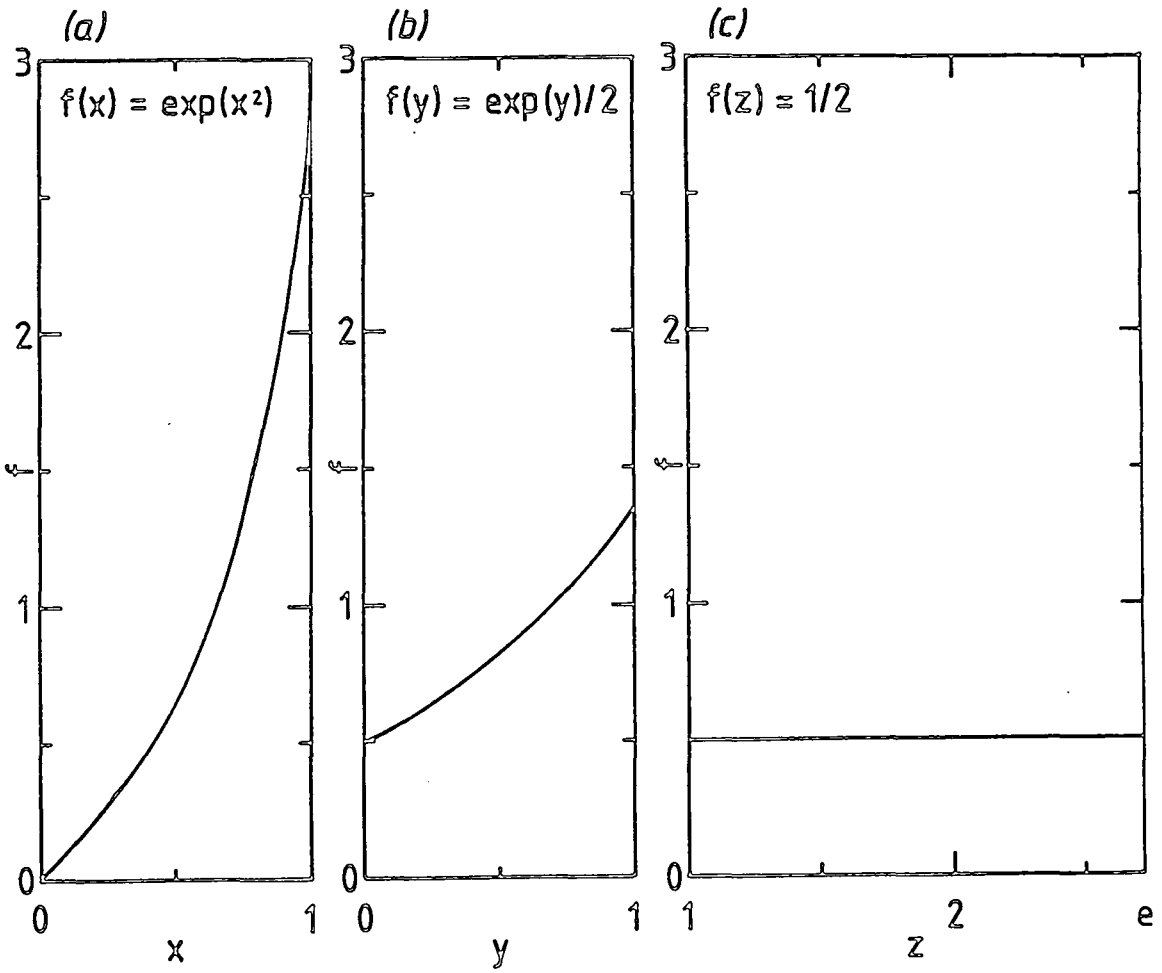

Figure A.1
The functions
(a) $f(x) = \exp(x^2)$
(b) $f(y) = {}^1/_2 \exp(y)$
(c) $f(z) = {}^1/_2$
between the limits of the integrals I_1 (Eq. A.3), I_2 (Eq. A.9) and I_3 (Eq. A.11). Note that the area under each curve is the same.

Table A.1

The results of a Monte Carlo evaluation with N values of x (or y) of the integrals $I_1(x)$ (of Eq.(A.3)) and $I_2(y)$ (of Eq.(A.9)).

N	I_1	I_2
10	1.01897	0.68077
10^2	0.83191	0.84451
10^3	0.87847	0.85603
10^4	0.85974	0.85652
10^5	0.85384	0.85917
10^6	0.85812	0.85894

random, the answers generated by the Monte Carlo will vary from run to run, particularly for low values of N.

The uncertainty in I (represented by the standard deviation, σ) is given by:[1]

$$\sigma = \sqrt{(V(f)/N)} \qquad (A.4)$$

where V(f) is the variance of the function f(x),

$$V(f) = \frac{1}{(b-a)} \int_a^b f(x)^2 \, dx - \left[\frac{1}{(b-a)} \int_a^b f(x) \, dx \right]^2 \qquad (A.5)$$

Hence, to improve the accuracy by an order of magnitude, 100 times as many points are required. This slow convergence means that, for low dimensional integrals, there are faster alternatives, e.g. the Trapezium rule, Simpson's rule, Romberg, &c. However, for n > 5 dimensions, the Trapezium rule converges more slowly than a Monte Carlo integration.

Since the standard deviation is proportional to $\sqrt{V(f)}$ it is possible to increase the accuracy by reducing the variance. Probably the most useful way of doing this is by importance sampling.[2]

A.2 Importance sampling

This involves a change of the integration variable, such that:

$$f(x) \longrightarrow f(x) \, dG(x)/g(x) \qquad (A.7)$$

Points are sampled according to G(x) rather than uniformly in the integration range, and f(x) is weighted by $g(x) = dG(x)/dx$. The

relevant variance is then V(f/g), which is small if g(x) has a similar shape to f(x).

Consider again the example $f(x) = x \exp(x^2)$ (see Fig. A.2(a)). The integral I_1 is formed by chosing points uniformly in x; some points are chosen where the function is large and some where it is small, such that the contribution to the integral for different xi varies considerably. Consider now the change of variable

$$G(x) = y = x^2 \qquad \text{(A.8a)}$$

with $$g(x) = 2x = 2/y \qquad \text{(A.8b)}$$

such that

$$I_2 = {}^1/_2 \int_0^1 \exp(y)\, dy \sim {}^1/_2 \left(\sum \exp(y_i)\right)/N \qquad \text{(A.9)}$$

From Fig. A.2(b) we see that the function is flatter and, hence, the contribution to the integral for different y_i varies rather less. The change of variable

$$G(x) = z = \exp(x^2) \qquad \text{(A.10a)}$$

with $$g(x) = 2x \exp(x^2) \qquad \text{(A.10b)}$$

allows us to write

$$I_3 = {}^1/_2 \int_1^e dz \sim \frac{e-1}{2} \left(\sum 1\right)/N = .859\ldots \text{ for all } N\,. \qquad \text{(A.11)}$$

The variance is reduced to zero and the answer is correct for all N. The function f(z) = 1 is flat (see Fig. A.2(c)).

As a further example, of direct relevance to many of the integrations in the work, consider a cross-section involving a particle resonance:

$$\sigma \sim \int_{s_a}^{s_b} \frac{ds}{((s-m^2)^2 + \Gamma^2 m^2)} \quad . \qquad (A.12)$$

The change of variables

$$G(s) = \theta = \tan^{-1}((s-m^2)/\Gamma m) \qquad (A.13a)$$

with $$g(s) = \Gamma m/((s-m^2)^2 + \Gamma^2 m^2) \qquad (A.13b)$$

yields

$$\sigma \sim \int_a^b \frac{d\theta}{\Gamma m} \qquad (A.14)$$

which is flat in θ; $V(f/g) = V(\Gamma m) = 0$.

The Monte Carlo method generalises to n dimensions:

$$I = \int f(x_j) \prod dx_j = {}^1/_N \sum_{i=1}^{N} f((x_j)_i) \prod_{j=1}^{n} (b_j - a_j) \quad . \qquad (A.15)$$

The standard deviation is again governed by (A.4); this method is particularly good for many dimensional integrals as the rate of convergence is essentially independent of n.

A.3 Monte Carlo simulation

A Monte Carlo program may be used to study experimental processes by simulating interactions event by event.

For exmple, we may be interested in a process the cross-section of which has the form

$$\sigma = \int S(x_j) \sum_{j=1}^{n} dx_j \quad . \qquad (A.16)$$

In the Monte Carlo analysis, the cross-section will be estimated by

$$\sigma_{MC} = {}^{1}/_{N} \sum_{i=1}^{N} S((x_j)_i) \prod_{j=1}^{n} (b_j - a_j) \ . \qquad (A.17)$$

$(x_j)_i$ are chosen randomly within the ranges $[a_j,b_j]$; thus, all values of x_j within these ranges are equally likely (if importance sampling is not being used), but each "event" is weighted by the integrand S and the product of the ranges (which, in practice, may be functions of other integration variables). The theoretical events with larger weighting correspond to experimentally more likely events; in a physical experiment each event has the same "weight" but, for dynamic and kinematic reasons, some events with particular configurations are more common. If importance sampling is used, it moves the theoretical simulation closer to reality by evening out the weighting but making some sets of values of x_j more likely than others.

One of the advantages of performing Monte Carlo simulations is the ease with which experimental "cuts" can be applied, without the need for reconfiguration of the integration limits (which may be non-trivial). For example, if a cut is required to represent an experimental trigger, we can build into the program a conditional statement such that the calculated cross section would correspond only to those events which would pass the experimental trigger. It may, in fact, be more efficient to make a new choice of variables, but in many cases the cut variable is related to the integration variables by a complicated function and such redefinition may be intractable.

References

Chapter 1

1. P.D.B. Collins and A.D. Martin, Hadron Interactions (Bristol; Adam Hilger, 1984), and references therein
2. F. Halzen and A.D. MArtin, Quarks and Leptons (New York; Wiley, 1984), and references therein
3. A. Bohm, *Proc. 20th Int. Conf. on High Energy Physics, Madison*, ed. L. Durand and L.G. Ponchom, AIP Conf. Proc. 68 (1980) 551
4. S.J. Brodsky and S.D. Drell, Phys. Rev. D22 (1980) 2236
5. F.J. Gilman, Phys. Rep. 4C (1972) 95
6. R.P. Feynman, Photon-Hadron Interactions (New York; Benjamin, 1972)
7. G. Arnison et al. (UA1 Collaboration), Phys. Lett. 147B (1984) 493
8. S. Adler, Phys. Rev. 177 (1969) 2426; J.S. Bell and R. Jackiw, Nuovo Cimento 51 (1969) 47
9. V.D. Barger, H. Baer, K. Hagiwara and R.J.N. Phillips, Phys. Rev. D30 (1984) 947
10. M.R. Pennington, Rep. Prog. Phys. 46 (1983) 393, and references therein
11. G. Arnison (UA1 Collaboration), Phys. Lett. 122B (1983) 103; 126B (1983) 398; 123B (1983) 115
12. M. Banner et al. (UA2 Collaboration), Phys. Lett. 122B (1983) 476; P. Bagnaia et al. (UA2 Collaboration), Phys. Lett. 129B (1983) 130; Z. Physik C20 (1983) 117
13. R.P. Feynman, Quantum Electrodynamics (New York; Benjamin, 1961)

14. H.D. Politzer, Phys. Rep. 14C

15. H.D. Politzer, Phys. Rev. Lett. 30 (1973) 1346

16. E. Reya, Phys. Rep. 69C (1918) 195

17. S.L. Glashow, Nucl. Phys. 22 (1967) 579; S. Weinberg, Phys. Rev. Lett. 19 (1967) 1264; A. Salam, *Proc. 8th Nobel Symp.*, ed. N. Svartholm (Stockholm; Arnqvist and Wiskell, 1968)

18. P.W. Higgs, Phys. Rev. Lett. 12 (1964) 132; 13 (1964) 508; F. Englert and R. Bront, Phys. Rev. Lett. 13 (1964) 321; G.S. Guralnik, C.R. Hagen and T.W.B. Kibble, Phys. Rev. Lett. 13 (1964) 585

19. G. 't Hooft, Nucl. Phys. B33 (1971) 167

20. Y. Nambu, Phys. Rev. Lett. 4 (1960) 380; J. Goldstone, Nuovo cimento, 19 (1961) 15; Y. Nambu and G. Jona-Lasinio Phys. Rev. 122 (1961) 345; 124 (1961) 246; J. Goldstone, A. Salam and S. Weinberg, Phys. Rev. 127 (1962) 965; S. Bluchman and A. Klein, Phys. Rev 131 (1962) 2363

21. M. Kobayashi and K. Maskawa, Prog. Theor. Phys. 49 (1973) 652

22. R.A. Flores and M. Sher, Ann. Physics 148 (1983) 95, and references therein

23. S. Coleman and E. Weinberg, Phys. Rev. D7 (1973) 1888

24. K.T. Mahanthappa and M. Sher, Phys. Rev. D22 (1980) 1711

25. L. Maiani, G. Parisi and R. Petronzio, Nucl. Phys. B158 (1979) 295; H.D. Politzer and S. Wolfram, Phys. Lett. B82 (1979) 242; errata, B83 (1979) 421

26. M.R. Pennington, *private communication*

27. L. Lyons, Prog. Part. Nucl. Phys. 10 (1983) 227

28. L. Susskind, Phys. Rev. D20 (1979) 2619

29. J.G. Taylor, Prog. Nucl. Phys. 12 (1983) 1, and references therein

30. J. Ellis, Proc. 1983 Symp. on Lepton and Photon Interactions at High Energies, ed. D.G. Cassel and D.L. Kreinick (Cornell University, 1983) 439

31. K.S. Stelle, Festschrift in honour of B. de Witt; P.C. West, *Proc. La Jolla Workshop*, January 1983, and references therein

32. P. van Nieuwenhuizen, Phys. Rep. 68C (1981) 189, and references therein

33. J. Wess and B. Zumino, Nucl. Phys. B70 (1974) 39; Phys. Lett. 49B (1974) 52; J. Iliopoulos and B. Zumino, Nucl. Phys. B76 (1974) 310

34. S. Dimopoulos and H. Georgi, Nucl. Phys. B193 (1981) 150; N. Sakai, Z. Physik C11 (1982) 153

35. S. Ferrara and B. Zumino, Nucl. Phys. B79 (1974) 413; L. Brink, J.H. Schwartz and J. Schenk, Nucl. Phys. B121 (1977) 77; F. Gliozzi, J. Schenk and D. Olive, Nucl. Phys. B122 (1977) 253

36. P. Fayet, Nucl. Phys. B113 (1976) 135

37. P. Howe, K.S. Stelle and P. Townsend, Nucl. Phys. B191 (1981) 445; S. Mandelstam, IHEPS Conf., Paris, J. Physique 43 (1982) n°12

38. S. Rajpoot, J.G. Taylor and M. Zaimi, Phys. Lett. 127B (1983) 347

39. E.Witten, Nucl. Phys. B188 (1981) 513; P. Fayet, in Studies in High Energy Phys. 3 (Harwood; 1981)

40. S. Ferrara and P. van Nieuwenhuizen, Phys. Rev. Lett. 37 (1976) 1669

41. E. Cremmer, B. Julia and J. Schenk, Phys. Lett. 76B (1978) 409

42. Th. Kaluza, Sitz. Preuss Akad. Wiss. Berlin Math Phys. K1 (1921) 966; O. Klein, Z. Physik 37 (1926) 895

43. M. Gell-Mann, talk at the *Washington meeting of the APS* (1977)

44. J. Ellis and D.V. Nanopoulos, Phys. Lett. 110B (1982) 44; R. Barbieri and R. Gatto, Phys. Lett. 110B (1982) 211; T. Inami and C.S. Lim, Nucl. Phys. B207 (1982) 533; B.A. Campbell, Phys. Rev. D28 (1983) 203; M.J. Duncan, Nucl. Phys. B221 (1983) 285; J.F. Donaghue, H.P. Nilles and D. Wyler, Phys. Lett. 128B (1983) 55

45. P. Fayet, Nucl. Phys. B90 (1975) 104; A. Salam and J. Strathdee, Nucl. Phys. B87 (1975) 85; G.R. Farrar and S. Weinberg, Phys. Rev. D27 (1983) 2732

46. P. Fayet, Phys. Lett. 69B (1977) 489; G. Farrar and P. Fayet, Phys. Lett. 76B (1978) 575

47. P. Fayet and J. Iliopoulos, Phys. Lett. 51B (1974) 461

48. S. Deser and B. Zumino, Phys. Rev. Lett. 38 (1977) 1433

Chapter 2

1. G. Arnison (UA1 Collaboration), Phys. Lett. 122B (1983) 103; 126B (1983) 398; 123B (1983) 115; M. Banner et al. (UA2 Collaboration), Phys. Lett. 122B (1983) 476; P. Bagnaia et al. (UA2 Collaboration), Phys. Lett. 129B (1983) 130; Z. Physik C20 (1983) 117

2. F.J. Hasert et al., Phys. Lett. 46B (1973) 121

3. S.L. Glashow, Nucl. Phys. 22 (1967) 579; S. Weinberg, Phys. Rev. Lett. 19 (1967) 1264; A. Salam, *Proc. 8th Nobel Symp.*, ed. N. Svartholm (Stockholm; Arnqvist and Wiskell, 1968)

4. B.W. Lee, *Proc. Int. Neutrino Conf., Achen*, 1976, ed. H. Faissner, H. Reithler and P. Zerwas (Braunschweig; Vieweg, 1977) p.704

5. C. Rubbia, P. McIntyre and D. Cline, *ibid.*, p.683

6. S. van der Meer, internal report CERN ISR-PO/72-31 (1972), unpublished; D. Mohl, G. Petrucci, L. Thorndahl and S. van der Meer, Phys. Rep. 58 (1980) 73; F.T. Cole and F.E. Mills, Ann. Rev. Nucl. Part. Sci. 31 (1981) 295, and references therein

7. G. Carron et al., Phys. Lett. 77B (1978) 353; G. Carron et al., IEEE Trans. Nucl. Sci. NS-26 No.3

8. UA1 proposal, CERN SPSC 78-6/P92 (1978); UA2 proposal, CERN SPSC 78-8/P93 (1978); UA3 proposal, CERN SPSC 78-15/P96 (1978); UA4 proposal, CERN SPSC 78-105/P114 (1978); UA5 proposal, CERN SPSC 78-10/P108 (1978); UA6 proposal, CERN SPSC 80-63/P148 (1980)

9. J.D. Bjorken, Proc. 3rd Int. Symp. on Electron and Photon Interactions, Stanford; R.P. Feynman, Phys. Rev. Lett. 23 (1969) 1415; J.D. Bjorken and E.A. Paschos, Phys. Rev. D10 (1969) 2973

10. R.P. Feynman, Photon-Hadron Interactions (New York; Benjamin, 1972)

11. V.N. Gribov and L.N. Lipatov, Yad. Fiz. 15 (1972) 781; 15 (1972) 1218

12. R.M. Barnett and D. Schlatter, Phys. Lett. 112B (1982) 475; R.M. Barnett, Phys. Rev. Lett. 48 (1982) 1657

13. G. Altarelli, R.K. Ellis and G. Martinelli, Nucl. Phys. B157 (1979) 461; G. Parisi, Phys. Lett. 90B (1980) 295

14. J.F. Owens and E. Reya, Phys. Rev. D17 (1978) 3003

15. M. Glück, E. Hoffmann and E. Reya, Z. Physik C13 (1982) 119

16. D.W. Duke and J.F. Owens, Phys. Rev. D27 (1984) 508

17. E. Eichten, I. Hinchcliffe, K. Lane and C. Quigg, Rev. Mod. Phys. 56 (1984) 1

18. G. Altarelli and G. Parisi, Nucl. Phys. B126 (1977) 298

19. D.H. Perkins, Introduction to High Energy Physics, 2nd ed. (Reading, Mass; Addison-Wesley, 1982)

20. CERN Courier 24 (1984) 227; 24 (1984) 269; 24 (1984) 375; 25 (1985) 52

Chapter 3

1. S.L. Glashow, Nucl. Phys. 22 (1967) 579; S. Weinberg, Phys. Rev. Lett. 19 (1967) 1264; A. Salam, *Proc. 8th Nobel Symp.*, ed. N. Svartholm (Stockholm; Arnqvist and Wiskell, 1968)

2. G. Arnison (UA1 Collaboration), Phys. Lett. 122B (1983) 103; 126B (1983) 398; 123B (1983) 115; M. Banner et al. (UA2 Collaboration), Phys. Lett. 122B (1983) 476; P. Bagnaia et al. (UA2 Collaboration), Phys. Lett. 129B (1983) 130; Z. Physik C20 (1983) 117

3. S. Coleman and E. Weinberg, Phys. Rev. D7 (1973) 1888; K.T. Mahanthappa and M. Sher, Phys. Rev. D22 (1980) 1711

4. L. Maiani, G. Parisi and R. Petronzio, Nucl. Phys. B158 (1979) 295; H.D. Politzer and S. Wolfram, Phys. Lett. B82 (1979) 242; errata, B83 (1979) 421; see also M.A. Beg, C. Panagiotakopoulos and A. Sirlin, Phys. Rev. Lett. 52 (1983) 883

5. R.A. Flores and M. Sher, Ann. Physics 148 (1983) 95, and references therein

6. J.G. Taylor, Prog. Nucl. Phys. 12 (1983) 1, and references therein

7. J. Ellis, M.K. Gaillard and D.V. Nanopoulos, Nucl. Phys. B106 (1976) 292

8. E. Wilzcek, Phys. Rev. Lett. 39 (1977) 1304

9. G. Arnison et al. (UA1 Collaboration), Phys. Lett. 147B (1984) 493

10. H. Georgi, S.L. Glashow, M. Machacek and D.V. Nanopoulos, Phys. Rev. Lett. 40 (1978) 692

11. R. Raito and T. Wada, Phys. Rev. D19 (1979) 941

12. J.N. Ng and P. Zakarauskas, Phys. Rev. D29 (1984) 876

13. P.D.B. Collins and A.D. Martin, Hadron Interactions (Bristol; Adam Hilger, 1984), and references therein

14. V.D. Barger, F. Halzen and W.-Y. Keung, Phys. Rev. D24 (1981) 1428

15. V.D. Barger, F. Halzen and W.-Y. Keung, Phys. Rev. D25 (1982) 1838

16. D.R.T. Jones and S.T. Petcov, Phys. Lett. 84B (1979) 440

17. L.-L. Chau, W.-Y. Keung and S.C.C. Ting, Phys. Rev. D24 (1981) 2862

18. P. Kalyniak, J.N. Ng and P. Zakarauskas, Phys. Rev. D29 (1984) 502

Chapter 4

1. G. Arnison et al. (UA1 Collaboration), Phys. Lett. 122B (1983) 103; G. Banner et al. (UA2 Collaboration), Phys. Lett. 122B (1983) 476

2. G. Arnison et al. (UA1 Collaboration), Phys. Lett. 139B (1984) 115

3. P. Bagnaia et al. (UA2 Collaboration), Phys. Lett. 139B (1984) 105

4. P.R. Harrison and C.H. Llewellyn-Smith, Nucl. Phys. B213 (1983) 223; errata, B223 (1983) 542

5. S. Dawson, E. Eichten and C. Quigg, Phys. Rev. D31 (1985) 1581

6. M. Gluck, E. Hoffman and E. Reya, Z. Physik C13 (1982) 119

7. S. Dimopoulos, S. Raby and F.A. Wilczek, Phys. Rev. D24 (1981) 1681; L.E. Ibanez and G.G. Ross, Phys. Lett. 105B (1982) 439; M.B. Einhorn and D.R.T. Jones, Nucl. Phys. B196 (1982) 475

8. J. Ellis, CERN preprint TH-3802 (1984), and references therein

9. H.E. Haber and G.L. Kane, Phys. Lett. 142B (1984) 212

10. J. Ellis and H. Kowalski, Nucl. Phys. B246 (1984) 189

11. V. Barger, K. Hagiwara and W.-Y. Keung, Phys. Lett. 145B (1984) 147

12. V. Barger et al., Phys. Rev. Lett. 53 (1984) 641

13. J. Ellis and H. Kowalski, Phys. Lett. 142B (1984) 441; E. Reya and D.P. Roy, Phys. Rev. Lett. 53 (1984) 881

14. M.J. Herrero et al., Phys. Lett. 145B (1984) 430

15. A. de Rújula, talk given at the *5th Topical Workshop on Proton-Antiproton Collider Physics*, Aosta (1985); CERN preprint TH-4148/85 (1985)

Chapter 5

1. R. Barbieri and S. Ferrara, Surv. High Energy Physics 4 (1983) 33, and references therein
2. G.F. Farrar and P. Fayet, Phys. Lett. 89B (1980) 191; R. Barbieri et al., Phys. Lett. 127B (1983) 458; N. Cabibbo, L. Maiani and S. Petrarca, Phys. Lett. 132B (1983) 195; S.K. Jones and C. Llewellyn-Smith, Nucl. Phys. B217 (1983) 145
3. M.K. Gaillard, L. Hall and I. Hinchcliffe, Phys. Lett. 116B (1982) 279
4. M. Kuroda et al., Phys. Lett. 127B (1983) 467; T. Kobayashi and M. Kuroda, Phys. Lett. 134B (1984) 271
5. I. Hayashibara et al., Phys. Lett. 158B (1985) 349
6. J.E. Johnson and S. Rudaz, Phys. Rev. D30 (1984) 1590
7. K. Hidaka, H. Komatsu and P. Ratcliffe, Phys. Lett. 150B (1985) 399
8. W. Bartel et al. (JADE Collaboration), Phys. Lett. 152B (1985) 385
9. G. Bartha et al. (ASP Collaboration), SLAC-PUB-3817 (1985)
10. H.E. Haber and G.L. Kane, Phys. Rep. 117 (1985) 75
11. S. Dawson, E. Eichten and C. Quigg, Phys. Rev. D31 (1985) 1581
12. M. Glück and E. Reya, Phys. Lett. 130B (1983) 423
13. N. Brown, *private communication*
14. K. Hagiwara and D. Zepperfield, DESY report 85-133 (1985)
15. T. Schimert, C. Burgess and X. Tata, Phys. Rev. D32 (1985) 707
16. T. Schimert and X. Tata, Phys. Rev. D32 (1985) 721

Chapter 6

1. A.R. Allan, E.W.N. Glover and A.D.Martin, Phys. Lett. 146B (1984) 247

2. A.R. Allan, E.W.N. Glover and S.L. Grayson, Nucl. Phys. B259 (1985) 77

3. A.R. Allan and A.D. Martin, Durham University preprint DTP/85/8 (1985) unpublished; A.R. Allan, N. Brown and A.D.Martin, Durham University preprint DTP/86/6 (1986) to be published in Z. Physik C

Appendix

1. F. James, Rep. Prog. Phys. 43 (1980) 73

2. R.Y. Rubenstein, Simulation and the Monte Carlo Method (New York; Wiley, 1981)

Envoi

The Red Queen shook her head. "You may call it 'nonsense' if you like," she said, "but *I've* heard nonsense, compared with which that would be as sensible as a dictionary!"

– from *Through the Looking-Glass* by Lewis Carroll